2014

Coordinated Voltage and Reactive Power Control of Power Distribution Systems with Distributed Generation

Esa A. Paaso
University of Kentucky, aleksi.paaso@uky.edu

STUDENT AGREEMENT:

I represent that my thesis or dissertation and abstract are my original work. Proper attribution has been given to all outside sources. I understand that I am solely responsible for obtaining any needed copyright permissions. I have obtained needed written permission statement(s) from the owner(s) of each third-party copyrighted matter to be included in my work, allowing electronic distribution (if such use is not permitted by the fair use doctrine) which will be submitted to UKnowledge as Additional File.

I hereby grant to The University of Kentucky and its agents the irrevocable, non-exclusive, and royalty-free license to archive and make accessible my work in whole or in part in all forms of media, now or hereafter known. I agree that the document mentioned above may be made available immediately for worldwide access unless an embargo applies.

I retain all other ownership rights to the copyright of my work. I also retain the right to use in future works (such as articles or books) all or part of my work. I understand that I am free to register the copyright to my work.

REVIEW, APPROVAL AND ACCEPTANCE

The document mentioned above has been reviewed and accepted by the student's advisor, on behalf of the advisory committee, and by the Director of Graduate Studies (DGS), on behalf of the program; we verify that this is the final, approved version of the student's thesis including all changes required by the advisory committee. The undersigned agree to abide by the statements above.

Esa A. Paaso, Student

Dr. Yuan Liao, Major Professor

Dr. Caicheng Lu, Director of Graduate Studies

COORDINATED VOLTAGE AND REACTIVE POWER CONTROL OF POWER DISTRIBUTION SYSTEMS WITH DISTRIBUTED GENERATION

DISSERTATION

A dissertation submitted in partial fulfillment of the
requirements for the degree of Doctor of Philosophy in the
College of Engineering
at the University of Kentucky

By

Esa Aleksi Paaso
Lexington, KY

Director: Dr. Yuan Liao, Associate Professor of Electrical Engineering

Lexington, Kentucky

2014

ABSTRACT OF DISSERTATION

COORDINATED VOLTAGE AND REACTIVE POWER CONTROL OF POWER DISTRIBUTION SYSTEMS WITH DISTRIBUTED GENERATION

Distribution system voltage and VAR control (VVC) is a technique that combines conservation voltage reduction and reactive power compensation to operate a distribution system at its optimal conditions. Coordinated VVC can provide major economic benefits for distribution utilities. Incorporating distributed generation (DG) to VVC can improve the system efficiency and reliability. The first part of this dissertation introduces a direct optimization formulation for VVC with DG. The control is formulated as a mixed integer non-linear programming (MINLP) problem. The formulation is based on a three-phase power flow with accurate component models. The VVC problem is solved with a state of the art open-source academic solver utilizing an outer approximation algorithm. Applying the approach to several test feeders, including IEEE 13-node and 37-node radial test feeders, with variable load demand and DG generation, validates the proposed control.

Incorporating renewable energy can provide major benefits for efficient operation of the distribution systems. However, when the number of renewables increases the system control becomes more complex. Renewable resources, particularly wind and solar, are often highly intermittent. The varying power output can cause significant fluctuations in feeder voltages. Traditional feeder controls are often too slow to react to these fast fluctuations. DG units providing reactive power compensation they can be utilized in supplying voltage support when fluctuations in generation occur. The second part of this dissertation focuses on two new approaches for dual-layer VVC. In these approaches the VVC is divided into two control layers, slow and fast. The slow control obtains optimal voltage profile and set points for the distribution control. The fast control layer is utilized to maintain the optimal voltage profile when the generation or loading suddenly changes. The MINLP based VVC formulation is utilized as the slow control. Both local reactive power control of DG and coordinated quadratic programming

(QP) based reactive power control is considered as the fast control approaches. The effectiveness of these approaches is studied with test feeders, utility load data, and fast-varying solar irradiance data. The simulation results indicate that both methods achieve good results for VVC with DG.

KEYWORDS: Power distribution, Voltage and VAR control, Mathematical programming, Distributed generation, Reactive power compensation

Esa Aleksi Paaso
Student's Signature

April 18, 2014
Date

COORDINATED VOLTAGE AND REACTIVE POWER CONTROL OF POWER DISTRIBUTION SYSTEMS WITH DISTRIBUTED GENERATION

By

Esa Aleksi Paaso

Dr. Yuan Liao
Director of Dissertation's Signature

Dr. Cai-Cheng Lu
Director of Graduate Studies Signature

April 18, 2014
Date

ACKNOWLEDGMENTS

I would like to thank my dissertation director and academic advisor Dr. Yuan Liao for his support and help towards completing my PhD degree. I have been fortunate enough to work with Dr. Liao for the past four years. I would also like to thank Dr. Aaron Cramer for providing help, ideas, and co-authoring a couple of papers with me. In addition to Dr. Liao and Dr. Cramer, special thanks to Dr. YuMing Zhang, Dr. Zongming Fei, and Dr. Joseph Sottile for their advice and willingness to serve in my dissertation advisory committee. I would also like to acknowledge Power and Energy Institute of Kentucky (PEIK) for the financial support for my PhD studies.

I would like to thank my wife, Becky, for her encouragement, support, and constructive criticism through my PhD studies. I would also like to thank my parents, Päivi and Esa, and my sister Annika for their support and encouragement through my studies.

TABLE OF CONTENT

LIST OF TABLES

LIST OF FIGURES

LIST OF ABBREVIATIONS

AI	Artificial intelligence
ANSI	American national standard institute
ANN	Artificial neural network
ANFIS	Artificial neural fuzzy interference system
BESS	Battery energy storage system
CVR	Conservation voltage reduction
DG	Distributed generation
DER	Distributed energy resources
DMS	Distribution management system
DSM	Demand side management
ESS	Energy storage system
IEEE	Institute of electrical and electronics engineers
LP	Linear programming
LTC	Load tap-changer
MILP	Mixed integer linear programming
MINLP	Mixed integer non-linear programming
MIP	Mixed integer programming
MPPT	Maximum power point tracking
MSE	Mean squared error
NLP	Non-linear programming
PV	Photovoltaic
LTC	Load-tap changing
RTU	Remote terminal unit
SCADA	Supervisory control and data acquisition
SVR	Static voltage regulator
VAR	Volt-ampere reactive
VVC	Voltage and VAR control
VVO	Voltage and VAR optimization

1. INTRODUCTION

Power distribution systems are integral parts of the electric power grid. These systems perform as links between the transmissions systems and end power users. Distribution systems deliver electric power to the customer. The transmitted power is not all delivered to the end users: some of the power is lost in the distribution systems.

1.1. Distribution loss

Distribution systems operate at lower voltage levels than their transmission counter parts. Equipment used for distribution is typically much smaller in terms of capacity than the equipment used for transmission. Moving electric power at a lower voltage increases the system loss. Lower voltages and less efficient equipment are major contributors to the distribution loss. It has been approximated that the distribution loss account for approximately four percent of the total power system load [1]. The majority of distribution loss occurs in the distribution lines and transformers: the main portion of this is due to resistive elements in the system. The loss due to the resistive elements is often referred to as resistive loss or I^2R loss [2]. The resistive loss is directly proportional to the resistance of the components and the square of the current magnitudes flowing in distribution systems.

This loss can have significant economic impacts. Not only are there fuel costs associated with the lost energy, but loss can also require added generation capacity. The power lost in the distribution systems – which still has to be transmitted through the transmission grid – totals up to even more distribution loss. Small improvements in distribution efficiency can contribute to large financial savings on utilities. These financial savings will have an effect on the cols of the utility to deliver power to customer.

The reduction in distribution loss can be indeed very beneficial for both the utility and the end power user.

1.2. Power factor correction

There are two ways to reduce the resistive loss: reducing the system resistance or reducing the currents. The reduction of distribution resistances is generally very expensive as it requires investing in new distribution system components, such as larger conductors on the distribution lines or new transformers. Since there are high costs associated with reducing distribution resistances, often the only viable option to reduce the resistive loss is to reduce the distribution current magnitudes. Application of capacitor banks to reduce net reactive power load is a well-established technique to reduce distribution current magnitudes [3]. Application of capacitor banks along the distribution feeders is commonly referred to as reactive power compensation and power factor correction. The distribution system load demand is typically variable, and thus, all or some of the installed capacitor banks can be controllable. With the application of the capacitor bank control, certain capacitor banks are only used when the system operates at load levels that require certain level of reactive power compensation, and can be switched off the other times. The control of capacitor banks is often referred in literature as VAR control or reactive power control.

1.3. Demand side management

The total power drawn from the transmission is the sum of distribution load demands and distribution loss. Reduction of loss is not the only option for decreasing the system total demand from the transmission system. The reduction in the total demand can also be achieved with the control of distribution system loads. Demand side management

(DSM) is one way to achieve such reductions [4]. In a DSM scheme, the utility company has direct control over certain loads that it can turn on or off as it desires. A typical DSM action would turn off some loads during the times of high consumption. DSM can be effective for reducing the overall system demand; however, it requires the utility to have an infrastructure to remotely control these loads. In addition to that, DSM does not provide a choice to the customer when the utility takes the demand reduction actions and turns off the power to their DSM load. The utility typically has to compensate for the customer to allow it to control the customer's power demand.

1.4. Conservation voltage reduction

Demand reduction is also obtainable with conservation voltage reduction (CVR) [5]. CVR reduces the load demand by reducing feeder service voltages. The typical distribution loads consist of constant impedance, constant current, and constant power loads. This load model structure is commonly referred to as a ZIP load model. With the load equations it can be shown that the load reduction is obtainable by reducing the service voltage for constant impedance and constant current loads. The active and reactive power loads at node *m* are described respectively by:

$$P_m = P_m^0 \left(a_l^P \left(\frac{|V_m|}{|V_m^0|} \right)^2 + b_l^P \left(\frac{|V_m|}{|V_m^0|} \right) + c_l^P \right) \tag{1.1}$$

and

$$Q_m = Q_m^0 \left(a_l^Q \left(\frac{|V_m|}{|V_m^0|} \right)^2 + b_l^Q \left(\frac{|V_m|}{|V_m^0|} \right) + c_l^Q \right) \tag{1.2}$$

where V_m is feeder service voltage at node *m*, V_m^0 is the rated voltage at node *m*, and P_m^0 and Q_m^0 are the rated real and reactive power demand. The portions of constant impedance, constant current, and constant power distribution loads are represented with

a_l^P, b_l^P, and c_l^P for real power loads and a_l^Q, b_l^Q, and c_l^Q for reactive power loads. With the reduction feeder service voltage at node *m*, the constant impedance portions and constant current portions are known to decrease. On the other hand, voltage reduction does not have an effect on constant power loads.

ANSI Standard C84.1 "Electrical Power System and Equipment – Voltage Ratings" has specified the voltage range, in which the utility must remain, when supplying electric power to its customers [6]. The normal steady-state service voltage range is between 114V-126V at the 120V base voltage level, which corresponds to ± 5% service voltage bandwidth. Traditionally most utilities have maintained the distribution voltage levels towards the higher end of the ANSI range. This is because the higher voltage levels are better suited for suddenly increasing power demand. The CVR scheme would maintain the voltage levels towards the lower end of the allowable range. The benefits achieved with CVR depend on the voltage drop along the distribution feeder. The attainable voltage reductions with CVR can be higher if the total voltage drops on a feeder are small [7].

The CVR is typically achieved by the control of voltage regulating devices in the distribution systems. In a traditional distribution system a load tap-changing (LTC) transformers and voltage regulators are the main voltage control devices. A LTC transformer is typically located at a distribution substation and controls the feeder source voltages. LTC mechanism on a transformer allows the number of turns in the transformer secondary winding to be selected in discrete steps. Step voltage regulators are devices to control feeder voltages. They can be located along the distribution line away from the substation and can be single phase or three phase devices. The step voltage regulators are

typically autotransformers with LTC mechanism on their series windings [8]. The regulators allow their output to vary as the system load varies. The voltage control is obtained by changing the number of turns of the series winding.

Certain distribution loads are reduced with application of CVR. These loads include resistive loads such as heating, cooking, and drying; standard incandescent lighting; and non-frequency-controlled motor loads operating below their nameplate values. Benefits of CVR are not limited to reducing the overall system consumption; CVR also reduces the customers' energy consumptions and save money on their electric bill.

1.5. Coordinated reactive power compensation and CVR

Power factor correction and CVR are known to provide improved efficiency for distribution systems. In a traditional distribution system the switchable capacitor banks, associated with VAR control, and voltage regulating devices, associated with voltage control, are the two main forms of control. In order to control these devices together, a global or feeder wide control is considered. For best results the global control should be formulated as an optimization problem. The goal of the optimal control is to develop and execute a control plan to minimize a specified objective function, such as minimization of energy consumption or minimization of distribution loss. Most objective functions for the optimal control are geared towards minimizing system loss, power demand, energy consumption, or a combination any combination mentioned objective functions. Early work in distribution automation has decoupled VAR and voltage control [9] [10] [11]. Decoupling forms two separate optimal control problems for the capacitor banks and for the voltage regulators. Although the decoupling the problems often yield to good

solutions, in order to achieve optimal control voltage and VAR control (VVC) need to be examined together.

In short, VVC is the control and operation of distribution control devices – including capacitor banks, LTC transformers, and voltage regulators – to perform power factor correction and demand reduction with CVR, to maintain acceptable distribution system operating voltages, and to operate the distribution system as efficiently as possible.

1.6. Challenges with integration of distributed generation to VVC

Distributed generation (DG) provides new challenges and opportunities for VVC. In a traditional distribution a single power flow is always present, the power flows from the substation to the loads. DG can introduce bi-directional power flow to the distribution system so power flows back to the distribution substation from the DG sites. The bi-directional power flow was introduced by DG and will have an effect on the global VVC. DG such as battery energy storage systems (BESS) can have controllable real and reactive power output. But sources such as wind and photovoltaic (PV), have variable generation outputs that are generally dependent on the external conditions. PV generation, in particular, is connected to the distribution grid via power electronic interfaces that can be used for reactive power control. It is possible to control the reactive power injection by DG as a part of the global VVC. In order to be optimally controlled DG needs to be included in the overall distribution VVC problem. The inclusion of the DG units will complicate the overall problem, but the additional benefits achieved with DG outweigh the implementation difficulties.

1.7. Ideal VVC

In order to develop algorithms that best suited for VVC, the idealized approach is considered. An ideal VVC system is identified in [12] to have the following characteristics:

- Maintain a voltage profile that is within the ANSI specified limits in all parts of the distribution feeder.
- Maintain a near-unity power factor.
- Have an ability to perform self-monitoring.
- Allow for operator overrides.
- Have the capability to adapt to feeder reconfigurations.
- Have the capability to exploit Smart Grid devices.
- Provide optimal coordinated control.
- Allow for selectable control and operation objectives.

1.8. Contribution of this dissertation

The motivation behind the research was to develop a new approach for VVC with intermittent DG. The methods use combined traditional VVC equipment together with controllable DG to provide coordinated fast acting voltage and VAR control for distribution systems. The main contributions of this dissertation are listed as follows:

- A new method for formulating and solving a distribution system VVC as a MINLP problem is introduced. With the proposed approach that a distribution system VVC can be solved without making assumptions, such as linearization, in the problem formulation. The effectiveness of the MINLP is studied with a number of test feeders including the IEEE 13 node and IEEE 37 node radial

distribution test feeders. The framework for the studied method is presented also in [13].

- The analytical VVC approaches, including the proposed MINLP based approach, are limited by their computational times for large distribution systems. The traditional VVC devices are also typically not fast enough to respond fast variations in DG caused by the intermittency of the source. It has been proposed that local reactive power at feeder nodes with DG could be used to limit voltage fluctuations in the feeder. Approach to minimize voltage fluctuation at specific feeder nodes is presented. The goal of the approach is to limit voltage fluctuations downstream from the DG devices. The proposed local control approach is also studied with several test feeders. The local control approach as a part of the feeder wide optimal control is presented in [14].
- In order to reduce two or more DG units to take counteracting control actions a novel approach for fast global reactive power control is presented. The approach utilizes quadratic programming constrained by classical sensitivity analysis to find optimized reactive power injections by the DG to minimize voltage variations across the feeder. The approach is presented to produce good results with high PV penetrations on several test feeders. The approach is based on the work presented in [15].
- Finally the dissertation presents, a dual-layer VVC with the proposed MINLP approach making the long-term control decisions and proposed fast-acting local control approach [14] making the control decisions on short term. The effectiveness of the dual layer control approaches is studied with test system, real

life variable utility load data, and with PV generation determined from measured irradiance patterns. The dual-layer control shows promise for on-line VVC approach as it can find the optimal operation point of the feeder and keep constant voltages across the feeder with changing generation.

1.9. Dissertation outline

A literature review of existing VVC techniques is presented in chapter 2. Chapter 3 presents the modeling required for formulating distribution system VVC as a MINLP. The results of case studies to validate the proposed VVC algorithm are shown in chapter 4. The fast local reactive power control is described in chapter 5, and the fast global reactive power control is discussed in detail in 6. The dual layer VVC approach with local reactive power control is presented in chapter 7. The conclusions of the dissertations are drawn in chapter 8.

2. LITERATURE REVIEW

Multiple methods to perform the distribution system VVC have been studied. Most of these methods combine reactive power control and CVR to some degree. Some recent methods have considered DG as a part of the VVC problem. The main purpose of the VVC is to provide the customers with high quality electric power while simultaneously reducing the system loss or overall power demand. There are several existing approaches developed for VVC of power distribution systems, which can be summarized as follows:

- Standalone VVC
- Rule-based VVC
- Distribution model based analytical voltage and VAR optimization (VVO)
- Artificial intelligence (AI) techniques for VVO

2.1. Standalone VVC

Standalone VVC is managed by independent, individual, standalone voltage regulation, and reactive power compensation devices. In a traditional distribution scheme these devices include voltage regulators, LTC transformers, and switchable capacitor banks. The devices are controlled individually based on the local conditions at their location on the feeder. Some of the control parameters of these devices include: the local power factor, load currents, feeder voltages, reactive power flow, ambient temperature, time of day, day of week, and operating season. The strengths of the standalone control approaches include their low cost of installation, lack of reliance on field communications, and scalability to many feeders. There are significant drawbacks to the standalone approaches as well: they generally have no self-monitoring features and lack

coordination between control devices. Due to these issues, standalone VVC may not be able to block counteracting control actions that two or more distribution control devices take. The control may reach optimal state for brief moments, but in typical operations the control is not optimal. The control of the standalone devices is often based on one directional power flow, and thus, standalone control may not effectively handle high penetration of DG with reversed power flow. Some of the existing standalone VVC approaches are described in the following paragraphs.

An early digital control technique for local static voltage regulators (SVRs) is presented in [16]. The basic design philosophy and field trial experiences of a microprocessor based local voltage regulator control are presented. It is proposed that an ideal voltage regulator control should have data-gathering and communication capabilities [16]. The paper also presents detailed solution for the hardware and the software necessary for the control action. It shows the microprocessor sampling and RMS calculations also the steps the software takes to determine whether to it needs to raise or lower the SVR tap-position. The method takes in account reverse power flow where the control operations for the Tap-positions are ceased until the power flow resumes to its original direction [16]. When this paper was published these controllers had been in service for several years and proven capable for local control. Drawbacks to the presented method are the controllers did not communicate with each other and the control was not optimal. The local microprocessor controlled SVR controllers and have been developed more since this paper was published, but the overall idea in them still remains the same.

Compensator circuit design for SVRs is described and demonstrated in [17]. The compensator circuit measures the regulator output current and output voltage constantly

then delivers that information to the voltage regulator tap-changer. The purpose for the compensator circuit is to allow for a local control of the voltage-regulator device. The compensator circuit will change the LTC tap position based on the information from the sensors. The desired output voltage level is set to the specified voltage setting and the compensator circuit will adjust the tap position to keep the voltage constant at the specified level. There is a bandwidth associated with the tap settings, as the tap position is an integer value. The bandwidth defines variance of the regulation point voltage centered on the desired voltage level [17]. The method is effective for controlling the local voltages, by keeping the secondary voltage of the SVR at a constant value, but in reality the set point values are typically set conservatively far from the optimal operating point.

Power factor correction is a well-known technique to reduce the net reactive power load in distribution systems by adding shunt capacitors. In [18] a technique for automated local power factor compensation is presented. The method uses a VAR-metric relay to control closing and releasing the capacitor banks. The node injection current and the node voltage are measured with current and potential transformers at the node where the capacitor bank is located. The power factor and the reactive power requirement are calculated with the information provided by the sensors. The relay regulates the compensator device actions based on its settings [18]. This technique is powerful for local power factor control, but it does not provide control for the overall reactive power of the power system. The technique might be optimal at the local node, but does not provide optimal control for the whole distribution system. Often used by industrial

customers the power factor correction technique is to reduce their apparent power load consumption [18].

A micro-controller based power factor control device is presented in [19]. Both hardware and software design of the control device are described. The hardware architecture includes the relays, capacitor banks, microcontroller, and signal conditioning units. Much like in [18], the current and voltage are measured and those signals are conditioned for the microcontroller. The microchip makes the decision whether to turn the capacitor banks on or off based on the reactive power demand and power factor. The control signals are sent from the microprocessor to the relays that control the capacitor banks. The capacitor bank control is local and will not achieve optimal state for the entire system. With the local approach two capacitor banks may perform counter acting control decisions in certain feeder loading cases.

The aforementioned techniques control the local voltages and the local power factors in a distribution system. They lack knowledge about the overall system and are limited in terms the integration of the DG. They also do not converge to the optimal control solutions for the entire distribution system. These systems, however, are easy and inexpensive to implement and in many cases they improve the power quality and efficiency.

2.2. Rule based VVC

In a rule based VVC, the distribution control devices are typically monitored and controlled by the distribution utility's Supervisory Control and Data Acquisition (SCADA) system. In a typical rule based approach, SCADA handles the voltage and reactive power decisions by separate processes. Reactive power control rules are set to

control the capacitor banks and voltage control rules are set to reduce system demand through CVR. The control operations are based on a stored set of predetermined rules specific for the distribution feeder. Turning on a capacitor bank when the power factor goes below 0.9 or dropping a tap on a voltage controller if the end of the line voltage goes above 116V are examples of simple SCADA control rules. In the rule based VVC systems the system data is brought back to SCADA through substation remote terminal units (RTUs). RTUs are utilized to handle the device monitoring and control. The VVC processor is built in the distribution SCADA and has a set of rules for the control actions, the processed control actions are sent back to the devices via the same RTUs. The SCADA based VVC systems require a two-way communication channel between the field devices and the distribution control center.

The SCADA based VVC is more complicated than the standalone control approach. Moreover, SCADA based VVC techniques have several advantages over the standalone VVC systems. The SCADA based VVC systems are capable of self-monitoring due to the extensive measurement network. The self-monitoring feature the SCADA based VVC can handle disturbances and possible system emergencies far more efficiently than the standalone VVC approaches. Drawbacks to the SCADA based VVC approaches exist as well: these methods are more complicated than the standalone approaches and require widespread field communications. The SCADA based VVC is generally not able easily to adapt to the changes in feeds configurations, due to the fact that the control rules have been determined in advance. Although, the overall efficiency is often improved compared to the standalone approaches, the rule based VVC typically does not yield to the optimal control solutions. Often rule based approaches have been

used for distribution systems with a single directional power flow. For this reason these approaches may not adapt well for systems with high DG penetration and bi-directional power flow.

Operation and advantages of an early SCADA based reactive power control, called CAPCON, developed by Virginia Electric and Power Company are discussed in [20]. The proposed approach considers only the capacitor bank control. In this method the SCADA computer decides every 15 minutes whether or not each shunt capacitor bank needs to be turned on or off. The service voltage and power factor are improve with the coordinated reactive power control approach. The reactive power and voltage limits have been predetermined for the CAPCON algorithm and control actions within the 15 minute operational interval will only be taken if the preset limits have been exceeded. The system allows for overrides to certain network actions from the distribution SCADA operators. The CAPCON has significant benefits in both distribution loss reduction and fuel cost reduction of the generation [20]. The CAPCON system also allows for global feeder wide real time system control. One of the flaws of the proposed system is that the decision rules have been predetermined for the system. Due to the predetermined rule set the CAPCON system does not adapt easily to the changes in the distribution system. Also the CAPCON system only considers the capacitor bank control without the considering the voltage regulator actions. The system efficiency can be further improved with coordinated control of both voltage regulators and capacitor banks.

The control method proposed in [21] is geared to improve the performance of standalone VVC by utilizing the distribution SCADA in the control. The control of the voltage regulators utilizes the voltage drop characteristics of the feeder. The control of

the capacitor banks utilizes the local measurements of power factor for the reactive power control in the substation. The capacitor control problem and the voltage control problem are decoupled from each other. However, both sub-problems communicate with each other through the high-level VVC implemented to distribution SCADA system [21]. The system has a set of pre-determined rules that it follows for both control sub-problems. The system receives information about the distribution system state through the distribution SCADA. The case study presented in [21], displays the effectiveness of the proposed method; the system demand is shown to decrease over the standalone approaches. The rule based solution approach however is not able to achieve the optimal control of the distribution system.

An expert system for VVC of distribution systems is proposed in [22]. An expert system is a computer program designed to behave like a human distribution expert. The system has an extensive knowledge base and is capable of solving problems that require using the information in the knowledge base [22]. The proposed expert system has three components: knowledge base where system knowledge is stored, interference engine where the decisions are made, and the user interface that is connected to the distribution SCADA. The rule base stores network related data including voltage limits, control actions, reactive power limits, etc. The inference engine is used to determine the control decision from the information and control rules stored in the knowledge base. The method uses a sensitivity tree method for the interference base that will be able to react on voltages that exceed their predetermined bounds [22]. The sensitivity tree method can be effective in the development of an expert system used to control a large distribution system. According to [22], the system nonlinearity needs to be fairly low for this type of

expert system to be utilized in the distribution system VVC. The proposed expert system handles both voltage regulator and capacitor control together, but is unable to provide optimal solution in most cases.

The expert system presented in [23] and [24] combines technical and theoretical expertise with human expertise to build the knowledge base for the expert system. While keeping the voltage levels of the system within the allowable range, the expert system provides the values of the reactive power levels to be injected to the distribution system in order to reduce the system peak power and energy loss. The decision engine uses various determination processes to calculate the voltage profile of a feeder and to determine the distribution system control actions. In distribution control model the expert system provides decision of which capacitor is switched on and for how long according to net dollars saving, voltage profile of the system buses, and maintenance and repair cycle of the capacitor [23]. The main advantage of the proposed expert system is the ability to interact with human operator. The proposed system can accept the human expert's recommendations and perform the output accordingly. The decision making process can be overridden by the network controller at any stage and it will incorporate changes in the system configuration.

The expert system can be interfaced with the distribution SCADA and human operator via its input and output interface. A case study of an expert system has been presented in [24]. The case study shows that the proposed expert system has major financial benefits for a distribution network. The expert system relies heavily on historic load demand data for knowledge and decision base [24]. Therefore, utilities that do not have extensive demand history might not benefit from the proposed system as much as

the utilities with extensive demand history. The expert system seems to provide a good control solution for the network problem; it appears that the computational time associated with the approach is very reasonable for the distribution feeders.

Another approach for development of an expert system for an utility voltage correction is studied in [25]. The approach consists of controlling shunt reactive power compensation and transformer tap positions. The proposed system is designed to help the system operator to make the control decision to minimize system loss and reduce number of control actions. When the paper was published the system had been implemented to six substations in a utility distribution system. The expert system draws real time data from the SCADA and uses it along with the feeder information stored in the knowledge base to make control decisions. The control decisions are then fed back to the power system via the SCADA communication system [25]. The decision engine on the expert system bases its control actions on the sensitivity information in the knowledge base. The expert system inputs from SCADA include the operation controls; voltages and currents at each bus; and loads at each bus. The outputs of the proposed system include the suggested control actions. In order to achieve optimality with the expert system the rules of the system have to be predetermined so well that optimality can be reached. If the rules are not perfect, the optimality is not likely. The system is capable of keeping the voltages within the limits and controlling reactive power, but optimality is likely not achieved.

Some existing techniques for rule based VVC were introduced in this section. The techniques include straightforward rules such as voltage and power factor limits and more involved rules introduced by the expert systems. Some of the studied rule based approaches use SCADA provided information about the system as the main triggers for

the control actions, whereas the other studied methods rely more heavily on historic load demand data. Rule based VVC provides significant advantages over the standalone VVC. These advantages include capability to block counter acting control actions and keeping the voltage level within the specified limits at all parts of the system. The optimal operating conditions are still unlikely with most of these techniques. The rule based systems are generally designed for single directional power flow that restricts the inclusion of large quantities of DG into these systems. Some of the more advanced expert systems, however, do have the knowledge and decision bases to take large DG quantities in account.

2.3. Analytical VVC

The goal of the analytical VVC is to model the VVC as a mathematical optimization problem. The goal of the formulation is to develop and to execute a coordinated optimal switching plan for all control devices in distribution feeder. The control is performed to achieve minimized value for the system objective function. The objective functions differ based on the utility and its needs. Most objective functions are geared to minimize the energy consumption and/or system loss. The voltages are required to be kept within the ANSI specified operational voltage levels. The installed distribution analytical and distribution model based VVC approaches often use the distribution SCADA along with the Distribution Management System (DMS) to determine the optimal control actions. Typically, these systems can estimate the state of the distribution system based on the data from the SCADA and the distribution network model. An optimization solver is then used to determine the optimal control settings for the

distribution devices. With the optimal control solutions determined the control is sent to the distribution devices in order to be implemented in the feeder.

The advantages of analytical VVC over the standalone and rule based VVC approached include: the capability to produce an “optimal solution”, flexibility to operate under varying objectives, and ability to handle complex feeder arrangements. The optimal or near optimal solution may only be achieved if the system is modeled accurately. The analytical VVC approaches may not be limited to one-directional power flow, and thus, can be suitable for feeders with high penetration of DG. With this said these systems are not perfect. Implementation of analytical VVC system comes often with high implementation costs. Regardless of that, the coordinated and centralized VVC is one of the most desirable functions within the distribution automation (DA) and DMS [26]. Analytical solutions are the basis for typical DMS based control. Generally the problem of capacitor banks and voltage regulators is very complex and difficult to solve since it involves, integer, binary, and complex numbers; and has both linear and non-linear equations.

A discrete optimization approach for coordination of switched capacitor banks and tap-changing transformers is presented in [27]. It is noted that the combinatorial problem involving capacitor and voltage regulator positions becomes extremely computationally intensive to solve. The analytical objective based solution method will minimize the loss, include voltage constraints, and consider combinatorial aspects of discrete control formulation applicable to distribution systems. In the proposed method the coordination problem is approximated by a constrained discrete quadratic optimization using the results from the corresponding unconstrained continuous problem

[27]. The objective function the problem uses a weighted sum of power consumption, voltage violations, and device tap-changes. The distribution system loss is approximated in [27]. The error present in approximations has also been studied in [27]: the approximate formula for loss is quite accurate and conservative in the sense that the estimated losses are slightly larger than the actual losses. The algorithms are efficient for large systems in the sense that their run and test results confirmed the theoretical predictions of the paper. The algorithm presented is effective for VVC. The results do not typically yield to the optimal solution in real life systems because approximations were made in the optimization. Overall the analytical optimization algorithm in [27] seems to have outperformed most of its predecessor in terms of accuracy and computational time.

Dynamic programming is another analytical approach studied for VVC. A dynamic programming algorithm for the distribution system VVC is presented in [28]. To reach the optimal dispatch the proposed method uses load forecasts to estimate the real and reactive power loads for a given time. The load forecasts are imported to a mathematical model of a system to ensure that the voltage limits will not be violated when VVC is performed. The system model is included to reduce computational burden for the dynamic programming approach [28]. The dynamic programming approach divides the complicated optimization problem into less complicated optimization problems. Dynamic programming creates state diagram and search paths for the each possible setting of LTCs and capacitor banks. The proposed approach then reduces the number of search paths and the number of possible configurations to the few most likely configurations. With the state reduction, the proposed method can find near optimal

solution with reduced computational effort [28]. The proposed method has been implemented to a utility distribution system with promising results. The method proposed has shown that it can produce near optimal solution; yet, the method still relies heavily on load forecasts and produces typically a near optimal solution. The actual optimal solution will require significantly more computational power.

Oriented discrete coordinate descent method based VVC approach is studied in [29]. In this method, all partial derivatives of an objective function with respect to discrete control variables are calculated for initial conditions. Then the system is moved in the direction of the largest derivative to the next point. In the proposed method the variable with the largest partial derivative is considered as the first search direction. This process is repeated until no further minimization of the objective function can be achieved [29]. The proposed approach uses so called “soft constraints”. Soft constraints are not imposed as constraints for the optimization, but rather as a penalty factor for the cost function. The proposed algorithm is fairly time consuming since it needs to calculate power flow for all of the optimization steps. An efficient power flow solver is also essential for accurate control results. The test results of the proposed algorithm indicate satisfactory computational speed for on-line operations in a small system [29]. Accurate network model and fast power flow calculations are necessary for the success of this method. Also the method may find a local minimums rather than the global minimum that is desired. The method may become very time consuming with a larger system.

A study of the VVC implementation and its effects to a distribution system are studied in [30]. The algorithm described in [29] is used in this study. The main components of the algorithm are: computation of the real time power flow solution and

the initial objective function, then applying the optimization technique. The optimization method calculates the optimal combination of capacitor bank states and transformer tap changer position with respect to the objective function. The algorithm is integrated to SCADA and DMS that provide the real time network data including power consumption and switch positions. The DMS based VVC was installed to a utility distribution feeder and the economics of the VVC were studied. The test results showed an immediate decrease in injected power of 1.4% to 1.6% in a utility distribution system. The experimentally derived values are dependent on many factors such as customer load patterns, distribution system characteristics, etc. However, the test results show trends in the desired direction.

Reference [31] introduces voltage and VAR optimization (VVO) system that is based on analytical computation. The presented system has an US patent [32] and is commercially available for the distribution utilities with the ABB DMS. The VVO system combines advanced optimization techniques with accurate modeling of distribution systems. It can handle various different types of system including: single and multi-phase, and delta and wye connected. The application can optimize distribution systems effectively with online application speeds [32]. In this approach the VVO problem is formulated as sequence of VAR only optimization and voltage regulator optimization problems. The VAR problem is formulated as mixed integer quadratic programming (MIQP) problem and the voltage optimization as a sequence of linear programming (LP) problems [31]. The VVO system also has a detailed model of each of the possible system components such as transformers, loads, and power lines. The VVO

program is implemented to the DMS. From the system graphic user interface the system operator can initiate the VVO along with other system operations.

Some of the analytical solutions to the VVC problem have been introduced in this section. These methods use analytical tools such as partial derivatives, DP, and LP to solve the complex mixed integer programming (MIP) problem. These methods provide significant advantages over the two VVC approaches discussed in previous sections. Including optimal or near optimal solution with respect to the objective functions. These approaches are not perfect: they make assumptions, linearize the problem, decouple the problem, find local minimums, are highly dependent on accurate network model, and take long time to compute. Analytical approaches, however, can be very efficient for optimal control of a distribution system, thus, finding a new analytical approach is a major task of the research presented in this dissertation.

2.4. Artificial intelligence based VVC

Artificial intelligence (AI) provides alternatives to overcome some of the limitations of the analytical methods. The artificial intelligence algorithms can shorten the VVC computational times and make the approaches more suitable for real time applications. Reduced computational times can yield to more efficient operation of the physical VVC control devices. Some of the AI techniques that can be applied to the distribution system VVC include artificial neural networks (ANNs), fuzzy techniques, hybrid systems, and genetic algorithm (GA) approaches [33].

An ANN based approach for VVC is presented in [34]. The goal of the ANN is to reach a preliminary dispatch schedule for capacitor banks and LTCs. The inputs of the proposed ANN include the real and reactive power of the substation transformer, bus

voltages around the system, whereas the outputs are the capacitor statuses, and LTC tap positions [34]. The ANN is also combined with a fuzzy DP method that determines the final dispatch from the preliminary values from the proposed ANN solution. The ANN is trained to produce optimal setting for the VVC devices based on the calculated optimal conditions under the network model. The preliminary results from ANN can result to several preliminary states for the optimal control; therefore, a Fuzzy DP solution is introduced to reach the final dispatch schedule [34]. The research concludes that the method proposed can yield into accurate control actions for capacitor banks and LTCs while keeping the computational burden at very low stage during the operation [34]. The proposed method can yield to good solutions in with online control applications. Sufficient training is necessary for the operation of the proposed method. Without adequate training some of the conditions may result in control actions far from the optimal control schedule.

An interacting set of fuzzy Mamdani controllers for distribution VVC is introduced in [35]. A complex rule base is proposed to interact with a Newton-Raphson power flow solver in iterative steps until the control is determined. The fuzzy system consists of a controller for each distribution control device. Each fuzzy block reacts to the voltage and power flow violations and determines a device status accordingly. The controller is triggered from the device status, voltage violations, efficiency, etc. Set of new device statuses is tested with the power flow solver and the solution is then re-examined with fuzzy controllers to produce an improved control settings. The steps form a continuous loop until control settings converge, or if inconclusive, until a certain number iterations have been performed [35]. The proposed method is validated with a

utility distribution system and has shown promise to produce similar control actions more than 15 times faster than simulated annealing based methods [35]. The main purpose for this controller is to stay within the voltage and current limits of the system; the optimal solution is not the top priority of the control approach. Optimality can be reached at times, but in many cases, the controller produces a coordinated device dispatch that is within the acceptable boundaries and fails to reach the optimal solution for the entire system.

A fuzzy based method for distribution VVC is proposed in [36]. The proposed method is based on annealing and is employed for the fuzzy based problem. The method forms a function called “energy function” to determine the efficiency of the solution. The efficiency function is expressed as a sum of membership functions, voltage deviations, and control variables. An initial solution is first determined and then one of the control configurations is perturbed to create a neighbor solution. The proposed algorithm determines the benefit of the neighbor solution and iteratively new solutions for all the control parameters will be found. The method uses a power flow solver in parallel to confirm that there are no voltage violations with the solutions. Annealing method includes a randomly acceptable process to prevent the solution to be trapped to a local minimum, but find the global minimum. The technique proposed can reduce the time required for search of the optimal solution [36]. A study of the method in a utility substation and five feeders was also presented; the results concluded that the method was effective for finding an optimal solution for a power distribution system. However the computational time can be large for a large distribution system. For this reason, the proposed method may not be suitable for real-time applications.

A VVC system using a time-interval based approach is presented in [37]. The time interval based control strategy decomposes the load forecasts into several sequential load levels. A GA process is used to determine the load level portioning and dispatch scheduling for LTCs and switchable capacitor banks. The proposed strategy improves the voltage profile and reduces the distribution loss for an entire day across the entire distribution system. The number of switching operations of the control devices is also kept within the specified daily tolerance. The algorithm assumes that the number of load levels in a day is known. A GA is employed to determine the start and end times for each load level based on the load forecast. Another GA is then used for the VVC problem; the method forms a fitness function to find the minimum energy loss while keeping the voltage violations at a minimum. It also adopts a canonical GA to find the optimal solution for the fitness function [37]. After the calculation, the optimal solution is verified with a parallel load flow algorithm. The proposed algorithm is capable of improving the voltage profile and reducing loss, however the method relies heavily on accurate load forecasts for the distribution system. The method is also not a real time solution, and thus, does not respond changes in load automatically.

The authors of [38] propose an optimal distribution voltage control with DG utilizing a GA based approach. The GA is a learning algorithm that imitates the evolution of organisms. The controller limits the number of operation based on the GA. This expedites approximating the solution from the feasible area of a large scale optimization problem [38]. The proposed technique will be able to take distributed generation in account to find the optimal solution, a PV system is demonstrated in [38]. The proposed GA method requires a reliable communication infrastructure. Overall, GA Based methods

seem to provide solution for the optimization problem with a sufficient degree of accuracy.

Some existing AI based approaches for VVC were discussed in this section. The AI methods show promise of producing results comparable to the analytical solvers. The potential advantage of the AI based method can be the shorter processing times and less computational burden. The existing methods are not ideal, some take long time to process, require extensive communication architecture, are good for only off-line control, require extensive training, etc. The large scale deployment of AI based approaches is contingent about the utilities trust on the AI solutions; there is often a certain amount of uncertainty about the AI solution as they are often determined without human interaction.

3. MINLP BASED VVO FORMULATION

The purpose of voltage and VAR optimization (VVO) is to operate distribution system feeders at their most efficient operating conditions. In many cases, that means the minimized load demand drawn from the distribution substation. The traditional distribution feeder control devices include: capacitor banks, LTC transformers, and voltage regulators. Distributed energy resources such as PV and wind generation can also participate to the VVO with developments in DG. Inverter coupled DG, such as PV, can provide reactive power injection to the distribution feeder in addition to the real power it generates, as discussed for example in [39] [40] [41]. It is also possible to control the reactive power injection by the wind generation in addition to the real power generated.

As discussed in the previous chapter there are multiple methods for VVC and VVO that have been studied and implemented. The analytical approaches consider VVC as a mathematical programming problem. Some of the existing analytical techniques are discussed in previous section. Some other techniques include non-linear programming (NLP) with interior point algorithm with discretization penalties to limit the switch operations in distribution feeders [42] and mixed integer linear (MILP) programming with distributed generation participating to the VVO [43].

Distribution system VVO with DG can be formulated as a mixed integer non-linear programming (MINLP) problem. The problem is constrained by the feeder power flows, line current and node voltage bounds, distribution device control, and the limitations of the DG. This section contains the general discussion of formulating a distribution system VVO problem as a MINLP problem. The section also discusses the solution approach taken for the VVO as MINLP problem.

The approach to formulate and solve a distribution system VVO with DG as a MINLP problem has significant advantages over previously studied algorithms. The MINLP approach adds value to distribution VVO as it reduces the need for linearization in problem formulation and the need to transform continuous values into discrete values. The presented MINLP based VVO approach solves the optimization problem for single and three-phase distribution feeder, works well with different load types, incorporates integer decisions, allows for two directional power flow, and accepts non-linear load, current, and control equations. The simulations of test cases indicate the MINLP based formulation and solution method are promising for yielding the optimal control solutions effectively. The work presented in this section is based on the techniques and work further discussed in [13].

3.1. General MINLP problem

Mixed integer non-linear programming (MINLP) combines the combinatorial nature of mixed integer programming (MIP) and difficulties of non-linear programming (NLP). Both MIP and NLP are complex problems to solve and are NP-hard problems by themselves [44]. Solving MINLP problems is thus very difficult. The general MINLP formulation is presented as follows:

$$mininmize\ F(x)$$

$$Constrained\ by:$$

$$Ax \leq b$$

$$A_{eq}x = b_{eq}$$

$$l_b \leq x \leq u_b$$

$$C(x) \leq d$$

$$C_{eq}(x) = d_{eq}$$

$$x_i \in Z$$

where *F(x)* is the objective function to be minimized, *A* and *b* define linear inequality constraints, A_{eq} and b_{eq} define linear equality constraints, l_b and u_b are the bounds that constrain *x*, *C(x)* and *d* define non-linear inequality constraints, $C_{eq}(x)$ and d_{eq} define the non-linear equality constraints, *Z* is the integer set, and x_i is the subset of *x* restricted to be integers. The solution approach is implemented in this section for the MINLP model.

3.2. MINLP solution approach

Direct formulation and solution of VVO as a MINLP problem has been difficult due to the fact that commercial optimization solvers cannot generally solve MINLP problems. A direct MINLP formulation of VVO can be presented and solved with advances in open-source MINLP solvers. The MINLP approach provides value to VVO since it reduces the need for linearization in problem formulation and the need to transform continuous values into discrete values. This chapter presents a new formulation method for VVO problem with DG as a direct MINLP problem. The presented method is also discussed in [13].

Distribution system VVO is formulated as an MINLP problem. Commercial optimization solvers, such as IBM ILOG CPLEX, are known to be unable to solve MINLP problems. However, recently there has been great academic interest in new MINLP solvers. Basic open-source mixed integer (BONMIN) solver is an open-source state-of-the-art optimization solver developed for solving general MINLP problems [45]. BONMIN has several optimization algorithms suitable for MINLP problems including branch-bound, outer approximation (OA), Quesada Grossman branch-cut, and hybrid OA

based branch-cut. OPTI Toolbox is a third-party toolbox developed to interface open-source optimization solvers with Matlab [46]. The solvers included in the OPTI Toolbox include the BONMIN optimization solver. The presented solution approach in this section utilizes the OPTI Toolbox to solve the distribution VVO as an MINLP problem in Matlab and to solve it with BONMIN.

In the studies performed for the BONMIN optimization algorithms the OA algorithm showed the best performance for fast and accurate convergence for distribution VVO problem. It was noted in [45] that it is not uncommon for one algorithm to outperform the others solution algorithms within the solver. The general idea of the OA algorithm is to relax the MINLP problem into MILP and NLP sub-problems and iteratively solve these problems until the optimal solution is reached. The OA algorithm used in BONMIN code is described in detail in [47], [48].

3.3. Optimization objective function

The objective function considered in the proposed approach is to minimize the real power drawn from the substation. The objective function is constrained by node voltage and branch current limits, feeder power flow, and other physical limitations of the distribution feeder. The objective function, the real power drawn from the substation, is mathematically stated as follows:

$$F = real(\boldsymbol{V_s} \boldsymbol{I_s}^*) \tag{3.1}$$

where F represents the objective function to be minimized, $\boldsymbol{V_s}$ is the vector containing three-phase source voltages for the system, $\boldsymbol{I_s}$ is a vector containing the three-phase currents drawn from the source, $*$ represents the conjugate of the complex value, and $real()$ represents the real part of the complex value. In order to be used with the

BONMIN optimization solver (3.1) has to be described with its Cartesian representations of complex node voltages and currents. This is necessary as the optimization solver is unable to handle complex representations. The decoupled Cartesian form of (3.1) can be mathematically written as:

$$F = \sum_{g \epsilon p} \sum_{k \in B_r} (V_s^x(g) I_{sk}^x(g) + V_s^y(g) I_{sk}^y(g)) \quad (3.2)$$

where B_r is the set of branches connected to the substation, , $I_{sk}^x(g)$ and $I_{sk}^y(g)$ are the Cartesian presentations of g-phase current in branch k, $V_s^x(g)$, $V_s^y(g)$ are Cartesian representations of source voltage of phase g at substation, and p is the set of phases that the branch currents are drawn from.

3.4. Distribution component models

Distribution system components models used for describing the distribution system VVC as a MINLP problem are presented in this section. The component models are key elements for accurate formulation of the VVC problem to match the system model with the physical phenomenon in distribution feeders. Some of the component models are described in [13], but a more comprehensive listing of different distribution components for the presented MINLP formulation is presented in this section.

3.4.1. Distribution lines

The distribution lines are modeled with the exact line segment model presented in [8]. The exact model can be used to represent single-phase, two-phase, and three-phase distribution lines. As the basis for the modeling the three-phase exact line segment model, presented in, will be used. To represent single-phase and two-phase lines some rows and columns of the impedance and admittance matrices of the three-phase line model are set to zero. The distribution lines are modeled as three-phase Π-equivalent circuits, the series

line impedance is modeled between the end of the line nodes and the line capacitance is modeled to occur at both ends of the distribution line.

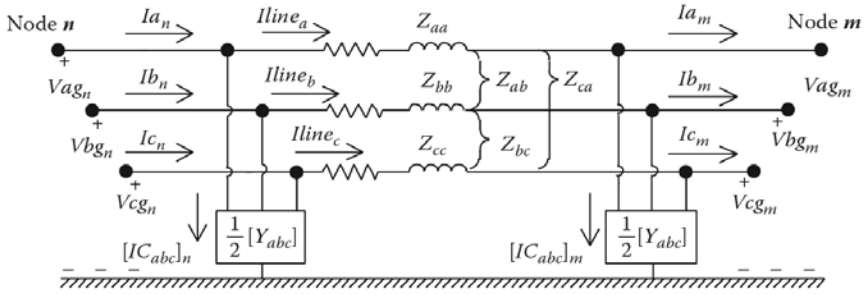

Figure 1: Distribution system three-phase Π-equivalent exact line segment model

The three phase line impedance matrix, $\boldsymbol{Z_{abc}}$, and shunt admittance matrix, $\boldsymbol{Y_{abc}}$, are presented by:

$$\boldsymbol{Z_{abc}} = \begin{bmatrix} Z_{aa} & Z_{ab} & Z_{ac} \\ Z_{ba} & Z_{bb} & Z_{bc} \\ Z_{ca} & Z_{cb} & Z_{cc} \end{bmatrix} \tag{3.3}$$

And

$$\boldsymbol{Y_{abc}} = \begin{bmatrix} Y_{aa} & Y_{ab} & Y_{ac} \\ Y_{ba} & Y_{bb} & Y_{bc} \\ Y_{ca} & Y_{cb} & Y_{cc} \end{bmatrix} \tag{3.4}$$

The line impedance, presented in (3.3) can be decoupled into the resistance and reactance matrices. The decoupling is necessary for the use of the distribution line model to be used in the optimization formulation as the optimization solvers are incapable of handling complex representations. The decoupled form of (3.3) is presented as follows:

$$\boldsymbol{Z_{abc}} = \begin{bmatrix} Z_{aa} & Z_{ab} & Z_{ac} \\ Z_{ba} & Z_{bb} & Z_{bc} \\ Z_{ca} & Z_{cb} & Z_{cc} \end{bmatrix} = \begin{bmatrix} R_{aa} & R_{ab} & R_{ac} \\ R_{ba} & R_{bb} & R_{bc} \\ R_{ca} & R_{cb} & R_{cc} \end{bmatrix} + j \begin{bmatrix} X_{aa} & X_{ab} & X_{ac} \\ X_{ba} & X_{bb} & X_{bc} \\ X_{ca} & X_{cb} & X_{cc} \end{bmatrix} \tag{3.5}$$

where R_{aa} for example is the self-resistance of phase A, and X_{ab} for example is the mutual reactance between phases A and B.

The shunt admittance model is assumed only to consist of the capacitive element of the line. For this reason, the resistive components of $\boldsymbol{Y_{abc}}$ matrix will have values of zero. As presented in [49] the mutual capacitances between the distribution lines are typically much smaller than the self-capacitance of the line. For this reason it is a common practice to model only the self-susceptance values and set the mutual susceptance values as zeros:

$$\boldsymbol{Y_{abc}} = \begin{bmatrix} Y_{aa} & Y_{ab} & Y_{ac} \\ Y_{ba} & Y_{bb} & Y_{bc} \\ Y_{ca} & Y_{cb} & Y_{cc} \end{bmatrix} \approx j \begin{bmatrix} B_{aa} & 0 & 0 \\ 0 & B_{bb} & 0 \\ 0 & 0 & B_{cc} \end{bmatrix} \tag{3.6}$$

where B_{aa} is the self-susceptance of phase A. The susceptance is defined as the imaginary part of the admittance and is measured in units of Siemens

The voltage and current equations for the distribution lines are determined from Figure 1. The current leaving the node *n*, $\boldsymbol{I_{abcn}}$, is the sum of current flowing into node *m*, $\boldsymbol{I_{abcm}}$, and the shunt currents due to the line capacitance occurring at both ends of the distribution line, $\boldsymbol{I_{Cabcn}}$ and $\boldsymbol{I_{Cabcm}}$.

$$\boldsymbol{I_{abcn}} = \boldsymbol{I_{abcm}} + \boldsymbol{I_{Cabcn}} + \boldsymbol{I_{Cabcm}} \tag{3.7}$$

The line current flowing through the series impedance, $\boldsymbol{I_{abcl}}$, is the summation of the current entering the node *m*, and shunt current occurring at node *m*:

$$\boldsymbol{I_{abcl}} = \boldsymbol{I_{abcm}} + \boldsymbol{I_{Cabcm}} \tag{3.8}$$

The voltage at node *n*, $\boldsymbol{V_{abcn}}$ is the sum of voltage at node *m*, $\boldsymbol{V_{abcm}}$, and the voltage drop across the distribution line. The voltage drop can be determined by multiplying the line impedance matrix, $\boldsymbol{Z_{abc}}$, by the line current found in equation (3.8).

$$\boldsymbol{V_{abcn}} = \boldsymbol{V_{abcm}} + \boldsymbol{Z_{abc}}\boldsymbol{I_{abcl}} \tag{3.9}$$

In order to be included into the optimization problem the voltage equations need to be decoupled into the Cartesian representations. In the Cartesian where $\boldsymbol{V_{abcn}}^{\boldsymbol{x}}$ and $\boldsymbol{V_{abcn}}^{\boldsymbol{y}}$ are for example the respectively the real and imaginary part of the complex representations of the node voltages formulated for use as linear constraints in the MINLP VVO problem formulation:

$$\boldsymbol{V_{abcn}}^{\boldsymbol{x}} - \boldsymbol{V_{abcm}}^{\boldsymbol{x}} - \boldsymbol{R_{abc}}\boldsymbol{I_{abcl}}^{\boldsymbol{x}} + \boldsymbol{X_{abc}}\boldsymbol{I_{abcl}}^{\boldsymbol{y}} = \mathbf{0} \tag{3.10}$$

and

$$\boldsymbol{V_{abcn}}^{\boldsymbol{y}} - \boldsymbol{V_{abcm}}^{\boldsymbol{y}} - \boldsymbol{X_{abc}}\boldsymbol{I_{abcl}}^{\boldsymbol{x}} - \boldsymbol{R_{abc}}\boldsymbol{I_{abcl}}^{\boldsymbol{y}} = \mathbf{0} \tag{3.11}$$

where the impedance matrix is decoupled to the resistance and reactance matrices, and the line current to its Cartesian representations.

The shunt current injection caused by the line capacitance is modeled to occur at both ends of the line segment. As previously discussed the susceptance imaginary component of the shunt admittance is typically only considered. The current caused by the shunt admittance at node *m* can be written as:

$$\boldsymbol{I_{Cabcm}} = \frac{\mathbf{1}}{\mathbf{2}}\boldsymbol{Y_{abc}}\boldsymbol{V_{abcm}} = j\frac{\mathbf{1}}{\mathbf{2}}\boldsymbol{B_{abc}}(\boldsymbol{V_{abcm}}^{\boldsymbol{x}} + j\boldsymbol{V_{abcm}}^{\boldsymbol{y}}) \tag{3.12}$$

where $\boldsymbol{B_{abc}}$ is the matrix containing the self-susceptances of the distribution line as described by (3.6). The shunt current equations can be decoupled Cartesian representations form the complex from and the Cartesian representations will be used as the linear constraints to describe shut current injection:

$$\boldsymbol{I_{Cabcm}}^{\boldsymbol{x}} + \frac{\mathbf{1}}{\mathbf{2}}\boldsymbol{B_{abcm}}\boldsymbol{V_{abcm}}^{\boldsymbol{y}} = \mathbf{0} \tag{3.13}$$

and

$$\boldsymbol{I_{Cabcm}}^{\boldsymbol{y}} - \frac{\mathbf{1}}{\mathbf{2}}\boldsymbol{B_{abc}}\boldsymbol{V_{abcm}}^{\boldsymbol{x}} = \mathbf{0} \tag{3.14}$$

where the ${I_{Cabcm}}^{x}$ and ${I_{Cabcm}}^{y}$ are the real and imaginary part of the complex representation of the shunt current at node *m*. Because of the capacitive component the susceptance values will be negative and thus cause a current injection to the distribution line.

3.4.2. Transformer

Distribution transformers are found all across the distribution feeders: from the substation to the customer connection. The two winding transformer approximate equivalent circuit is used to model distribution transformers. The primary side impedance is referred to the secondary side of the transformer without introducing a significant error [8], [50]. The two-winding approximate transformer equivalent is shown in Figure 2.

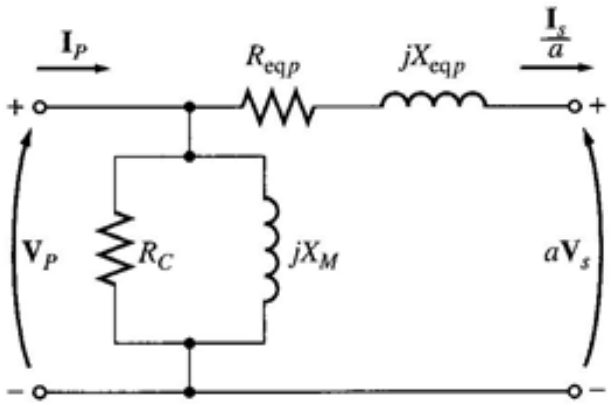

Figure 2: Two-winding approximate transformer model

For a two-winding approximate transformer model, the secondary voltage can be written as the function of primary voltage, turns ratio, and the equivalent secondary side total approximate impedance:

$$V_s = \frac{V_p}{a} - Z_{eq} I_s \tag{3.15}$$

where V_s is the secondary side voltage, $V_p$is the primary side voltage, a is the transformer turns ratio, Z_{eq} is the total impedance referred to the transformer secondary side, and I_s is

the transformer secondary side current. In order to be used as constraints of the VVO MINLP problem, (3.15) has to be decoupled into its Cartesian representations:

$$V_s^x - \frac{V_p^x}{a} + R_{eq} I_s^x - X_{eq} I_s^y = 0 \tag{3.16}$$

and

$$V_s^y - \frac{V_p^y}{a} + X_{eq} I_s^x + R_{eq} I_s^y = 0 \tag{3.17}$$

where R_{eq} and X_{eq} are the transformer equivalent resistance and reactance; V_p^x, V_p^y, V_s^x, and V_s^y are the transformer primary side and secondary side voltages; and I_s^x and I_s^y are the transformer secondary currents.

The current relationships in a two winding transformers can be found with the same approach. The primary side current is the summation of transformer secondary side current and the current in the transformer excitation branch, as follows:

$$I_p = \frac{I_s}{a} + I_{ex} \tag{3.18}$$

where I_p is the primary side current, I_{ex} is the current in the excitation branch, and $I_s$is the secondary side current.

The current equation in (3.18) has to be decoupled in order to be used as constraints in MINLP VVO formulation. In decoupled form (3.18) can be written as follows:

$$I_p^x - \frac{I_s^x}{a} - I_{ex}^x = 0 \tag{3.19}$$

and

$$I_p^y - \frac{I_s^y}{a} - I_{ex}^y = 0 \tag{3.20}$$

where I_{ex}^x and I_{ex}^y are Cartesian presentations of excitation branch currents of the transformer.

The two winding transformer model can be extended to three-phase distribution transformers. The three-phase distribution transformers can be connected with delta-wye, wye-delta, wye-wye, delta-delta, and open delta-open wye connections. The voltage equations in three-phase can be presented for all transformer connections as follows:

$$\boldsymbol{V_{abcs}^{x} - A^{-1}V_{abcp}^{x} + R_{eq}I_{s}^{x} - X_{eq}I_{s}^{y} = 0} \quad (3.21)$$

and

$$\boldsymbol{V_{abcs}^{y} - A^{-1}V_{abcp}^{y} + X_{eq}I_{s}^{x} + R_{eq}I_{s}^{y} = 0} \quad (3.22)$$

where $\boldsymbol{V_{abcs}^{x}}$, $\boldsymbol{V_{abcs}^{y}}$, $\boldsymbol{V_{abcp}^{x}}$, and $\boldsymbol{V_{abcp}^{y}}$ are the Cartesian representations of three-phase secondary and primary voltages of the transformer, $\boldsymbol{A}$ is the matrix of turns ratios, $\boldsymbol{R_{eq}}$ is the matrix of transformer total resistances**,** $\boldsymbol{X_{eq}}$ is the matrix of transformer total reactances, and $\boldsymbol{I_{s}^{x}}$ and $\boldsymbol{I_{s}^{y}}$ are the Cartesian representations of three-phase secondary currents of the transformer. The $\boldsymbol{A}$, $\boldsymbol{R_{eq}}$, and $\boldsymbol{X_{eq}}$ matrices are dependent on the transformer connections.

Similar to the voltage equations, the current equations can be represented in three phases as well:

$$\boldsymbol{I_{abcp}^{x} - A^{-1}I_{abcs}^{x} - I_{ex}^{x} = 0} \quad (3.23)$$

and

$$\boldsymbol{I_{abcp}^{y} - A^{-1}I_{abcs}^{y} - I_{ex}^{y} = 0} \quad (3.24)$$

where $\boldsymbol{I_{abcp}^{x}}$ and $\boldsymbol{I_{abcp}^{y}}$ are the Cartesian representations of three-phase primary side currents, $\boldsymbol{I_{abcs}^{x}}$ and $\boldsymbol{I_{abcs}^{y}}$ are the Cartesian representations of three-phase secondary side currents, and $\boldsymbol{I_{ex}^{x}}$ and $\boldsymbol{I_{ex}^{y}}$ are the Cartesian representations of three-phase excitation

branch currents of the transformer. All transformer voltage and current equations can be expressed as linear equality constraints in the VVO MINLP formulation.

3.4.3. Load tap-changing transformer and voltage regulator

Common devices for regulating the distribution system voltages are LTC transformers at the distribution substations and line voltage regulators along the distribution feeders. These devices are typically autotransformers that have variable turn ratios. The voltage regulation devices are capable of adjusting their secondary side voltages up or down from the primary side voltages by selecting turn ratios. The LTC mechanism allows the device to change the turn ratio in integer steps. The autotransformer can be visualized as a two winding transformer with a solid connection between the secondary and the primary side of the transformer. Two winding approximate transformer model is shown in Figure 2.

It is common that voltage regulators can adjust the voltage levels ±10% usually this is done in 32 discrete steps. Each step is equivalent to 0.75 V on a 120V voltage base. Typically the series impedance and the shunt admittance of voltage regulators are small; therefore, they can be neglected from the equations [8]. However, if that is not the case, it is possible to include the impedance and admittance into the voltage regulator equations.

The voltage and current relationships of a voltage regulator are described similar to the three-phase transformer equations in the decoupled form, as follows:

$$\boldsymbol{V}^{\boldsymbol{x}}_{\boldsymbol{abcs}} - \boldsymbol{A}^{-\mathbf{1}}\boldsymbol{V}^{\boldsymbol{x}}_{\boldsymbol{abcp}} = \mathbf{0} \tag{3.25}$$

$$\boldsymbol{V}^{\boldsymbol{y}}_{\boldsymbol{abcs}} - \boldsymbol{A}^{-\mathbf{1}}\boldsymbol{V}^{\boldsymbol{y}}_{\boldsymbol{abcp}} = \mathbf{0} \tag{3.26}$$

$$\boldsymbol{I}^{\boldsymbol{x}}_{\boldsymbol{abcp}} - \boldsymbol{A}^{-\mathbf{1}}\boldsymbol{I}^{\boldsymbol{x}}_{\boldsymbol{abcs}} = \mathbf{0} \tag{3.27}$$

and

$$\boldsymbol{I}^{\boldsymbol{y}}_{\boldsymbol{abcp}} - \boldsymbol{A}^{-\mathbf{1}}\boldsymbol{I}^{\boldsymbol{y}}_{\boldsymbol{abcs}} = \mathbf{0} \tag{3.28}$$

The entries of $\boldsymbol{A}$ matrix depend on the configuration of the voltage regulating devices. For example, for a common case without phase shifts, $\boldsymbol{A}$ matrix is a diagonal matrix described as:

$$\boldsymbol{A} = \begin{bmatrix} a_a & 0 & 0 \\ 0 & a_b & 0 \\ 0 & 0 & a_c \end{bmatrix} \tag{3.29}$$

where a_a, a_b, and a_c are the turn ratios for each three phases and for example a_a is defined as:

$$a_a = 1 + S_t T_{pa} \tag{3.30}$$

where S_t is the discrete per unit step size of a voltage regulator and T_{pa} is an integer tap-position decision for phase A.

There are voltage regulators with ganged tap-position control where the tap position for all three-phases will be the same. Un-ganged control of voltage regulators is the more common control. In un-ganged control all three phases of the voltage regulator may have different control decisions. The voltage regulator equations are non-linear equality constraints and are included in $C_{eq}(x)$ and d_{eq} constraints in the MINLP formulation.

3.4.4. Capacitor bank

The purpose of the capacitor banks is to provide reactive power support to the distribution system. The capacitor banks should be modeled as controllable shunt capacitances that can be turned on or off based on system needs. Shunt capacitor banks are modeled as negative constant impedance reactive power loads. The amount of reactive power provided by the capacitor banks is directly proportional to the square of

the capacitor bank voltage. The capacitor bank control can be implemented with binary variable or integer values. Figure 3, shows model of a three-phase capacitor bank. Similar to voltage regulating devices the capacitor bank control can be ganged or un-ganged controlled.

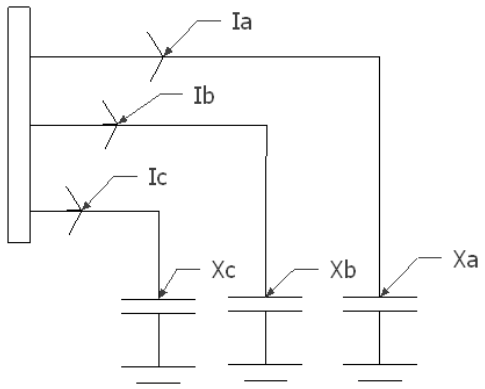

Figure 3: Shunt Three- Phase Capacitor Bank Model

The capacitor bank will not have real power output, but will have controllable reactive power output. A single phase real and reactive power injection by the capacitor bank is described as follows:

$$P_C = 0 \tag{3.31}$$

and

$$Q_C + Q_C^0 \left(\frac{|V_C|^2}{|V_C^0|^2}\right) C_d = Q_C + Q_C^0 \left(\frac{\left(\sqrt{(V_C{}^x)^2 + (V_C{}^y)^2}\right)^2}{|V_C^0|^2}\right) C_d = 0 \tag{3.32}$$

where C_d is the capacitor decision variable, V_C is the operating voltage at capacitor bank location, Q_C is the total controllable reactive injection power at capacitor location, P_C is the real power injection by the capacitor banks, and Q_C^0 and V_C^0 are the rated reactive power and voltage.

The current injection caused by the reactive power at the capacitor bank location is calculated from apparent power equation:

$$S_c = V_c I_c{}^* = \left(V_c^x + jV_c^y\right)\left(I_c^x - jI_c^y\right) \tag{3.33}$$

where S_c is the apparent power output of the capacitor bank, V_c is the capacitor bank operational voltage, I_c is the capacitor bank current injection, and * denotes the complex conjugate. The apparent power equation (3.33) is solved for the Cartesian component representations of the current injection:

$$I_c^x - \left(\frac{P_c V_c^x + Q_c V_c^y}{(V_c^x)^2 + (V_c^y)^2}\right) = 0 \tag{3.34}$$

and

$$I_c^y - \left(\frac{P_c V_c^y - Q_c V_c^x}{(V_c^x)^2 + (V_c^y)^2}\right) = 0 \tag{3.35}$$

where I_c^x and I_c^y are the Cartesian representations of the single-phase capacitor bank current injections, and V_c^x and V_c^y are the Cartesian representation of the capacitor voltages. By substituting (3.31) and (3.32) into (3.33) and (3.34) constraints are:

$$I_c^x + \left(Q_C^0 \left(\frac{C_d V_c^y}{|V_C^0|^2}\right)\right) = 0 \tag{3.36}$$

and

$$I_c^y - \left(Q_C^0 \left(\frac{C_d V_c^x}{|V_C^0|^2}\right)\right) = 0 \tag{3.37}$$

The current injections by capacitor banks are non-linear equality constraints and are included in $C_{eq}(x)$ and d_{eq}constraints in the MINLP formulation.

3.4.5. Distribution load

The distribution system loads are presented as combinations of constant impedance, current, and power loads. The presentation of loads as combinations of

constant impedance (Z), current (I), and power (P) is often referred to as ZIP load model in literature, e.g. in [51]. With that presentation, the load real and reactive power, P_m and Q_m, at node *m* are functions of node voltage as described by:

$$P_m = P_m^0 \left(a_l^P \left(\frac{|V_m|}{|V_m^0|} \right)^2 + b_l^P \left(\frac{|V_m|}{|V_m^0|} \right) + c_l^P \right) \tag{3.38}$$

and

$$Q_m = Q_m^0 \left(a_l^Q \left(\frac{|V_m|}{|V_m^0|} \right)^2 + b_l^Q \left(\frac{|V_m|}{|V_m^0|} \right) + c_l^Q \right) \tag{3.39}$$

where V_m^0, P_m^0, and Q_m^0 are rated node voltage, rated real and reactive power respectively; a_l^P, b_l^P, c_l^P, a_l^Q, b_l^Q, and c_l^Q represent the percentages of constant impedance, current, and power loads respectively; and V_m is the node operating voltage. P_m and Q_m are real and reactive load power at node *m* at the operating voltage. The sum of real power load percentages a_l^P, b_l^P, and c_l^P, as well as the sum of reactive power load percentages a_l^Q, b_l^Q, and c_l^Q have to equal unity.

The load demand equations are non-linear equality constraints are described as follows for MINLP problem formulation:

$$P_m - P_m^0 \left(a_l^P \left(\frac{(V_m^x)^2 + (V_m^y)^2}{|V_m^0|^2} \right) + b_l^P \left(\frac{\sqrt{(V_m^x)^2 + (V_m^y)^2}}{|V_m^0|} \right) + c_l^P \right) = 0 \tag{3.40}$$

$$Q_m - Q_m^0 \left(a_l^Q \left(\frac{(V_m^x)^2 + (V_m^y)^2}{|V_m^0|^2} \right) + b_l^Q \left(\frac{\sqrt{(V_m^x)^2 + (V_m^y)^2}}{|V_m^0|} \right) + c_l^Q \right) = 0 \tag{3.41}$$

where V_m^x and V_m^y are the Cartesian representations of the voltage at node *m*. The power constraints are included as non-linear equality constraints in $C_{eq}(x)$ and d_{eq}constraints in the MINLP formulation.

The load currents can be calculated from the load power demand and load voltages. At node *m* load current is calculated from Cartesian voltage and power representation. Load current equations are non-linear equality constraints and are included in $C_{eq}(x)$ and d_{eq} in the MINLP VVO formulation:

$$S_m = V_m I_m{}^* = \left(V_m^x + jV_m^y\right)\left(I_m^x - jI_m^y\right) \tag{3.42}$$

$$I_m^x - \left(\frac{P_m V_m^x + Q_m V_m^y}{(V_m^x)^2 + (V_m^y)^2}\right) = 0 \tag{3.43}$$

$$I_m^y - \left(\frac{P_m V_m^y - Q_m V_m^x}{(V_m^x)^2 + (V_m^y)^2}\right) = 0 \tag{3.44}$$

where I_m^x and I_m^y are the Cartesian representations of load currents at node *m*.

Three-phase distribution loads can be connected to either delta or wye, wye loads can be grounded or ungrounded. Delta loads are dependent on the phase to phase voltages and Wye loads are dependent on the phase to neutral voltages.

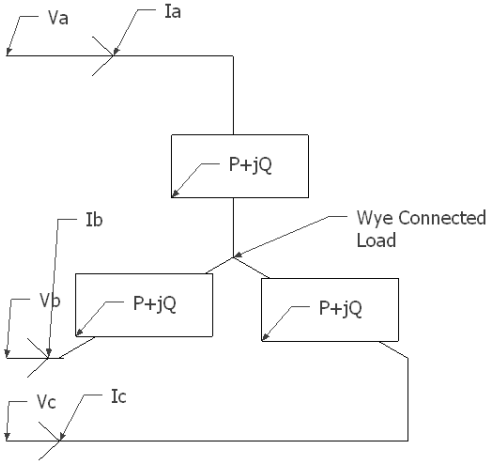

Figure 4: Wye connected load model

A simplified Wye connected load is shown in Figure 4. All the line currents go through the load component into a common neutral n terminal. In a Wye connected load

the total power is the summation of the all three phases of the load. The notation for the complex powers and voltages for all three phases are:

$$S_a = |S_a|\underline{/\theta_a} = P_a + jQ_a \text{ and } |V_a|\underline{/\delta_a} \quad (3.45)$$

$$S_b = |S_b|\underline{/\theta_b} = P_b + jQ_b \text{ and } |V_b|\underline{/\delta_b} \quad (3.46)$$

$$S_c = |S_c|\underline{/\theta_c} = P_c + jQ_c \text{ and } |V_c|\underline{/\delta_c} \quad (3.47)$$

where S_a, S_b, and S_c are per phase apparent power, P_a, P_b, and P_c are per phase real power, Q_a, Q_b, and Q_c are per phase apparent power, δ_a, δ_b, and δ_c are the line-to-neutral voltage angles, and θ_a, θ_b, and θ_c are per phase power factor angles. The Cartesian load current representations described in (3.41) and (3.42) are used to for three phase wye-connected loads.

A simple model of a Delta-connected load is shown in Figure 5. The loads are connected between the two phase and the currents through the load elements are combinations of the two line currents for the load component.

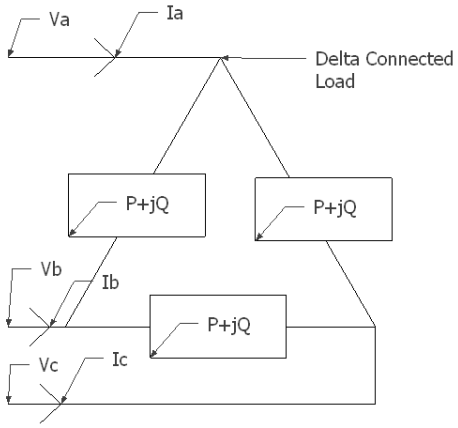

Figure 5: Delta connected load model

The notation for the specified complex powers and voltages are described by the following equations:

$$S_{ab} = |S_{ab}|\underline{/\theta_{ab}} = P_{ab} + jQ_{ab} \text{ and } |V_{ab}|\underline{/\delta_{ab}} \quad (3.48)$$

$$S_{bc} = |S_{bc}|\underline{/\theta_{bc}} = P_{bc} + jQ_{bc} \text{ and } |V_{bc}|\underline{/\delta_{bc}} \quad (3.49)$$

$$S_{ca} = |S_{ca}|\underline{/\theta_{ca}} = P_{ca} + jQ_{ca} \text{ and } |V_{ca}|\underline{/\delta_{ca}} \quad (3.50)$$

For delta connected loads a simple transform based on the Kirchhoff's current laws at the each node of a Delta connected load can be applied to the load currents in to determine line currents. In matrix form the equation is described as:

$$\begin{bmatrix} IL_a \\ IL_b \\ IL_c \end{bmatrix} = \begin{bmatrix} 1 & 0 & -1 \\ -1 & 1 & 0 \\ 0 & -1 & 1 \end{bmatrix} \cdot \begin{bmatrix} I_{ab} \\ I_{bc} \\ I_{ca} \end{bmatrix} \quad (3.51)$$

where IL_a, IL_b, and IL_c are the line currents I_{ab}, I_{bc}, and I_{ca} are the line-line delta connected load currents. The Cartesian load current representations described in (3.43) and (3.44) are also used to for three phase delta-connected loads.

Loads that utilize only one or two phases of the available three-phases of a power system are quite common. All of the load models, both Delta connected and Wye connected, can be extended for two-phase and single-phase loads. The load currents of the missing phases can be set to zero. The currents present in the loads are calculated by using the equation described on above sections.

3.4.6. Source/substation connection

The distribution source or substation connection is modeled as an infinite source node. An infinite source node means that the node voltages remains constant and no frequency change occurs regardless of changes in node loading [37]. The three-phase node voltages have the same magnitudes, but the phases are 120 degrees apart. The three-phase infinite source model is shown in Figure 6. The source may have a series

impedance or shunt impedance component, these can be modeled the same way as the distribution lines described in Section 3.4.1.

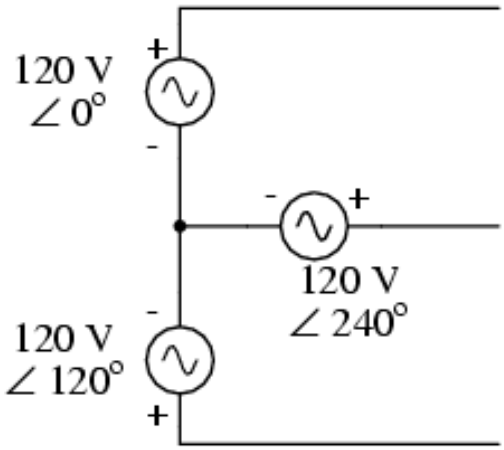

Figure 6: Infinite distribution three-phase source model

3.4.7. Distributed generation

Distributed generation (DG) can be utilized as a part of VVC strategy. Some DG devices can provide reactive power injection to the distribution system for voltage support and power factor correction. For example, photovoltaic (PV) generation, which is connected to the grid via a power electronic interface, can be used for reactive power support as a part of coordinated VVC. The DG units, capable for reactive power support, are constrained by their apparent power limits and real power outputs. The current injection into the distribution feeder depends on the voltage level at which the DG operates.

Inverter coupled DG, such as PV inverters, can source and sink reactive power based on the system need. Not only can PV inverters be used for constant reactive power support, but they can also serve as fast-acting static VAR controllers to limit voltage fluctuations caused by intermittent generation. The power output of a PV generator varies largely with the sunlight intensity and irradiance conditions. The output of the PV

inverter is not bounded by the generation, but rather by its apparent power limit. If apparent power limit is larger than the PV real power generation, then it is possible to control the reactive power supplied or consumed by the inverter [39] [52]. Figure 7 displays the four-quadrant operations of an inverter, a typical PV inverter will operate in the first or the fourth quadrant, where the inverter is supplying real power and consuming the reactive power. With advanced controls the inverter can vary its real power output in a very fast manner.

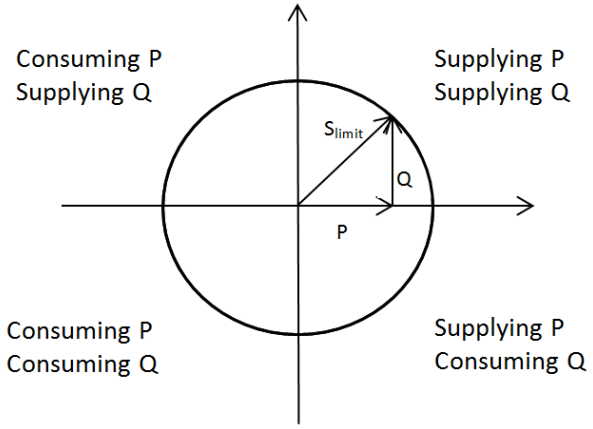

Figure 7: Four-quadrant inverter operations

The reactive power injection of a PV inverter is limited by its maximum apparent power, S_{max}, and real power generation, P_{DG}. Mathematically, the reactive power injection is bounded by:

$$-\sqrt{{S_{max}}^2 - {P_{DG}}^2} \leq Q_{DG} \leq \sqrt{{S_{max}}^2 - {P_{DG}}^2} \tag{3.52}$$

where Q_{DG} is the real power output of the DG device. The reactive power generation bounds of a DG source are included in the variable bounds l_b and u_b of the MINLP VVO of the distribution feeder.

The current injection of the DG depends on the real and reactive power injection by the device. The DG sources can be modeled as negative constant power distribution loads. The Cartesian representations of the current injection are described by:

$$I_{DG}^{x} + \left(\frac{P_{DG}V_{DG}^{x}+Q_{DG}V_{DG}^{y}}{(V_{DG}^{x})^{2}+(V_{DG}^{y})^{2}}\right) = 0 \tag{3.53}$$

And

$$I_{DG}^{y} + \left(\frac{P_{DG}V_{DG}^{y}-Q_{DG}V_{DG}^{x}}{(V_{DG}^{x})^{2}+(V_{DG}^{y})^{2}}\right) = 0 \tag{3.54}$$

where $I_{DG}^{x}$and I_{DG}^{y} are the Cartesian representations of the current injections caused by the distributed generation, V_{DG}^{x} and V_{DG}^{y} are the Cartesian representations of DG operational voltage.

It is often possible that the real power output of the DG can be limited from the maximum value for the external conditions. Limiting of the DG real power output is often referred to as curtailment. With curtailment the real power output of the DG unit at time *t*, $P_{DG}(t)$, is limited by the maximum real power output at that time. The reactive power output at time *t*, $Q_{DG}(t)$, is not bounded by the maximum real power output, but by the apparent power limit and the actual real power generation at time *t*. For the DG with the possibility of curtailment the bounds for real and reactive power generation are written mathematically as follows:

$$0 \leq P_{DG}(t) \leq P_{DGmax}(t) \tag{3.55}$$

and

$$-\sqrt{{S_{max}}^2 - P_{DG}(t)^2} \leq Q_{DG}(t) \leq \sqrt{{S_{max}}^2 - P_{DG}(t)^2} \tag{3.56}$$

where $P_{DGmax}(t)$ is the maximum real power output of the DG at time *t*. For the most economic use of the distribution feeder it is typically best to let the DG operate at its maximum real power output.

Distributed energy storage (DES) is defined as group of small energy storage units typically on the distribution side of the electric grid [53]. DES and DG with controllable real power output should be modeled similar to DG sources with possibility for curtailment. The key difference to the PV sources without curtailment is that the real power generation can now be controlled too and it should be considered as one of the system variables. The system variables are bounded by the l_b and u_b in the MINLP formulation, but since the $P_{DG}(t)$ in (3.56) is a variable $Q_{DG}(t)$ is not bound by the variable bounds but rather by the non-linear inequality constraints $C(x)$ and d. This model slightly complicates the VVO formulation.

3.5. Distribution power flow

The distribution power flow constraints are developed with the help of the ladder iterative power flow approach [8]. The idea of ladder iterative power flow approach is to perform a series of node voltage determining forward sweeps and use the calculated voltages for current determining backward sweeps until the solution converges. The approach has been shown to have fast convergence and good performance for balanced and unbalanced three-phase distribution feeders [8]. The power flow constraint used in the MINLP formulation is written the same way as the voltage and current equations of

the ladder iterative power flow approach. As the optimization solver cannot use complex numbers, all complex numbers are decoupled into their Cartesian forms.

3.5.1. Voltage equations

The node voltages are calculated with forward sweeps in the ladder iterative power process. The voltage equations (3.10) and (3.11) for distribution lines, (3.21) and (3.22) for transformers, and by (3.25) and (3.26) for voltage regulating devices are used. The initial currents are all set to zero and the tap positions of the voltage regulators are at their mid points. The first forward sweep produces a constant voltage profile with all currents initially set equal to zero.

3.5.2. Current equations

The distribution system currents are calculated with a backward voltage sweep, where the node voltages, determined by the forward sweep, are used to calculate the load current, (3.43) and (3.44), the currents caused by the DG real and reactive power injections, (3.53) and (3.54), the shunt currents produced by the line capacitances, (3.13) and (3.14), by the controllable discrete shunt currents introduced by the distribution capacitor banks, (3.34) and (3.35), by the transformer current equations, (3.19) and (3.20), and by voltage regulator current equations (3.27) and (3.28).

The currents through distribution lines and capacitor banks are the summations of load currents, generation currents, and shunt currents at the end node and downstream from the transformer or the distribution line. Mathematically the decoupled line current equations for three-phase distribution currents can be written as:

$$\boldsymbol{I_{abcl}}^{\boldsymbol{x}} = \sum_{\boldsymbol{i \in D}} (\boldsymbol{I_{Cabc}}^{\boldsymbol{x}}(i) + \boldsymbol{I_{DGabc}}^{\boldsymbol{x}}(i) + \boldsymbol{I_{Labc}}^{\boldsymbol{x}}(i)) \tag{3.57}$$

and

$$\boldsymbol{I_{abcl}}^{\boldsymbol{y}} = \sum_{\boldsymbol{i}\in\boldsymbol{D}}(\boldsymbol{I_{Cabc}}^{\boldsymbol{y}}(i) + \boldsymbol{I_{DGabc}}^{\boldsymbol{y}}(i) + \boldsymbol{I_{Labc}}^{\boldsymbol{y}}(i)) \quad (3.58)$$

where $\boldsymbol{I_{abcl}}^{\boldsymbol{x}}$ and $\boldsymbol{I_{abcl}}^{\boldsymbol{y}}$ are Cartesian representations of complex line currents through the distribution line, $\boldsymbol{I_{Cabc}}^{\boldsymbol{x}}(i)$ and $\boldsymbol{I_{Cabc}}^{\boldsymbol{y}}(i)$ are Cartesian representations of the shunt currents at node *i*, $\boldsymbol{I_{DGabc}}^{\boldsymbol{x}}(i)$ and $\boldsymbol{I_{DGabc}}^{\boldsymbol{y}}(i)$ are Cartesian representations of the DG current injections at node *i*, $\boldsymbol{I_{Labc}}^{\boldsymbol{x}}(i)$ and $\boldsymbol{I_{Labc}}^{\boldsymbol{y}}(i)$ are Cartesian representations of the load currents at node *I*, and $\boldsymbol{D}$ is the set of nodes including the distribution line end node and all nodes downstream from the end of the distribution line.

The transformer secondary side currents are also summations of load, shunt, and DG currents on the secondary side of the transformer. Mathematically they are represented in their decoupled form as:

$$\boldsymbol{I_{abcs}}^{\boldsymbol{x}} = \sum_{\boldsymbol{i}\in\boldsymbol{Xs}}(\boldsymbol{I_{Cabc}}^{\boldsymbol{x}}(i) + \boldsymbol{I_{DGabc}}^{\boldsymbol{x}}(i) + \boldsymbol{I_{Labc}}^{\boldsymbol{x}}(i)) \quad (3.59)$$

and

$$\boldsymbol{I_{abcs}}^{\boldsymbol{y}} = \sum_{\boldsymbol{i}\in\boldsymbol{Xs}}(\boldsymbol{I_{Cabc}}^{\boldsymbol{y}}(i) + \boldsymbol{I_{DGabc}}^{\boldsymbol{y}}(i) + \boldsymbol{I_{Labc}}^{\boldsymbol{y}}(i)) \quad (3.60)$$

where $\boldsymbol{I_{abcs}}^{\boldsymbol{x}}$ and $\boldsymbol{I_{abcs}}^{\boldsymbol{y}}$ are the distribution transformer secondary side currents, and $\boldsymbol{Xs}$ is a set of nodes on the secondary side of the distribution transformer.

3.6. Formulation of the MINLP problem from distribution power flow

3.6.1. Linear distribution component constraints

As a summary of the equations presented in section 3.3 the linear constraints of the MINLP VVO formulation include:

- Distribution line voltage drops
- Shunt currents introduced by distribution line capacitances
- Transformer voltage and current equations

- Distribution line currents

3.6.2. Non-linear distribution component constraints

As a summary of the equations presented in section 3.3 the non-linear constraints of the MINLP VVO formulation include:

- Distribution loads
- Distribution load currents
- The current injections by the DG
- The current injections by the capacitor banks
- The voltage and current relationships of voltage regulating devices
- The reactive generation limits by the DG if there is a possibility for curtailment with the DG source. (Non-linear inequality constraint)

3.6.3. Voltage bounds

The distribution voltages are bounded by the ANSI standard in the US [6]. The voltage bounds are described with non-linear inequality constraints in the MINLP VVO formulation. The constraints are formed by the voltage magnitudes determined from the Cartesian representations. The voltage magnitudes are calculated by taking a square root of the summation of their complex components. The voltages bounds are included in $C(x)$ and d of the MINLP VVO formulation. Mathematically the voltage bounds are presented by:

$$V_{ll} \leq \sqrt{(V_m^x)^2 + \left(V_m^y\right)^2} \leq V_{lu} \tag{3.61}$$

where V_m^x and V_m^y are the Cartesian representations of the node voltage at node m, V_{ll} is the lower voltage limit, V_{lu} is the upper voltage limit. The ANSI standard the lower and upper voltage limits are 95% and 105% of the rated node voltages. If the power flow is

modeled with per unit (pu) system, then the voltage bounds are respectively 0.95 pu and 1.05 pu.

3.6.4. Line current bounds

The distribution lines have maximum allowed current limits. The limits are determined by the conductor manufacturers to prevent overloading the distribution lines. Exceeding the current limits may cause conductors to overheat and potentially even to fail. The line current magnitude is calculated by taking the square root of the summation of the Cartesian line current representations. The line current magnitude is limited by the maximum line current limit specified by the conductor manufacturer. Mathematically the line current bounds are described as:

$$\sqrt{(I_{line}^{x})^2 + \left(I_{line}^{y}\right)^2} \leq I_L \tag{3.62}$$

where I_{line}^{x} and I_{line}^{y} are the Cartesian representations of the line currents and I_L is the maximum allowable line current. The line current bounds are included in $C(x)$ and d of the MINLP VVO formulation.

3.6.5. Integer and continuous decision variables

The decision variables in the MINLP VVO formulation include integer and continuous decisions. The integer variables include:

- Voltage regulator tap-positions
- LTC transformer tap positions
- Capacitor bank switch positions

The devices with continuous controllable decision variables in MINLP VVO formulation include:

- The reactive power injection commands for DG

- The real power DG injection commands for controllable DG or devices with opportunity for curtailment

4. MINLP BASED VVO RESULTS WITH TEST FEEDERS

This chapter presents test results achieved with studied MINLP based VVO algorithm that was introduced in previous chapter. Based on the IEEE 37-node radial distribution test feeder the test system studied include an 8-node radial distribution test feeder, 10-node radial distribution test feeder, 13-node test feeder based on the IEEE 13-node radial distribution test feeder, and 37-node radial distribution test feeder. The feeder power flow was modeled in the decoupled form, because it constraints for the problem formulation and the decision variables included continuous and discrete decisions.

4.1. Single-phase 4-node distribution test feeder

A small 4-node single-phase distribution test feeder with a line voltage regulator and two capacitor banks was first studied with the VVO MINLP approach. The small test system was used to display the initial functionality and effectiveness of the proposed MINLP VVO approach. Figure 8 displays the 4-node single-phase distribution test feeder used for the initial MINLP VVO study.

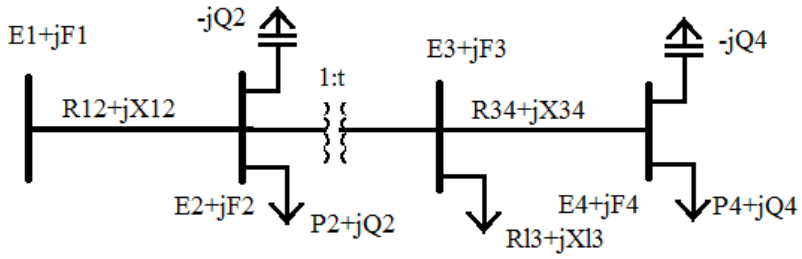

Figure 8: Single-phase 4-node radial distribution test feeder.

The test feeder, in Figure 8, has four distribution nodes, an infinite source at node one, two constant power loads at nodes two and four, a constant impedance load at node three, two distribution line segments between nodes one and two as well as three and four, a step voltage regulator between nodes two and three, and two switchable constant

impedance capacitor banks at nodes two and four. Finding the optimal tap position for the voltage regulator and optimal switch positions for the two capacitor banks in is the goal of the optimization. The objective for the optimization is to minimize the real power drawn from the substation at node 1. The test case was solved with the BONMIN MINLP solver with the constant values described in Table 4.1.

Table 4.1: 4-node test feeder constant component values

Constant	**Value**	**Constant**	**Value**	**Constant**	**Value**
E_1	1.05 pu	X_{34}	0.010 pu	P_4	4.00 pu
F_1	0.00 pu	R_{l3}	1.00 pu	Q_4	4.00 pu
R_{12}	0.005 pu	X_{l3}	1.00 pu	X_{2c}	-0.2 pu
$\mathbf{X_{12}}$	0.010 pu	P_2	2.00 pu	X_{4c}	-0.2 pu
R_{34}	0.005 pu	Q_2	2.00 pu	-	-

The voltage regulator between nodes two and three has ten positions upward and downward, which can increase or decrease the voltage by total of 10%. Each tap position downward reduces the primary voltage by one percent. Therefore, the equations for tap potion becomes from (3.30):

$$t = 1 + 0.01T_p \tag{4.1}$$

The 4-node test feeder was solved with the BONMIN MINLP solver with the constant values described in Table 4.1. The minimized cost was calculated to occur for the specified conditions when the control was as described in Table 4.2. All constraints were satisfied and all optimization variables were within their bounds.

Table 4.2: 4-node test feeder optimal control

Device	Control setting
Voltage regulator	-3
Capacitor bank at node two	0
Capacitor bank at node four	1

The capacitor bank at node two is at its OFF position. The capacitor bank at node four is at its ON position. The voltage regulator is set to drop the voltage level between nodes two and three by three percent. The minimized real power drawn from the substation under the constant load conditions was equal to 7.2925 per unit. The voltage profile for the optimally controlled 4-node test feeder is shown in Figure 9 below. The voltage profile is drawn as function of distance from the substation. The nodes two and three are located 10 distance units from the substation while bus four is located 20 units from the substation.

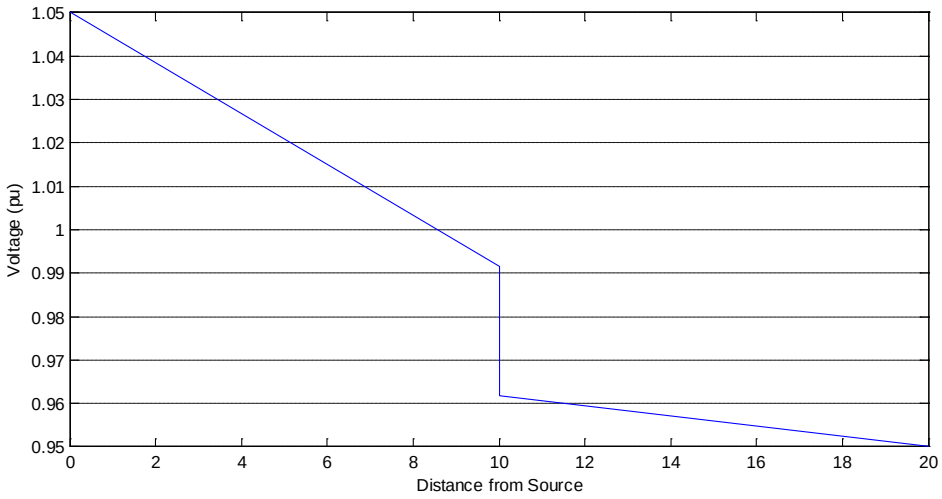

Figure 9: Optimal voltage profile for 4-node radial distribution test feeder

The solved optimal control was confirmed by performing a series of power flow studies for the test system with varying combination of control commands. The power drawn from the substation was recorded for each control setting and the power values for conditions where none of the constraints were violated were compared against each other. The control solved by the MINLP VVO approach drew the least amount of power without violating the optimization constraints.

4.2. Three-phase 8-node distribution test feeder

The presented MINLP based VVO approach was applied to an 8-node three-phase distribution feeder shown in Figure 10. The feeder loading was unbalanced. The system had two line voltage regulators between nodes two and three as well as four and five. The feeder also had two capacitor banks at nodes four and six. The system also had an inverter coupled PV generation source at node eight. The PV source was to be used to provide reactive power support to the system. The substation source connection was modeled as an infinite voltage source at rated, 12.47 kV, voltage and the abc-phase sequence. Branch, load, and component parameters for the test feeder are described in Table 4.3. Two loading conditions were used for the study: medium and heavy loading conditions. The heavy loading conditions were defined as 120% of the medium loading conditions.

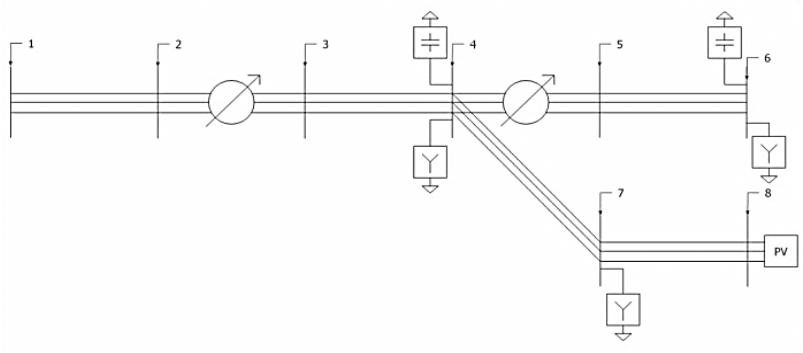

Figure 10: 8-node radial distribution test feeder

Table 4.3: 8-node radial distribution system component and loading description

Branches					
Starting node	Ending node	Z_s	Z_m	B_s	B_m
N1	*N2*	*.005 + j.01pu*	*.001+j.002pu*	*0*	*0*
N3	*N4*	*.005 + j.01pu*	*.001+j.002pu*	*0*	*0*
N5	*N6*	*.005 + j.01pu*	*.001+j.002pu*	*0*	*0*
N4	*N7*	*.005 + j.01pu*	*.001+j.002pu*	*0*	*0*
N7	*N8*	*.005 + j.01pu*	*.001+j.002pu*	*0*	*0*
Spot loads (100%)					
Node	P (A,B,C)	Q(A,B,C)	Constant Z	Constant I	Constant P
N4	*80,80,60 kW*	*40,50,60 kVAR*	*20%*	*0%*	*80%*
N6	*120,90,100 kW*	*80,90,70 kVAR*	*20%*	*0%*	*80%*
N7	*120,140,150 kW*	*60,75,90 kVAR*	*20%*	*0%*	*80%*
Voltage Regulators					
Starting node	Ending node	Z_e	Z_m	Step	Control
N2	*N3*	*0.01 + j0.02pu*	*Infinity*	*0.01 pu*	*[-10,10] ϵ Z*
N4	*N5*	*0.01 + j0.02pu*	*Infinity*	*0.01 pu*	*[-10,10] ϵ Z*
Capacitor Banks			**PV Generators**		
Location	Q (per phase)	Control	Location	P (per phase)	S_{max} (per phase)
N4	*150 kVAR*	*[0,1] ϵ Z*	*N8*	*50 kW*	*100 kVA*
N6	*150 kVAR*	*[0,1] ϵ Z*			

All feeder branches have same pu impedance values, the three-phase lines have both self-impedance and mutual-impedance between the phases. The overhead branches are short and the line capacitances are negligible. All loads are modeled as spot lodes at nodes four, six, and seven. The distribution loads are modeled to consist of 80% constant power loads, and 20% of constant impedance loads. The loading was unbalanced for the three-phases as seen on the spot load section of Table 4.3. The line voltage regulators

were modeled to have a transformer model with variable turns ratios for each phase. The line voltage regulators were modeled to have series impedance components on their secondary sides. As un-ganged control was assumed for both line voltage regulators the control of each phase of the voltage regulator was treated as an independent control variable,. Each phase of the voltage regulators had ten discrete control steps both upward and downward. The capacitor banks were modeled as 150 kVAR shunt capacitances for each phase and the control of capacitor banks is also un-ganged. The control was modeled as binary values, to determine if the shunt capacitor bank is switched on or off. The PV generator at node eight was assumed to inject 50kW for each phase. The apparent power limit for each phase of the PV inverter was 100 kVA leaving 86.6 kVAR of available reactive power for reactive power compensation.

The optimization was performed with the presented MINLP based VVO approach and the results are shown in Table 4.4. In the presented approach the control decisions were determined for each phase of the voltage regulators, capacitor banks, and PV inverter. In the determined control settings a power flow program was executed to determine the optimal voltage profile for control settings. The optimal voltage profile for medium loading conditions is shown in Figure 11. The voltage profile indicates that the node voltages throughout the feeder are within their ANSI specified limits.

The BONMIN solver, interfaced with Matlab via OPTI toolbox, was able to reach the optimal control solution in 2.83s for medium load and 3.15s for heavy load. To confirm the optimality of the solution a series of load flow studies was performed with parallel power flow solver implemented to Matlab. The feeder control parameters were varied and the real power demand for each combination of control parameters was

recorded. From the series of power flow studies it was determined that varying any of the parameters would not reduce the power demand without violating the constraints. The optimality of the solution was confirmed.

Table 4.4: Optimal control of 8-node radial distribution test feeder

Optimal Control	Medium load (100%)	Heavy load (120%)
Control Device	Phase A, B, C settings	Phase A, B, C settings
Voltage Regulator 23 Control	[-3, -2, -1]	[-2, -1, 1]
Voltage Regulator 45 Control	[0, 0, -1]	[0, 0, 0]
Capacitor Bank 4 Control	[0, 0 , 0]	[1, 1 , 0]
Capacitor Bank 6 Control	[1, 1, 1]	[1, 1, 1]
PV8 Reactive Power (kVAR)	[70.44, 68.28 ,66.02]	[0.00, 0.00 ,63.72]
Solution		
Power demand	709.36 kW	906.42 kW
Computational time	2.83 seconds	3.15 seconds
Solver iterations	21	25

The optimal voltage regulator settings are shown in Table 4.4 for medium and heavy loading conditions. The control of capacitor banks is also shown. When comparing the medium and heavy loading condition more reactive power compensation is connected to the feeder as the power demand by the loads is increased. It is assumed that the PV inverters are only allowed to operate in control mode where they inject both real and reactive power to the distribution feeder. The PV inverter is disabled from being able to consume reactive power. The solution part of Table 4.4 indicates that the solver is able to converge to the optimal solution in 21 iterations for medium loading conditions, and in

25 iterations for the heavy loading conditions. There is a slight increase in processing times for these two conditions. The total real power demand from the substation was observed to increase from approximately 710 kW to 910 kW, which is slightly over 20 % increase in demand when the PV generation is also considered. The increased demand is a function of loss and the load demand, with the higher loss and node voltages in heavy loading case the increased consumption, can be explained.

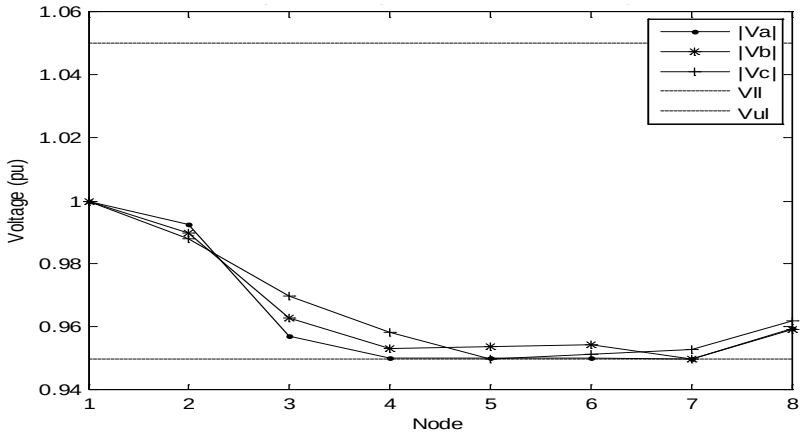

Figure 11: Optimal voltage profile for 8-node radial distribution test feeder under medium loading conditions.

The results show that the optimization algorithm performs well for the 8-node distribution test feeder in the study. The MINLP algorithm is able to converge to the optimal control solution in reasonable amount of time.

4.3. Three-phase 10-node distribution test feeder

The MINLP based VVO approach is applied in this section to a 10-node three-phase test feeder. The test feeder studied in this section is shown in Figure 12. The loading of the test feeder was unbalanced for the three phases. The 10-node test feeder was derived from the 8-node test feeder. The test feeder had two voltage regulators between nodes two and three and nodes four and five. The test feeder also had two

capacitor banks connected to the nodes four and six and two PV sources connected to nodes eight and ten. The feeder parameters, component, and control device settings are shown in Table 4.5.

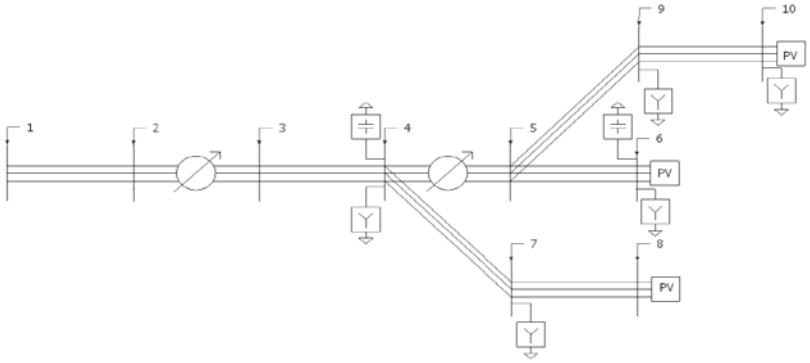

Figure 12: 10-node radial distribution test feeder

The parameters discussed in Table 4.5 include the distribution branches, distribution loads, voltage regulator configurations, capacitor bank settings, and information about the PV sources connected to the distribution system. All feeder branches have same pu impedance values and the three-phase lines have both self-impedance and mutual-impedance between the phases. The overhead branches are short and the line capacitances are negligible. All loads are modeled as spot lodes at nodes four, six, seven, nine, and ten. The distribution loads are modeled to consist of 1/3 constant power loads, 1/3 constant current loads, and 1/3 constant impedance loads. The loading was unbalanced for the three-phases as seen in the spot load section of Table 4.5. The line voltage regulators were modeled the same way as in 8-node test feeder.

The line voltage regulators were modeled to have series impedance on their secondary sides. Un-ganged control was assumed for both line voltage regulators. Each phase of each voltage regulator had ten discrete control steps both upward and downward. The capacitor banks were modeled as 150 kVAR shunt capacitances for each

phase, the capacitor bank control was also un-ganged. The control was modeled as binary values determining if the shunt capacitor bank is switched on or off. The PV generators at node eight and ten were assumed to inject 100 kW each to each phase. The apparent power limits for each phase of the PV inverters were 200 kVA leaving 173.2 kVAR of available power for reactive power compensation.

Table 4.5: 10-node radial distribution test feeder component and loading description

Branches					
Starting node	Ending node	Z_s	Z_m	B_s	B_m
N1	*N2*	*0.005 + j0.01pu*	*0.001+j0.002pu*	*0*	*0*
N3	*N4*	*0.005 + j0.01pu*	*0.001+j0.002pu*	*0*	*0*
N5	*N6*	*0.005 + j0.01pu*	*0.001+j0.002pu*	*0*	*0*
N4	*N7*	*0.005 + j0.01pu*	*0.001+j0.002pu*	*0*	*0*
N7	*N8*	*0.005 + j0.01pu*	*0.001+j0.002pu*	*0*	*0*
N5	*N9*	*0.005 + j0.01pu*	*0.001+j0.002pu*	*0*	*0*
N9	*N9*	*0.005 + j0.01pu*	*0.001+j0.002pu*	*0*	*0*
Spot loads (100%)					
Node	P (A,B,C)	Q(A,B,C)	Constant Z	Constant I	Constant P
N4	*60,60,100 kW*	*100,40 ,50 kVAR*	*33.3%*	*33.3%*	*33.3%*
N6	*100,120,120 kW*	*100,100,80kVAR*	*33.3%*	*33.3%*	*33.3%*
N7	*80,80,80 kW*	*30,20,50 kVAR*	*33.3%*	*33.3%*	*33.3%*
N9	*75,75,75 kW*	*50,30,80 kVAR*	*33.3%*	*33.3%*	*33.3%*
N10	*110,160,110kW*	*30,30,50 kVAR*	*33.3%*	*33.3%*	*33.3%*
Voltage Regulators					
Starting node	Ending node	Z_e	Z_m	Step	Control
N2	*N3*	*0.01 + j0.02pu*	*Infinity*	*0.01 pu*	*[-10,10] ϵ Z*
N4	*N5*	*0.01 + j0.02pu*	*Infinity*	*0.01 pu*	*[-10,10] ϵ Z*
Capacitor Banks			**PV Generators**		
Location	Q (per phase)	Control	Location	P (per phase)	S_{max} (per phase)
N4	*150 kVAR*	*[0,1] ϵ Z*	*N8*	*100 kW*	*200 kVA*
N6	*150 kVAR*	*[0,1] ϵ Z*	*N10*	*100 kW*	*200 kVA*

The results for the 10-node test feeder optimal control are shown in Table 4.6 for medium and heavy loading conditions. The optimal voltage profile for the medium loading conditions is shown in Figure 13. The presented optimization approach with the BONMIN algorithm was able to produce the optimal solutions in 4.02s for the medium loading condition and 4.48s for the heavy loading condition. The voltage regulator tap

positions were raised as the system loading was increased. The capacitor banks were switched on for both medium and heavy loading conditions. These computational times were slightly longer than the times for the 8 node radial distribution test feeder. The computational time was slightly larger for the heavy loading case as it was with the 8-node distribution test feeder.

Table 4.6: Optimal control of 10-node radial distribution test feeder

Optimal Control	Medium load (100%)	Heavy load (120%)
Control Device	Phase A, B, C settings	Phase A, B, C settings
Voltage Regulator 23 Control	[-4, -3, -3]	[-4, -1, -1]
Voltage Regulator 45 Control	[0, 1, 1]	[1, 1, 2]
Capacitor Bank 4 Control	[1, 1, 1]	[1, 1, 1]
Capacitor Bank 6 Control	[1, 1, 1]	[1, 1, 1]
PV8 Reactive Power (kVAR)	[-34.08,-19.66, 30.45]	[11.99, -30.24,51.96]
PV10 Reactive Power (kVAR)	[86.98, 54.21, 96.72]	[98.51, 77.16, 90.32]
	Solution	
Power demand	772.58 kW	1,064.24kW
Computational time	4.02 seconds	4.48 seconds
Solver iterations	30	36

To confirm the optimality of the solution a series of load flow studies was performed with a custom Matlab power flow solver. The study was performed to determine whether varying any of the control feeder parameters would reduce the power demand without violating one or more feeder constraints. The results of the study

confirmed that the reached solution for both loading cases was optimal and varying one or more system control settings could not reduce the power demand.

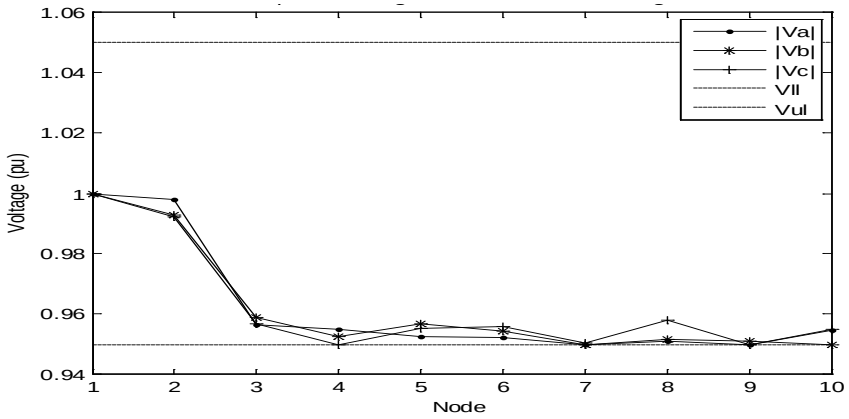

Figure 13: Optimal voltage profile for 10-node radial distribution test feeder under medium loading conditions.

The overall power demand from the substation increased by 21.3% as the load demand increased by 20% while the PV generation remained at constant level. The power demand is a function of load powers and the power loss in the system. The load power demands are functions of voltage and as the voltage increases so does the total power demand. The increase in voltage regulator tap-positions contributed to the increase in total power demand as it increased some of the node voltages is also larger line currents along the feeder contributed to the increased total power demand.

4.4. IEEE 13-node radial distribution test feeder

In this section the proposed MINLP based VVO approach was applied to a 13-node three phase unbalanced distribution test feeder based on the IEEE 13-bus radial distribution feeder. The feeder is shown in Figure 14. The IEEE test feeder is further discussed in [49]. The branch configurations and the lengths of the branches are stated in [54]. The VVO was calculated for two unbalanced loading conditions, the medium

loading conditions and heavy loading. The medium loading conditions are shown in Table 4.7, and heavy loading conditions are 120% of the medium loading conditions. The 13-node test feeder has spot and distributed loads, two controllable capacitor banks at nodes 611 and 675, a voltage regulator right downstream from the substation connection between nodes 650 and 632, and two three-phase PV plants with reactive power compensation capabilities at nodes 634 and 680. The capacitor bank at node 675 has eight 50kVAR reactive power steps for each phase. The control of the capacitor bank is modeled with integer values rather than with binary values as in previous test feeders. The capacitor bank at node 611 is a single-phase capacitor banks and has four 50 kVAR reactive power steps for phase C.

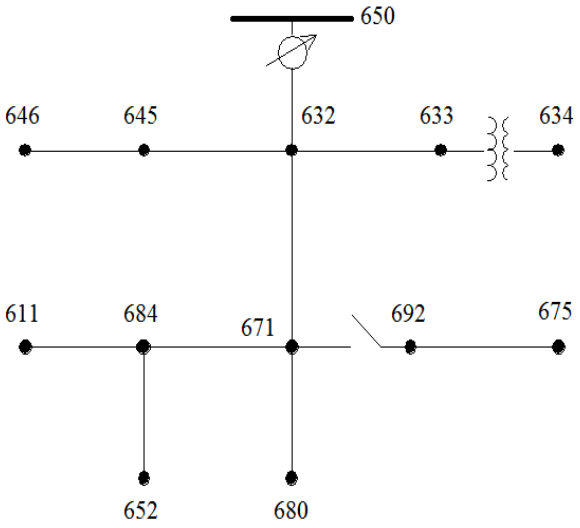

Figure 14: IEEE 13 node radial distribution test feeder

The PV plants, connected to nodes 634 and 680, and have each 100 kW per phase output with apparent power limit of 125 kVA for each phase. For the two test cases the PV plants were assumed to have full real power output. The optimization results are shown in Table 4.8. The corresponding optimal per unit voltage profile is shown in Table

4.9 for the medium loading case. The symbol '-', in Table 4.9 designates that the corresponding phase does not exist in the feeder. The computational times for the test system were 11.73s and 12.47s for medium and heavy loads, respectively. The computational time increased with increasing system size and complexity. Heavy loading conditions also slightly entail more computational times in all three test feeders.

Table 4.7: Three phase apparent power load for 13-node test system under medium loading conditions

Node	Load type	Phase A	Phase B	Phase C
634	Constant PQ	160+j110 kVA	120+j90 kVA	120+j90 kVA
645	Constant PQ	0	170+j125 kVA	0
646	Constant Z	0	230+j132 kVA	0
652	Constant Z	128+j86 kVA	0	0
671	Constant PQ	385+j220 kVA	385+j220 kVA	385+j220 kVA
675	Constant PQ	485+j190 kVA	68+j60 kVA	290+j212 kVA
692	Constant I	0	0	170+j151 kVA
611	Constant I	0	0	170+j80 kVA
Distributed load: 632-671	Constant PQ	17+j10 kVA	66+j38 kVA	117+j68 kVA

The optimal control of the 13-node radial distribution test feeder indicates that the voltage regulator setting increases as the loading increases more reactive power compensations is also switched on as the power demand increases. The computational time increased also slightly when the system loading was increased. However, the

number of iterations was slightly reduced. The total power consumption of the distribution feeder was shown to increase slightly over 20% with the increase in load levels, like in the other test cases the increase in load level is due to the increase in operational voltages and increased line loss, due to distribution currents.

Table 4.8: Optimal control of 13 node radial distribution test feeder

Optimal Control	Medium Load (100%)	Heavy Load (120%)
Control Device	Phase A, B, C settings	Phase A, B, C settings
Voltage Regulator Control	[1,-3, 2]	[3, -2,7]
Capacitor Bank 675 Control	[2, 3, 8]	[3, 3, 8]
Capacitor Bank 611 Control	[4] - Phase C only	[4] - Phase C only
PV680 Reactive Power (kVAR)	[63.19, 75.00,75.00]	[45.54, 75.00,75.00]
PV634 Reactive Power (kVAR)	[75.00, 58.19,42.33]	[75.00, 75.00,45.37]
Solution		
Power demand	2,898 kW	3,630 kW
Computational time	11.73 seconds	12.47 seconds
Solver iterations	32	27

Table 4.9: Optimal voltage profile for the IEEE 13-node radial distribution test feeder under medium loading conditions

Node	$\|V_A\|$ (pu)	$\|V_B\|$ (pu)	$\|V_C\|$ (pu)
650	1.0000	1.0000	1.0000
632	0.9811	0.9645	0.9787
671	0.9573	0.9697	0.9516
680	0.9593	0.9714	0.9541
692	0.9573	0.9697	0.9516
675	0.9508	0.9704	0.9510
633	0.9800	0.9642	0.9776
634	0.9809	0.9648	0.9783
645	-	0.9538	0.9774
645	-	0.9508	0.9755
684	0.9554	-	0.9508
611	-	-	0.9500
652	0.9500	-	-

The optimality of the solution was confirmed with a series of the power flow studies around the calculated optimal conditions for the distribution feeder. The obtained solutions indicate that the presented optimization approach was able to converge to minimized power demand for the more complicated 13-node test feeder.

4.5. IEEE 37-node radial distribution test feeder

The presented MINLP based VVO approach was applied to a much larger test feeder in this section. The test feeder is a radial feeder with 37 distribution nodes and is modeled after the IEEE 37 node distribution test feeder. The IEEE 37 node radial distribution test feeder is further discussed in [49] and [55]. A single line diagram of the test feeder is shown in Figure 15. The same test system is used for the dual-layer VVC test case in [14] and in Chapter 7.

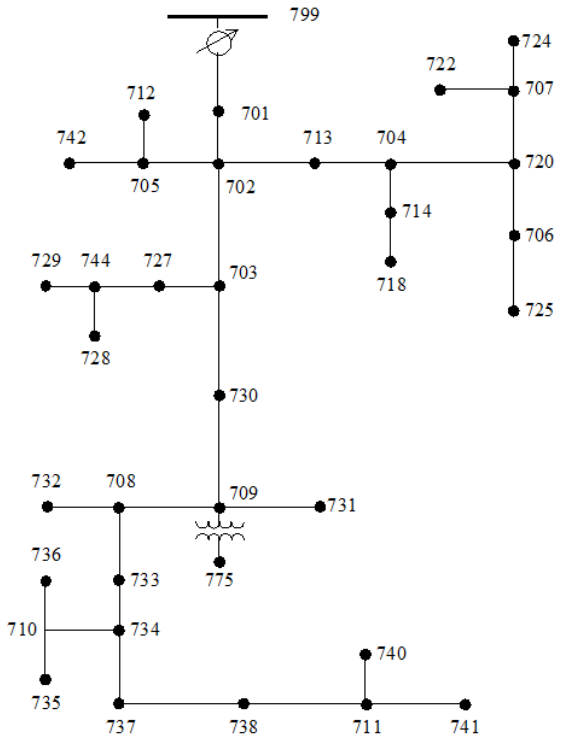

Figure 15: 37-node radial distribution test feeder

Between nodes 799 and 701 the test feeder has a voltage regulator at the distribution substation connection. The voltage regulator is used for the main voltage control of the feeder. Three PV sources are added to the nodes 727, 732, and 736. The VVO algorithm is applied to a constant loading condition with two PV generation conditions considered 100% and 50% of the rated generation capacity. The 100% of generation is 300 KW by each PV inverter and 50 % generation is 150 kW by each by each PV inverter. The apparent power limit is 125% of the maximum PV generation 375 kVA. The optimal control settings, determined by the VVO approach, for both PV generation conditions are shown in Table 4.10. The first column in Table 4.10 defines the control setting. The second through seventh column display the control setting for each phase with 50% and 100% PV output.

Table 4.10: Optimal control for 37-node radial test system with PV generation installed to the nodes 727, 732, and 736 under 50% and 100% generation.

	50% PV generation			**100% PV generation**		
Phase	A	B	C	A	B	C
Voltage regulator control	-1	-3	-2	-1	-3	-2
VAR injection at node 727	-114.6	-114.6	-85.54	-49.53	-65.58	-75.00
VAR injection at node 732	-48.30	-68.41	-114.6	-22.38	-6.046	-75.00
VAR injection at node 736	-22.25	-25.53	-114.6	-18.34	0.758	-75.00
Power demand	2003.70 kW			1543.20 kW		

As determined from Table 4.10 the powers demand from the substation decreases as the PV generation increases. With the increased generation the PV inverters are not able to inject as much reactive power to the distribution system, and therefore, the total reactive power injected is reduced when the generation increases. For this study no capacitor banks were connected to the distribution feeder. The optimal voltage profile for each phase of the 37-node test feeder with 100% PV generation is shown in Table 4.11.

The optimality of both control solutions were again confirmed with a series of the power flow studies around the calculated optimal conditions for the distribution feeder. The obtained solutions indicate that the presented optimization approach was able to converge to minimized power demand for the 37-node test feeder.

Table 4.11: Optimal voltage profile for 37-node radial distribution test feeder with 300 kW PV sources installed to the nodes 727, 732, and 736, with rated PV generation.

Node	Phase A	Phase B	Phase C
799	1.0000	1.0000	1.0000
701	0.9794	0.9772	0.9742
702	0.9754	0.9753	0.9689
703	0.9709	0.9773	0.9671
730	0.9679	0.9791	0.9637
709	0.9668	0.9795	0.9633
708	0.9649	0.9813	0.9623
733	0.9618	0.9825	0.9609
734	0.9584	0.9844	0.9582
737	0.9519	0.9862	0.9563
738	0.9500	0.9869	0.9546
711	0.9503	0.9873	0.9525
740	0.9504	0.9875	0.9518
741	0.9504	0.9875	0.9514
710	0.9616	0.9849	0.9583
735	0.9620	0.9817	0.9587
736	0.9628	0.9857	0.9582
732	0.9666	0.9824	0.9631
731	0.9672	0.9775	0.9636
727	0.9704	0.9782	0.9674
744	0.9691	0.9781	0.9673
728	0.9687	0.9777	0.9669
729	0.9685	0.9781	0.9674
705	0.9757	0.9736	0.9671
712	0.9759	0.9737	0.9658
742	0.9758	0.9720	0.9673
713	0.9751	0.9726	0.9670
704	0.9743	0.9683	0.9660
720	0.9762	0.9618	0.9637
707	0.9776	0.9519	0.9640
722	0.9777	0.9508	0.9640
724	0.9778	0.9500	0.9642
714	0.9764	0.9608	0.9639
718	0.9765	0.9600	0.9640
706	0.9738	0.9682	0.9661
725	0.9712	0.9686	0.9664
775	0.9668	0.9795	0.9633

5. FAST LOCAL REACTIVE POWER CONTROL OF DG

This section presents an approach for fast reactive power distributed local control of multiple DG sources. In this section inverter coupled PV sources are considered, but the approach is also applicable to other DG sources with ability to control their reactive power injection fast. The work presented here is derived from the work presented in [56], but extended to multiple inverters and larger distribution systems in this section. The local control approach presented here is also studied as a second-layer control approach for the dual-layer VVC presented in [14]. The dual-layer control approach with distributed local reactive power controllers is discussed in detail in Chapter 7 of this dissertation.

5.1. Introduction

High penetration of distributed energy resources (DER) in distribution feeders is desirable for their environmental and economic impacts. Integration of renewable DG often presents significant technical challenges to the distribution feeders. Technical challenges are particularly substantial with PV generation. The intermittency of the PV generation, due to fast changing irradiance conditions, may cause large fluctuations in the feeder voltages. In some cases the fluctuations in generation can cause significant power quality issues, such as feeder operational voltage bounds, to be exceeded. As traditional feeder control is performed mostly with slow-acting mechanical control devices it is typically too slow to respond to the fast fluctuations in PV generation.

Studies for PV sources have indicated that solar irradiance levels can change as much as sixty percent in a one-second time interval [57] [58] [59]. The solar irradiance is mostly responsible for the generation output of the PV units, but the panel operating

temperature and other factors also affects the generation. Practically all PV systems installed today are equipped with fast-acting maximum power point trackers (MPPT) to maximize the real power output of the PV source. MPPT tracks the changes in irradiance conditions and moves the PV system operating point along the power hyperbola until maximum power output is reached [60]. Advanced MPPT control algorithms can track the irradiance changes almost instantaneously, in 50 milliseconds or less [61]. PV generation output changes practically simultaneously to the irradiance conditions with the assumed fast MPPT tracking. Traditional feeder control devices, such as voltage regulators, load tap-changer (LTC) transformers, and capacitor banks, are often too slow to respond to the fast irradiance fluctuations. The slow response times of the traditional distribution control devices are some of the main limiting factors for higher DG penetration to distribution feeders.

Non-traditional control approaches need to be considered to allow more DG penetration. If the voltage fluctuations, caused by the intermittency of DG sources, can be eliminated or reduced more PV generation could be interconnected to the distribution feeders. Perhaps the most common approach for limiting the voltage fluctuations is to replace the lost PV generation with real power injection from other sources. A few methods of using battery backup systems to provide real power injection in place of lost PV generation are studied in [62], [63], and [64]. Limiting the rate of change in DG by storing energy in capacitors is studied in [65] [66]. Replacing the lost PV generation with real power injection with fast control algorithm can be very effective. Unfortunately adding the energy storage system to the feeders is often very expensive.

Another approach considered for limiting the voltage fluctuations is injecting reactive power in the place of lost real power generation. PV generation units are DC devices that are connected to the AC distribution grid via power electronic inverter interfaces. Using advanced inverter controls the PV units are able to provide reactive power injection to the distribution feeder, as widely noted in literature, e.g. [39] [41] [52] [67] [68]. Distribution feeder loss can be reduced and higher levels of PV generation can be interconnected to the distribution feeders when the voltages can be kept close to constant with application of fast reactive power compensation by PV inverters. The PV inverters with the fast reactive power compensation capability are often referred to as smart inverters, e.g. in [68]. Some VVC approaches have considered the smart inverters to be used as a part of scheduled and dispatched feeder control [38] [43] [69] [70]. Although scheduled reactive power control is effective, the computational times of the analytical VVC algorithms are the main obstacles for online use of the VVC algorithms [31]. This is especially true in feeders with large PV systems and high intermittency. Due to the computational burden and slow response nature of mechanical control devices, the VVC systems are unable to respond to irradiance variations in real time, and thus voltage fluctuations are very likely.

This section describes distributed control approach for multiple PV inverters to limit the fast voltage fluctuations in distribution feeders. The approach utilizes a local linear controller to control the reactive power output of the smart PV inverts. The local linear controller is set to minimize the voltage fluctuations at the main feeder tie points closest to the PV generation source. The classical sensitivity approach is utilized to find the ideal control coefficient for the local linear controller. The rest of this chapter is

organized as follows Section 5.2 discusses the classical voltage sensitivity approach, Section 5.3 describes the theory for finding the optimal substitution factors to minimize voltage fluctuations at main feeder tie nodes, case studies and their results for the distributed control are discussed in Section 5.4, and the conclusion of the chapter follows in Section 5.5.

5.2. Classical sensitivity approach

The classical sensitivity approach is utilized for determining the linear substitution factors for distributed local reactive power control. The distribution system voltages can be determined from the distribution system power flow. The distribution system power flow is a non-linear problem with multiple inputs. Mathematically the feeder voltages are written as a function of the real and reactive power demand, real and reactive power injection by distributed generation, and feeder control settings:

$$\boldsymbol{V} = f(\boldsymbol{P_l}, \boldsymbol{Q_l}, \boldsymbol{P_{DG}}, \boldsymbol{Q_{DG}}, \boldsymbol{u}) \quad (5.1)$$

where $\boldsymbol{V}$ is a vector of feeder voltages, $\boldsymbol{P_l}$ and $\boldsymbol{Q_l}$ are the real and reactive power demands, $\boldsymbol{P_{DG}}$ and $\boldsymbol{Q_{DG}}$ are the real and reactive power injections provided by the DG, $\boldsymbol{u}$ represents the control settings, and f denotes the governing equations relying on the distribution system topology and parameters. If the distribution system topology changes function f will be updated accordingly.

It is known and can be shown that around the feeder operating conditions. The feeder voltages vary in close to a linear manner with changing real and reactive power injection by the distributed generation, $\Delta\boldsymbol{P_{DG}}$ and $\Delta\boldsymbol{Q_{DG}}$ respectively. For this reason the voltage equation (5.1) can be reduced to a linear form:

$$|\boldsymbol{V}| \approx \boldsymbol{V_0} + \boldsymbol{A_P}\Delta\boldsymbol{P_{DG}} + \boldsymbol{A_Q}\Delta\boldsymbol{Q_{DG}} \quad (5.2)$$

where $\boldsymbol{V_0}$ is a vector containing the voltage magnitudes at the feeder operating point, $|\boldsymbol{V}|$ is a vector representing the magnitudes of feeder voltages as the DG outputs change, $\boldsymbol{A_P}$ and $\boldsymbol{A_Q}$ are voltage sensitivity coefficient matrices that are partial derivatives of $|\boldsymbol{V}|$ with respect to $\boldsymbol{P_{DG}}$ and $\boldsymbol{Q_{DG}}$ as defined in:

$$\frac{d|\boldsymbol{V}|}{d\boldsymbol{P_{DG}}} \approx \frac{\Delta|\boldsymbol{V}|}{\Delta\boldsymbol{P_{DG}}} = \boldsymbol{A_P} \quad (5.3)$$

$$\frac{d|\boldsymbol{V}|}{d\boldsymbol{Q_{DG}}} \approx \frac{\Delta|\boldsymbol{V}|}{\Delta\boldsymbol{Q_{DG}}} = \boldsymbol{A_Q} \quad (5.4)$$

The voltage fluctuations are defined as the difference between the actual voltage magnitude and the voltage at operating point. The feeder voltage fluctuations $\Delta|\boldsymbol{V}|$ can be mathematically written as:

$$\Delta|\boldsymbol{V}| \approx \boldsymbol{A_P}\Delta\boldsymbol{P_{DG}} + \boldsymbol{A_Q}\Delta\boldsymbol{Q_{DG}} \quad (5.5)$$

where

$$\Delta|\boldsymbol{V}| = |\boldsymbol{V}| - \boldsymbol{V_0} \quad (5.6)$$

The classical approach for voltage sensitivity analysis is utilized to determine $\boldsymbol{A_P}$ and $\boldsymbol{A_Q}$ in this section. For a good estimate a large number of distribution power flows needs to be performed with variable $\Delta\boldsymbol{P_{DG}}$ and $\Delta\boldsymbol{Q_{DG}}$ injection around the feeder operating point. The voltage magnitudes and the corresponding real and reactive power injections by the PV inverters are recorded for each power flow with the data points, a linear least squares fit was applied to (5.2), and the values for $\boldsymbol{A_P}$ and $\boldsymbol{A_Q}$were determined.

For the linear least square fit Matlab *linsolve()* function was utilized. The data is entered in a linear system form:

$$\boldsymbol{A_l X} = \boldsymbol{B_l} \quad (5.7)$$

where $\boldsymbol{A_l}$ contains the values for real and reactive power injection, $\boldsymbol{B_l}$ contains the voltage fluctuations, and $\boldsymbol{X}$ contains the corresponding voltage sensitivity coefficient matrices $\boldsymbol{A_P}$ and $\boldsymbol{A_Q}$. The function determines the values for the coefficient matrices by utilizing QR factorization with column pivoting for a system with a large number of power flow results. QR decomposition method is a common approach used for linear least squares fit problems.

For distribution system nodes the voltage sensitivities $\boldsymbol{A_P}$ and $\boldsymbol{A_Q}$ vary based on the node locations, system operating conditions, and control settings. The variations in sensitivities are typically small enough so that the sensitivity matrices do not need to be continuously updated. However, a periodic updating of the sensitivity matrices can improve the performance of the distributed local control. The closer to the true operating conditions the sensitivity matrices are determined the better the performance of the control will generally be. The results of the study presented in this chapter suggest that updating the sensitivity matrices should be performed at least when substantial changes in operating conditions occur. These changes in operating conditions could include significant changes in loading, generation, and control settings. The system wide updates for sensitivity matrices can be performed in parallel to the main control algorithm with a parallel power flow solver. The sensitivity matrix updates will not affect the performance of the control when the parallel power flow solver is used. The new voltage sensitivity matrices are calculated system wide and they can be delivered to the distributed control via distribution communication channels as necessary.

5.3. Local linear controller with substitution factors

Distributed linear controller is utilized for the distribution feeder fast reactive power control by the PV inverters. The goal of the control is to limit the voltage fluctuations in a distribution feeder. As solar irradiance is known to be highly variable it will cause significant fluctuations in real power outputs of PV inverters equipped with MPPTs. Traditional distribution feeder control is often too slow to respond to fast changes in irradiation, such as cloud transients, in real time. Applying distributed reactive power control for PV inverters can reduce the voltage fluctuations and allow for more DG integration to distribution feeder.

A local liner control method for short-term reactive power control of a single PV inverter for a small distribution system is presented in [56]. The method used in this section is based on a similar local control approach, but extended to multiple inverters and to a much larger distribution feeder. The substitution factors, used in a local linear controller, are selected to limit voltage fluctuations at certain feeder nodes. For the feeder wide voltage control the most promising results were achieved by selecting the substitution factors to minimize the voltage variations at main feeder tie nodes closest to the smart PV inverters. The general idea behind this control approach is to adjust the reactive power output of a PV inverter in response to the fluctuation in real power generation. Local linear controllers are used to control the reactive power injection. The controller used is expressed as:

$$Q(t) = Q_{ref} + \beta(P(t) - P_{ref}) \tag{5.8}$$

where P_{ref} is the reverence value of expected real power generated by the PV plant for the expected solar irradiance conditions, Q_{ref} is the PV inverter reactive power injection

reference point, β is a control parameter called the substitution factor, and $P(t)$ and $Q(t)$ are the actual real and reactive power injection by the PV inverter at time *t*.

Alternatively the equation (5.7) can be written as

$$\Delta Q = \beta \Delta P \tag{5.9}$$

where

$$\Delta Q = Q(t) - Q_{ref} \tag{5.10}$$

and

$$\Delta P = P(t) - P_{ref} \tag{5.11}$$

As noted in earlier in Section 3.4.7 the reactive power output of a PV inverter is constrained by the inverter apparent power limit and the real power injection:

$$-\sqrt{{S_{max}}^2 - P(t)^2} \leq Q(t) \leq \sqrt{{S_{max}}^2 - P(t)^2} \tag{5.12}$$

where $S_{max}$is the apparent power limit, $P(t)$ is the real power generation at time *t*, and $Q_{DG}(t)$ is the reactive power injection. The reactive power injection (5.8) by the local linear controller depends on the maximum apparent power limit as seen in:

$$Q(t) = Q_{ref} + \beta\big(P(t) - P_{ref}\big), if\ \left|Q_{ref} + \beta(P(t) - P_{ref})\right| \leq \sqrt{{S_{max}}^2 - P(t)^2} \tag{5.13}$$

$$Q(t) = \sqrt{{S_{max}}^2 - P(t)^2}, if\ \left(Q_{ref} + \beta(P(t) - P_{ref})\right) > \sqrt{{S_{max}}^2 - P(t)^2} \tag{5.14}$$

$$Q(t) = -\sqrt{{S_{max}}^2 - P(t)^2}, if\ \left(Q_{ref} + \beta\big(P(t) - P_{ref}\big)\right) < -\sqrt{{S_{max}}^2 - P(t)^2} \tag{5.15}$$

The substitution factor, β, is chosen for each PV inverter to limit the voltage fluctuations on the distribution feeder. In the approach presented in this chapter the substitution factors are selected in a way that they mainly limit the voltage changes at the main feeder tie nodes. These nodes are the main feeder nodes electrically closest to the

PV device. All downstream nodes depend on the voltages at the main feeder tie nodes limiting the voltage fluctuations at these nodes also directly limits the voltage fluctuations at the nodes downstream of the tie nodes.

The classical voltage sensitivity approach, described previously in section 5.2, is utilized for calculating the substitution factors. The goal of the control is to keep the voltage fluctuations at selected distribution feeder nodes at minimum. To minimize the voltage fluctuation at a certain node the change in voltage, $\Delta|\boldsymbol{V}|$, is set to zero in equation (5.5). With $\Delta|\boldsymbol{V}|$ set to zero for the targeted node (5.5) becomes:

$$\boldsymbol{A_P}\Delta\boldsymbol{P_{DG}} + \boldsymbol{A_Q}\Delta\boldsymbol{Q_{DG}} = \boldsymbol{0} \tag{5.16}$$

Next the equation (5.16) is solved for the change in reactive power, $\Delta\boldsymbol{Q_{DG}}$, which equals:

$$\boldsymbol{A_Q}\Delta\boldsymbol{Q_{DG}} = -\boldsymbol{A_P}\Delta\boldsymbol{P_{DG}} \tag{5.17}$$

and

$$\Delta\boldsymbol{Q_{DG}} = -\left(\boldsymbol{A_Q}\right)^{-\boldsymbol{1}}\boldsymbol{A_P}\Delta\boldsymbol{P_{DG}} \tag{5.18}$$

By comparing (5.18) to (5.9) a large similarity is obvious and (5.18) can be written mathematically as:

$$\Delta\boldsymbol{Q_{DG}} = \boldsymbol{\beta}\Delta\boldsymbol{P_{DG}} \tag{5.19}$$

where

$$\boldsymbol{\beta} = -(\boldsymbol{A_Q})^{-\boldsymbol{1}}\boldsymbol{A_P} \tag{5.20}$$

The three-phase substitution factor to minimize the voltage fluctuation at a main feeder tie node can be determined from the voltage sensitivity matrices determined for the feeder operating conditions. In reality the substitution factors are combinations of nonlinear functions with voltage levels, current injections, load demand, and feeder

controls as some their variables. However as the results, described later in this chapter, show the linearized solutions for voltage sensitivities are sufficient to provide a good control solution for the distribution feeder.

5.4. Local linear reactive power control results

The distributed control approach using local linear control was validated for two test feeders that were based on the IEEE 13 node and IEEE 37 node radial distribution test feeders. Each feeder was equipped with three PV sources along the feeder. Each PV inverter was equipped with a local linear PV controller.

5.4.1. Results for 13-node radial distribution test feeder

The modified IEEE 13 node distribution test system is described in detail in Section 4.4 and a single line diagram can be seen in Figure 14. The test feeder used for analysis in this section had three PV generators, instead of two, connected at nodes 634, 675, and 680. The voltage fluctuations for phase A with and without the local reactive and PV sources installed at nodes 634, 675, and 680 shown in Figure 16. The voltage fluctuations are significantly reduced with the distributed local reactive power control, which is indicated by the Figure 16. The PV systems installed at nodes 634, 675, and 680 each have a rated 1600 kW real power output. The generation profiles for a 30-minute study period are shown in Figure 17. The generation profiles are derived from the one-second global irradiance record collected at National Renewable Energy Laboratory (NREL) Solar Measurement Grid in Oahu, HI [71]. The data used for this study was collected on July 20, 2010. The specific locations used for the measurements were DH3, AP1, and AP6 on the NREL measurement grid. The locations are displayed on the map in [71].

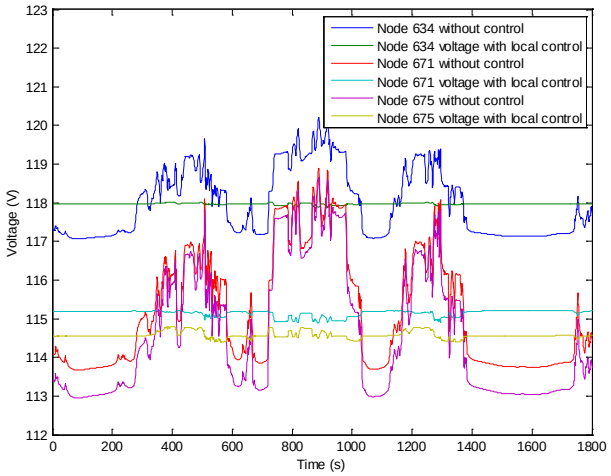

Figure 16: Phase A voltage fluctuations for the 13-node radial distribution test feeder with PV sources installed at nodes 634, 675, and 680.

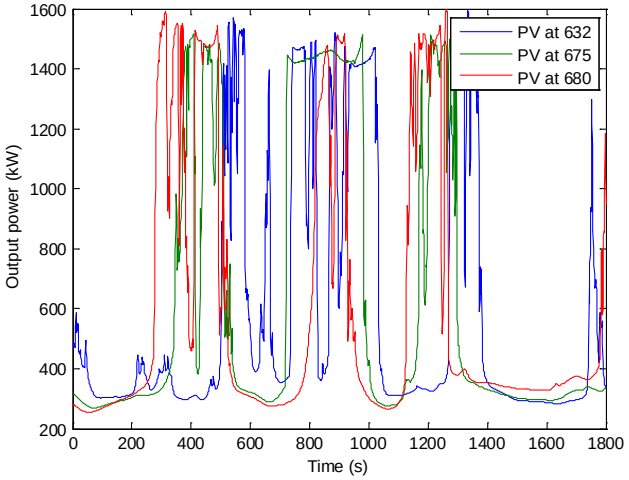

Figure 17: PV generation profiles for 1600 kW systems installed at nodes 634, 675, and 680.

The voltage fluctuations are further analyzed in Table 5.1. The first column of Table 5.1 describes the type of voltage fluctuation measured. The second and third columns display the fluctuations measured for the installed PV systems with and without the control. In the first column, PU denotes per unit, MSE_V denotes mean squared

voltage error from average voltage value, $Max_{\Delta V}$ denotes the maximum local peak to peak voltage variation at node 675, and Max_{Ve} denotes the maximum global voltage error. The maximum global voltage error is defined as the maximum difference between the actual voltages and the average voltage values.

Table 5.1: Voltage fluctuations with and without distributed reactive power control of PV inverters installed at nodes 634, 675, and 680.

Measurement	**With Q control**	**Without Q control**
PU MSE_V at node 675	6.05×10^{-7}	1.93×10^{-4}
PU $Max_{\Delta V}$ at node 675	2.94×10^{-3}	4.75×10^{-2}
PU global MSE_V	5.80×10^{-7}	5.84×10^{-5}
PU global Max_{Ve}	6.23×10^{-3}	3.37×10^{-2}

The results recorded in Table 5.1 indicate that the local reactive power control reduced the local MSE measured at 675 by 99.7%. The local voltage variations were reduced by 93.8% from 5.70V to 0.35 V on a 120 V base voltage. Global MSE for voltages was reduced by 99.0% and global voltage variation by 81.5% from 4.00V to 0.75V on a 120 V base voltage. The results show that the MSE of voltages were reduced by approximately two orders of magnitudes both locally and globally. The reductions in the maximum local voltage variations at node 675 and the maximum global voltage deviations were also significant. The studies performed for the 13-node test feeder demonstrated that the distributed control approach is effective for reducing voltage fluctuations caused by intermittency of PV generations.

5.4.2. Results for 37-node radial distribution test feeder

The presented local control approach was also applied to the 37-node radial distribution test feeder, which is already described in section 4.5. The single line diagram for the test system is shown in Figure 15. The 37-node test feeder used for analysis in this section had three PV generators, instead of two, connected at nodes 727, 732, and 736. The voltage fluctuations for phase A with and without the local reactive with PV sources installed at nodes 727, 732, and 736 are shown in Figure 18. The voltage fluctuations are also significantly reduced for the 37-node test feeder with the distributed local reactive power control. The PV systems installed at nodes 727, 732, and 736 have a rated 1600 kW real power output each. The generation profiles for a different 30-minute study period are shown in Figure 19. Similar to the 13-node test feeder the generation profiles are derived from the one-second global irradiance recorded collected at NREL solar Measurement Grid at Oahu, HI [71].

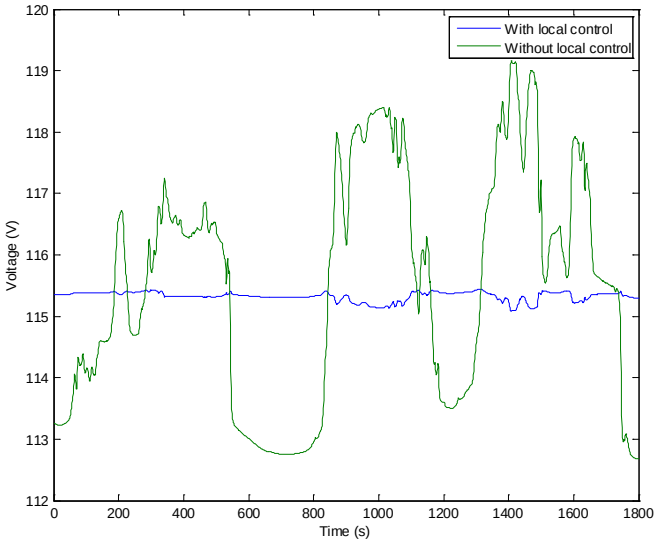

Figure 18: Voltage at node 741 of the 37-node test feeder with 1600 kW PV systems installed at nodes727, 732, and 736.

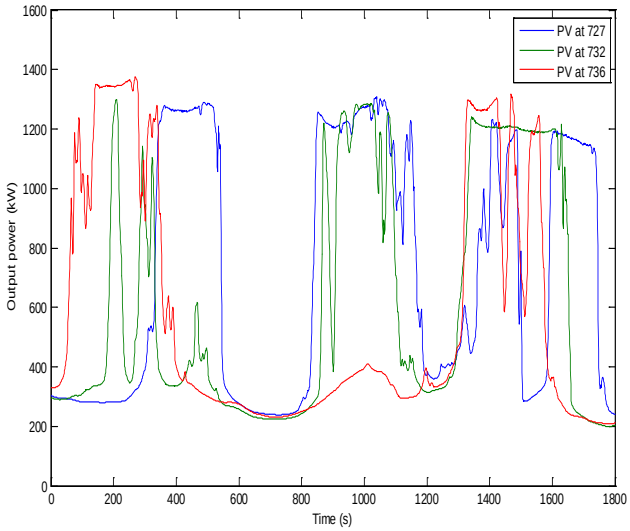

Figure 19: PV generation profiles for 1600 kW systems installed at nodes727, 732, and 736.

Table 5.2: Voltage fluctuations with and without distributed reactive power control of PV inverters installed at nodes 727, 732, and 736.

Measurement	**With Q control**	**Without Q control**
PU MSE_V at node 741	1.18×10^{-6}	2.43×10^{-4}
PU $Max_{\Delta V}$ at node 741	2.84×10^{-3}	5.33×10^{-2}
PU global MSE_V	1.30×10^{-6}	7.90×10^{-5}
PU global Max_{Ve}	6.16×10^{-3}	3.59×10^{-2}

The voltage fluctuations are further analyzed in Table 5.2. The columns and rows of Table 5.2 are described the same way as in Table 5.1. The results indicate that the local reactive power control reduced the local MSE measured at 741 by 99.5%. The local voltage variations were reduced by 94.7% from 6.40V to 0.34 V on a 120 V base voltage. Global MSE for voltages was reduced by 98.2% and global voltage variation by 82.3%

from 4.30V to 0.74V on a 120 V base voltage. The results show that the MSE of voltages were reduced by approximately two orders of magnitudes both locally and globally. The reductions in the maximum local voltage variations at node 675 and the maximum global voltage deviations were also significant. The studies performed for the 13-node test feeder demonstrated that the distributed control approach is effective for reducing voltage fluctuations caused by intermittency of PV generations.

5.5. Local control conclusions

This chapter presented an application of fast local reactive power control of PV inverters in distribution systems to limit voltage fluctuations caused by intermittency in PV generation. The proposed algorithm considered a local reactive power control of multiple PV inverters on a distribution feeder to minimize voltage fluctuations at main feeder tie nodes closest to the PV generator. With the target set on the main feeder, the voltage fluctuations were also similarly limited at the downstream feeder locations from the main feeder tie points. It is important to limit the fluctuations on the downstream nodes due to the voltage drop or rise on the distribution lines, their operational voltages are often the closest to the specified voltage limits.

The proposed distributed control approach was compared to a case without fast reactive power control and the method was shown effective for reducing voltage fluctuations significantly. The proposed algorithm was applied to modified IEEE 13 node and IEEE 37 node radial distribution test feeders, each with three PV plants. Multiple loading and generation conditions were considered to study the performance of the proposed algorithm. The results obtained displayed significant reductions in both the mean and maximum voltage fluctuations caused by the irradiance variations.

6. FAST GLOBAL REACTIVE POWER CONTROL OF DG

The fast global reactive power control approach for multiple PV inverters is presented in this chapter. Unlike the local control approach, presented in the previous chapter, the fast global reactive power control targets the voltage fluctuations at all nodes on the distribution feeder. The fast reactive power control approach formulates the reactive power injection by multiple PV inverters as a quadratic programming (QP) problem. The objective of the problem is to minimize the mean squared error between voltage set points and actual feeder voltages. The approach requires a fast communication channel between the PV devices. Because of the communication needs the approach is best suited for Smart Grid application. The work discussed in this chapter is based on the research work presented in [15] .

6.1. Introduction

The distribution power systems are expected to contain progressively more PV generation units in the future. The amount of PV generation that can be integrated into a power grid is limited due to reasons such as intermittency in generation. As mentioned in chapter 5 the solar irradiance is known to change as much as 60% in one second [57] [58] due to cloud movement and other external weather conditions. As PV penetration into the distribution feeder increases the intermittency in PV generation is known to cause power quality issues, including voltage fluctuations [72]. As the number of PV devices connected to the distribution system increases the voltage fluctuations are known to increase. The voltages in a distribution system are bounded by the ANSI standard in the US between 114V and 126V on a 120 V base [6]. The fluctuations in PV output can cause feeder voltages to exceed the ANSI bounds.

As previously discussed in chapter 5 the fluctuations in PV generation can be substituted with real power injection to limit the voltage fluctuations. Energy storage systems (ESSs) such as battery backup systems and capacitor systems can be used to provide the lost PV generation. The ESSs can be effective for limiting the voltage fluctuations as the rate of change in real power output can be limited. The existing ESSs are typically expensive to install and they also introduce loss to the system. The PV generation can also be controlled by curtailment. An active power control method for multiple PV generators is presented in [73]. The goal of the control to is to limit the rate of change in generation by using active power control. Using curtailment as the main control is not ideal, because as the maximum capacity of PV generation will not be utilized.

As also discussed in previous chapter 5, the voltage fluctuations can be limited by controlling the reactive power output of the PV generations. PV generation units, which are connected to the distribution grid via power electronic interfaces, are capable to inject and consume reactive power based on system demand. Reactive power injection by smart PV inverters is included in the VVC for example in the work presented in [13] [14] [38] [43]. Their computational algorithms and the response times of the mechanical distribution control devices, such as LTC transformers and voltage regulators, typically limit the VVC techniques. For these reasons VVC techniques are typically unable to limit the fast voltage fluctuations, caused by the intermittency, in real time.

A time-based strategy for power factor control at the point of common coupling is presented in [74]. The approach uses statistical analysis of generation data to control the power factor. Another approach for local control based on voltage sensitivity analysis is

presented in [75]. Local active power dependent control of multiple PV devices based on the sensitivity analysis is addressed in [76]. A complex mathematical model to consider multiple PV sources for voltage support by reactive power compensation is described in [77]. A local linear control based substitution factor approach is proposed in [56]. The distributed local linear control approach is extended to multiple PV inverters, target specific system nodes, and studied for a larger distribution system in chapter 5. The local control approach is also included as the fast reactive power control layer of a dual-layer VVC approach in [14] and Chapter 7. The local control is designed to adjust reactive power outputs of PV inverters based on the local generation conditions.

This chapter presents a new coordinated control approach to limit voltage variations in distribution feeders with PV generation. The approach utilizes quadratic programming (QP) to determine optimal reactive power injection schedule for multiple PV inverters to maintain close to constant feeder voltages. Unlike the local control approaches discussed earlier the presented coordinated control approach includes all reactive power injections to the problem and decides the injection to minimize voltage MSEs at all feeder locations. This prevents two PV inverters from taking counteracting control actions and also makes sure that the inverters operate at the optimal way to reduce voltage fluctuations. The approach requires a fast communication channel between the PV inverters and the centralized control. For this reason the presented coordinated control approach is ideal for smart grid applications.

The theory and application of the QP based coordinated control approach is presented in section 6.2. Case studies to validate the presented approach are discussed in section 6.3. The sections 6.4 and 6.5 present the results for the case studies. They are

derived from the original work presented in [15]. Section 6.6 concludes the technique discussed in this chapter.

6.2. Quadratic programming based global fast VAR control

The goal of the global reactive power control is to optimize reactive power injection of multiple PV inverters to limit voltage fluctuations at all feeder nodes. The control is formulated as a QP problem. The problem is constrained by the voltage sensitivity equations at the operating point, ANSI voltage bounds, and the reactive power injection limits of the PV inverters. The voltage sensitivity equations are determined from the classical sensitivity approach presented in section 5.2. The theory for QP is presented in following section 6.2.1 and formulation of the coordinated reactive power control of multiple PV inverters as a QP problem is presented in 6.2.2. The theory section is based on the original work presented in [15].

6.2.1. Quadratic programming

The proposed reactive power control is formulated as a standard QP problem. A QP problem is a mathematic optimization problem, which has quadratic terms in its objective function, is constrained by variable bounds, linear equality constraints, and linear inequality constraints. Commercial optimization solvers, such as IBM CPLEX, are able to efficiently solve standard QP problems to their optimality. The objective function of a standard QP problem is written as follows:

$$min_x \ \frac{1}{2}\boldsymbol{x}^T\boldsymbol{H}\boldsymbol{x} + \boldsymbol{f}^T\boldsymbol{x} \tag{6.1}$$

where $\boldsymbol{x}$ is the optimization variable vector, $\boldsymbol{H}$ is a matrix containing quadratic and bilinear terms, $\boldsymbol{f}$ is a vector containing linear terms, and T denotes the transpose of a vector.

The objective function (6.1) is constrained by the linear equality constraints, linear inequality constraints, and variable bounds. Mathematically the constraints of the optimization problem are presented as follows:

$$\boldsymbol{A_{eq}x = b_{eq}} \tag{6.2}$$

$$\boldsymbol{Ax \leq b} \tag{6.3}$$

$$\boldsymbol{lb \leq x \leq ub} \tag{6.4}$$

where $\boldsymbol{A_{eq}}$ and $\boldsymbol{b_{eq}}$ in (6.2) describe the linear equality constraints, $\boldsymbol{A}$ and $\boldsymbol{b}$ in (6.3) describe the linear inequality constraints, and $\boldsymbol{lb}$ and $\boldsymbol{ub}$ in (6.4) describe lower and upper bounds for the variable vector $\boldsymbol{x}$.

6.2.2. Formulation of the global reactive power control as a QP problem

The global fast reactive power control is formulated as a QP problem in this section. The QP problem is constrained by the classical voltage sensitivity analysis, which is described previously in section 5.2. In order to limit the global voltage fluctuations all nodes on the distribution feeder and the mean squared error (MSE) approach is utilized. The objective function to be minimized is written as a summation of squared voltage errors across the feeder.

$$\min \sum_{i=1}^{n} (e_i)^2 \tag{6.5}$$

where

$$e_i = V_{SP(i)} - V_i \tag{6.6}$$

where e_i represents the voltage deviation, or the voltage error, at node *i*, and *n* is the total number of nodes in the system, $V_{SP(i)}$ is the set point voltage at node *i*, and V_i is the actual voltage at node *i*. As seen in (6.6) the voltage deviation, or the voltage error, is defined as

the difference between set-point voltage and the node voltage calculated from the voltage sensitivity equations.

The optimization variables included in $\boldsymbol{x}$ the vector of voltages determined from voltage sensitivity constraints, $\boldsymbol{V}$;vector of changes in reactive power injection, $\Delta\boldsymbol{Q_{DG}}$; and vector of voltage errors $\boldsymbol{E}$. Mathematically the optimization variable vector is written as follows:

$$\boldsymbol{x} = [\boldsymbol{V} \quad \Delta\boldsymbol{Q_{DG}} \quad \boldsymbol{E}]^{\boldsymbol{T}} \tag{6.7}$$

where

$$\boldsymbol{V} = [V_1 \quad V_2 \quad \dots \quad V_n] \tag{6.8}$$

$$\Delta\boldsymbol{Q} = [\Delta Q_{DG1} \quad \Delta Q_{DG2} \quad \dots \quad \Delta Q_{DGn}] \tag{6.9}$$

$$\boldsymbol{E} = [e_1 \quad e_2 \quad \dots \quad e_n] \tag{6.10}$$

where the V_i is the voltage determined from the voltage sensitivity equations at node *i* and ΔQ_{DGi} is the change in reactive power injection at node *i*. For the nodes that do not have a PV inverter the entries for ΔQ_{DGi} are eliminated from the QP formulation as the reactive power injection at that node cannot change.

As the cost function is a summation of squared error terms and the $\boldsymbol{H}$ matrix contains the squared and bilinear terms, mentioned in (6.1). This can be written as a diagonal matrix with zero entries for ${V_i}^2$ and ${Q_i}^2$ components and ones for ${e_i}^2$ error components. Mathematically the $\boldsymbol{H}$ matrix is written as follows:

$$\boldsymbol{H} = \begin{bmatrix} \mathbf{0} & & \\ & \mathbf{0} & \\ & & \boldsymbol{I} \end{bmatrix} \tag{6.11}$$

where $\boldsymbol{I}$ denotes an identity matrix corresponding to the squared error terms. As the objective function formulation does not contain any linear terms $\boldsymbol{f}$ is a zero vector as defined below:

$$\boldsymbol{f} = [0 \quad 0 \quad ... \quad 0] \tag{6.12}$$

The linear equality constraints, described in (6.1), are written determined from the classical voltage sensitivity analysis and discussed in detail in section 5.2. It is known that around the feeder operating point, the voltages can be linearized as:

$$\boldsymbol{V} \approx \boldsymbol{V_0} + \boldsymbol{A_P}\Delta\boldsymbol{P_{DG}} + \boldsymbol{A_Q}\Delta\boldsymbol{Q_{DG}} \tag{6.13}$$

where $\boldsymbol{V_0}$ is a vector containing the voltage magnitudes at the feeder operating point, $\boldsymbol{V}$ is a vector representing the feeder voltage magnitudes as the DG outputs change, $\boldsymbol{A_P}$ and $\boldsymbol{A_Q}$ are voltage sensitivity coefficient matrices that are partial derivatives of $\boldsymbol{V}$, $\Delta\boldsymbol{P_{DG}}$ represent the change in real power injection by the DG, and $\Delta\boldsymbol{Q_{DG}}$ represent the change in reactive power injection by the DG. By replacing ≈ with an equals sign, and transferring the $\boldsymbol{A_Q}\Delta\boldsymbol{Q_{DG}}$ term to left side of the equals sign in (6.13), the first linear equality constraint equation is written as:

$$\boldsymbol{V} - \boldsymbol{A_Q}\Delta\boldsymbol{Q_{DG}} = \boldsymbol{V_0} + \boldsymbol{A_P}\Delta\boldsymbol{P_{DG}} \tag{6.14}$$

The second linear equality constraint equation can be determined from the error equations determined for a single node in (6.6). The error equation for all feeder nodes can be written as:

$$\boldsymbol{E} = \boldsymbol{V_{SP}} - \boldsymbol{V} \tag{6.15}$$

where $\boldsymbol{V_{SP}}$ is a vector containing the voltages at the set point. By transferring all components included in the variable vector $\boldsymbol{x}$ to the left hand side of the equal sign (6.15) can be re-written as:

$$\boldsymbol{V} + \boldsymbol{E} = \boldsymbol{V_{SP}} \tag{6.16}$$

With the formulation presented in (6.14) and (6.16) the linear equality constraints for QP problem formulation can be written as:

$$\boldsymbol{A_{eq}} = \begin{bmatrix} \boldsymbol{I} & -\boldsymbol{A_Q} & \boldsymbol{0} \\ \boldsymbol{I} & \boldsymbol{0} & \boldsymbol{I} \end{bmatrix} \tag{6.17}$$

and

$$\boldsymbol{b_{eq}} = \begin{bmatrix} \boldsymbol{V_0} + \boldsymbol{A_P}\Delta\boldsymbol{P_{DG}} \\ \boldsymbol{V_{SP}} \end{bmatrix} \tag{6.18}$$

In the presented QP based reactive power control problem the change in reactive power, $\Delta\boldsymbol{Q}$, included in the variable vector $\boldsymbol{x}$, is bounded by the reactive power limits of the PV inverters. The bounds for reactive power injection are dynamic as they depend on the real power generated by the PV inverter at time *t*, $P_{PV}(t)$, by the apparent power limit of the PV inverter S_l, and also by the reactive power injection at the operating point Q_{OP} at which the voltage sensitivities are determined:

$$-\sqrt{{S_l}^2 - P_{PV}^2(t)} - Q_{OP} \leq \Delta Q_{PV}(t) \leq \sqrt{{S_l}^2 - P_{PV}^2(t)} - Q_{OP} \tag{6.19}$$

The voltage deviations from the set point values, or the voltage errors, are set to be minimized, and therefore, are set to be unbounded to reduce the complexity of the formulation. The voltage standard between 114 V and 126 V on a 120V base voltage binds the ANSI distribution voltage standard. In terms of the rated voltage of the distribution feeder this means that the voltages are bounded between 95% and 105% of the rated distribution voltage, V_r. The variable vector upper and lower bounds $\boldsymbol{lb}$ and $\boldsymbol{ub}$ are written as:

$$\boldsymbol{lb} = [\boldsymbol{V_{lb}} \quad \Delta\boldsymbol{Q_{lb}} \quad -\infty] \tag{6.20}$$

$$\boldsymbol{ub} = [\boldsymbol{V_{ub}} \quad \Delta\boldsymbol{Q_{ub}} \quad \infty] \tag{6.21}$$

where

$$\boldsymbol{V_{lb}} = [0.95 \cdot V_r \quad \cdots \quad 0.95 \cdot V_r] \tag{6.22}$$

$$\boldsymbol{V_{ub}} = [1.05 \cdot V_r \quad \cdots \quad 1.05 \cdot V_r] \tag{6.23}$$

$$\Delta \boldsymbol{Q_{lb}} = \left[-\sqrt{\left(S_{l_1}\right)^2 - \left(P_{PV_1}(t)\right)^2} - Q_{OP_1} \quad \cdots \quad -\sqrt{\left(S_{l_n}\right)^2 - \left(P_{PV_n}(t)\right)^2} - Q_{OP_n} \right] \tag{6.24}$$

and

$$\Delta \boldsymbol{Q_{ub}} = \left[\sqrt{\left(S_{l_1}\right)^2 - \left(P_{PV_1}(t)\right)^2} - Q_{OP_1} \quad \cdots \quad \sqrt{\left(S_{l_n}\right)^2 - \left(P_{PV_n}(t)\right)^2} - Q_{OP_n} \right] \tag{6.25}$$

where $P_{PV_i}(t)$ is the total real power injected at node *i*, S_{l_i} is the PV inverter apparent power limit at node *i*, and Q_{OP_i} is the reactive power injected at the operating point at node *i*.

6.3. Case studies

To evaluate the performance of the presented coordinated control approach two distribution test feeders were used. Like in the case studies presented for the distributed control approach in Chapter 5 two test feeder based on the IEEE 13-node radial distribution test feeder and IEEE 37-node radial distribution test feeder were used. The test systems are described in detail in [49] [54] [55]. A one-line diagram of a 13-node distribution test feeder is shown in Figure 14. Similar to the case studies for the local control approach, three PV inverters were added to nodes 632, 675, and 680. In order to validate the performance of the proposed algorithm with different PV system sizes, small, medium, and large sized PV systems were considered. The size of each small system was set to 200 kW meaning that the total amount of the PV generation in the 13-node distribution feeder is approximately 15% of the load conditions for the feeder, as shown

in Table 4.7. The medium sized PV systems were selected as 900 kW each and large as 2000 kW each.

The 37 node test feeder used was also a three-phase distribution feeder modified from the IEEE 37 node radial distribution test feeder. A single line diagram of the test feeder is shown in Figure 15. As in case study in section 5.4.2 three PV inverters were connected to nodes 727, 732, and 736 of the 37-node distribution test feeder. Three PV systems sizes, small, medium and large, were also considered. The small system were sized at 150 kW this is slightly more than 15% of the total load of the 37-node distribution system as described in [55]. The medium sized PV systems were selected as 800 kW each and large as 1600 kW each.

Like in the case studies presented for the local reactive power control in chapter 5, the PV generation outputs were determined from the real-life one-second irradiance data recorded at NREL Solar Measurement Grid in Oahu, HI [71]. The same specific locations as described in section 5.4.1 were used. The use of one second irradiance data is appropriate because maximum power point tracking (MPPT) algorithms are capable of converging to the optimal real power output very quickly. The data used for this study was collected on July 20, 2010. The specific locations for the measurements were DH3, AP1, and AP6 on the NREL measurement grid. The locations are displayed on map in [71]. The irradiance data was converted into normalized PV generation levels. The normalized generation levels were then applied to the PV sources with their rated output power.

The feeder voltages were calculated with a custom Matlab program utilizing the ladder-iterative distribution power flow approach described in detail in [8]. The power

flow approach is based on Kirchhoff's current and voltage laws are known to converge fast for unbalanced radial distribution feeders. To solve the coordinated reactive power control as QP problem IBM CPLEX v.12.1 interfaced with Matlab was utilized. CPLEX was interfaced with Matlab using a third party optimization toolbox, OPTI Toolbox, discussed in [46].

The study performed for the two test systems evaluated the performance of the control in terms of local and global MSE of per unit voltages, local voltage variations, and global maximum voltage deviations from their set points during few 30-minute study intervals. Small, medium, and large PV systems were considered and compared for each test system. The results of the case studies are shown in the following sections 6.4 and 6.5.

6.4. Results for 13-node radial distribution test feeder

The first test system was a radial distribution feeder modified from the IEEE 13 node test feeder. The system consists of overhead and underground distribution lines, and system loading was highly unbalanced. The outputs of each PV source were determined from the irradiance patterns collected at the NREL Solar Measurement Grid, and are shown in Figure 20 for a 30-minute time interval around noon for the large PV systems. The irradiance data was collected on July 20, 2010 and the generation outputs were determined from the irradiance profiles. The PV generation variability was extremely large within the interval studied.

The objective of the coordinated reactive power control approach is to limit the global voltage fluctuations on the distribution feeder. For example, the phase C voltage fluctuations at node 675 are shown in Figure 21, Figure 22, and Figure 23 and

respectively for the small, medium, and large PV systems with and without the control. Figure 21, Figure 22, and Figure 23 demonstrate that large voltage fluctuations occur without the control, but these fluctuations can be significantly reduced with the global control.

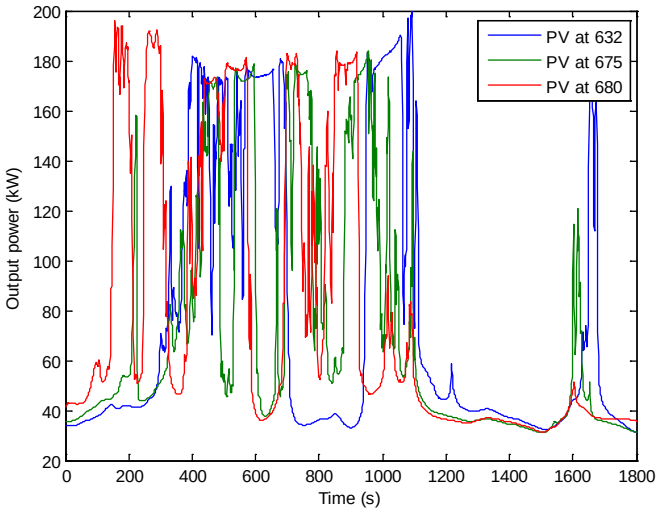

Figure 20: PV outputs for 200 kW PV systems installed at nodes 632, 675, and 680 on IEEE 13 node test feeder.

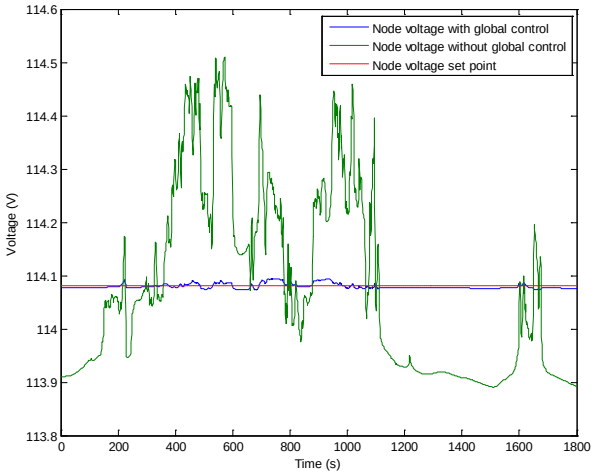

Figure 21: Phase C voltage measured at node 675 on the IEEE 13 node radial distribution test feeder with 200 kW PV systems installed at nodes 632, 675, and 680.

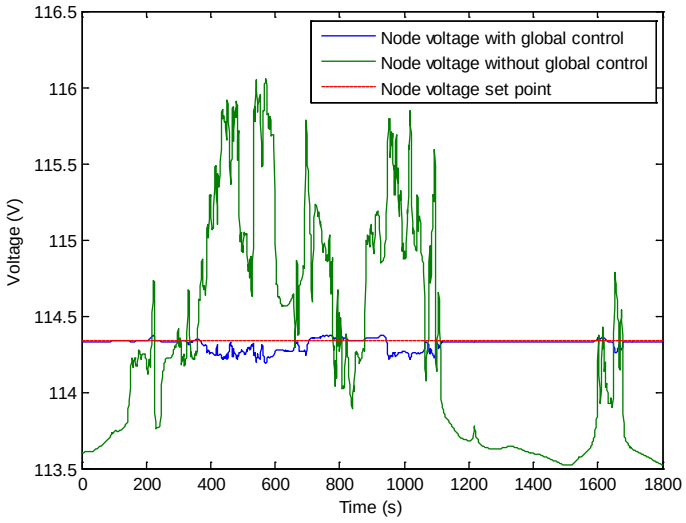

Figure 22: Phase C voltage measured at node 675 on the IEEE 13 node radial distribution test feeder with 900 kW PV systems installed at nodes 632, 675, and 680.

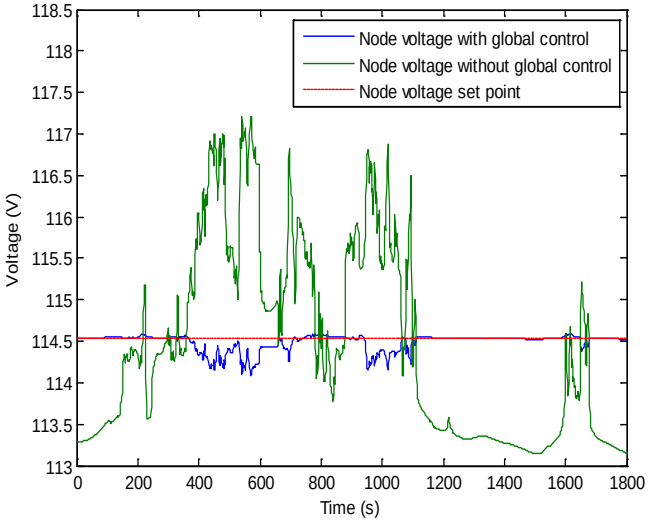

Figure 23: Phase C voltage measured at node 675 on the IEEE 13 node radial distribution test feeder with 1600 kW PV systems installed at nodes 632, 675, and 680.

The reactive power injected to the node 632 is recorded in Figure 24. The changes in reactive power injection, determined by the QP approach, are seen to follow the generation profile for PV source at node 632, presented in Figure 20. The reactive power

injection is significantly smaller than the real power injection and will not exceed the apparent power bounds set for the inverter.

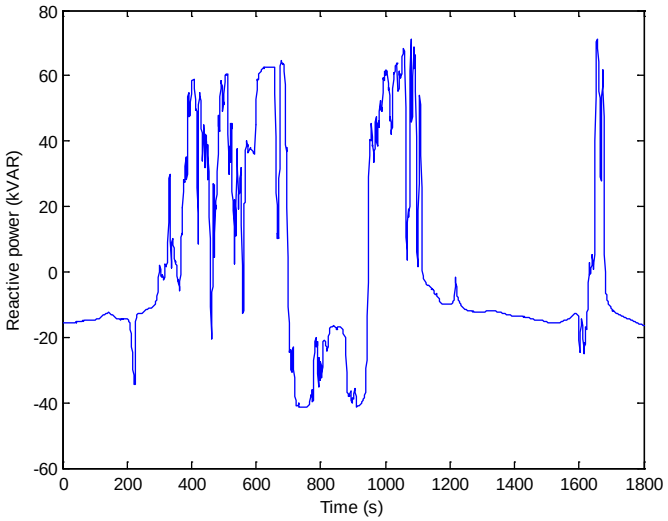

Figure 24: Reactive power injected to phase C at node 632 by the 900 kW PV inverter.

Table 6.1 displays the measured voltage fluctuation with and without the proposed control approach for the 13-node distribution test feeder. The first column describes the type of voltage fluctuation measured. The second through fifth columns display the fluctuations measured for the medium and large PV systems with and without the control. In the first column, PU denotes per unit, MSE_V denotes mean squared voltage error from voltage set points, $Max_{\Delta V}$ denotes the maximum local voltage variation at node 675, and Max_{Ve} denotes the maximum global voltage error. The maximum local voltage variation is defined as the difference between the maximum local voltage and the minimum local voltage measured during the study interval. The maximum global voltage error is defined as the maximum difference between the actual voltages and the voltage set points considering all of the system nodes. Percent reductions in voltage fluctuations are shown in Table 6.2.

Table 6.1: Voltage fluctuations with and without local control on the study interval for 13-node radial distribution feeder with 200 kW, 900 kW, and 1600 kW PV systems.

	200 kW systems		**900 kW systems**		**1600 kW systems**	
Measurement	Qc	No Qc	Qc	No Qc	Qc	No Qc
PU MSE_V at node 675	1.81×10^{-9}	2.06×10^{-6}	2.44×10^{-7}	3.54×10^{-5}	2.00×10^{-6}	9.69×10^{-5}
PU $Max_{\Delta V}$ at node 675	1.68×10^{-4}	5.20×10^{-3}	1.70×10^{-3}	2.11×10^{-2}	5.00×10^{-3}	3.44×10^{-2}
PU global MSE_V	19.4×10^{-9}	1.06×10^{-6}	1.04×10^{-7}	1.87×10^{-5}	9.13×10^{-7}	5.17×10^{-5}
PU global Max_{Ve}	1.48×10^{-4}	4.40×10^{-3}	2.10×10^{-3}	1.85×10^{-2}	5.9×10^{-3}	3.08×10^{-2}

Table 6.2: Reduction in voltage fluctuations for 13-node test system with PV systems installed at nodes 632, 675, and 680.

Reduction in	**200 kW systems**	**900 kW systems**	**1600 kW systems**
PU MSE_V at node 675	99.92%	99.31%	98.65%
PU $Max_{\Delta V}$ at node 675	96.81%	91.97%	86.11%
PU global MSE_V	99.98%	99.45%	98.65%
PU global Max_{Ve}	96.81%	88.42%	83.88%

The results in Table 6.2 show that the MSE of voltages were reduced by approximately two orders of magnitudes, both locally and globally, and the reductions were not significantly decreased between the small medium and large PV systems. The reductions in the maximum local voltage variations at node 675 and the maximum global voltage deviations were also significant. The best performance in terms of reductions was observed with the smallest PV systems. The studies performed for the 13-node test system demonstrated that the proposed approach is effective for reducing voltage fluctuations caused by intermittency of PV generations.

6.5. Modified IEEE 37 node radial distribution test feeder

The second test system selected was also a three-phase distribution feeder modified from the IEEE 37 radial node test feeder. Three PV inverters were connected to nodes 727, 732, and 736 of the 37-node test feeder. All of the distribution lines were underground and system loading was unbalanced. Three test system sizes were considered. The small system were sized 150 kW each, medium systems were 800 kW each, and large systems 1600 kW each. Another 30-minute time interval around noon was selected for the 37-node test system: this interval also showed large variability in PV generation. The outputs of the PV generation were determined from the irradiance patterns collected at the NREL Solar Measurement Grid on July 20, 2010. The outputs of the PV generation units are shown in Figure 25 for the 800 kW PV systems.

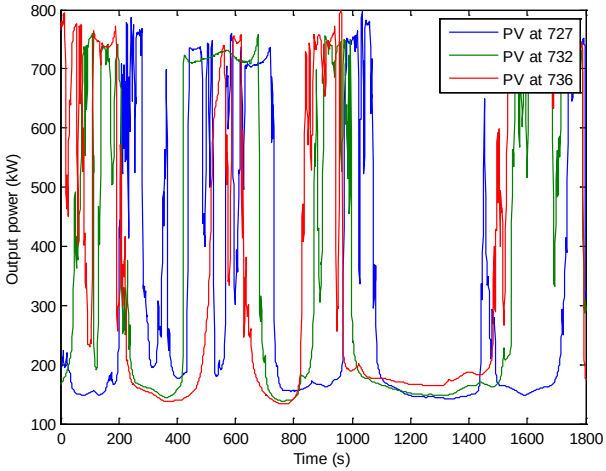

Figure 25: PV outputs for 800 kW PV systems installed at nodes 727, 732, and 736.

The presented global reactive power control limits the voltage fluctuations at each node of the feeder. For example, phase A voltage variations at node 741 are shown in Figure 26, Figure 27, and Figure 28 and respectively for the small, medium, and large PV systems with and without the control. Figure 26, Figure 27, and Figure 28 demonstrate that large voltage variations occur without the coordinated reactive power control, but the voltage variations are significantly reduced with the coordinated global voltage control. In the large system the maximum voltage variations on phase A at node 741, shown in Figure 28, are observed as high as 7.47 V on 120 V base voltage without the control, but are reduced to less than 0.94 V with the coordinated reactive power control. That is reduction of almost 85%. By observation of Figure 26, Figure 27, and Figure 28 the fluctuations were significantly reduced with the global control. Table 6.3 displays the voltage fluctuation with and without the proposed control for the 37-node radial distribution test feeder. The rows and columns of Table 6.3 are described same as Table 6.1 rows and columns.

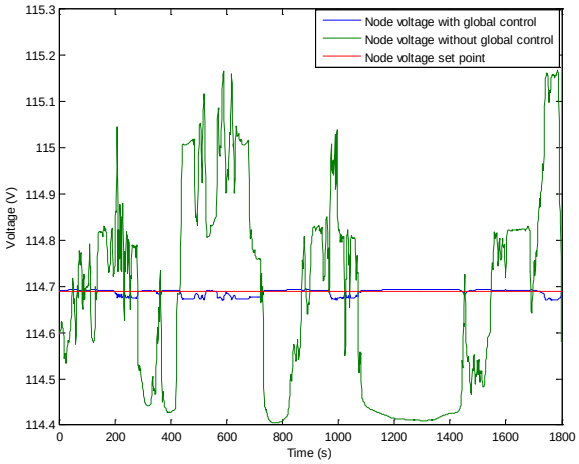

Figure 26: Phase A voltage measured at node 741 on the IEEE 37 node radial distribution test feeder with 150 kW PV systems installed at nodes 727, 732, and 736.

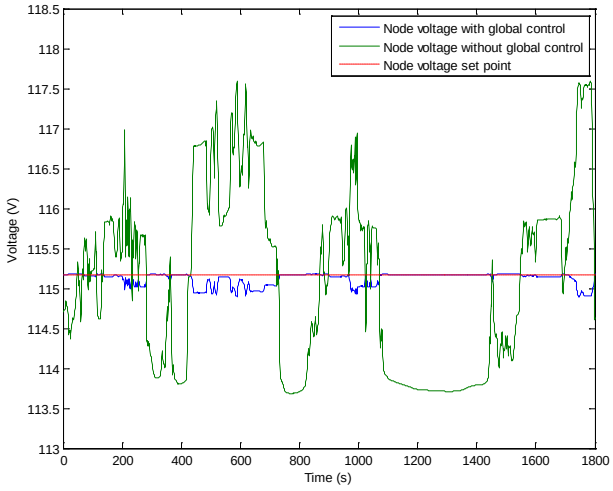

Figure 27: Phase A voltage measured at node 741 on the IEEE 37 node radial distribution test feeder with 800 kW PV systems installed at nodes 727, 732, and 736.

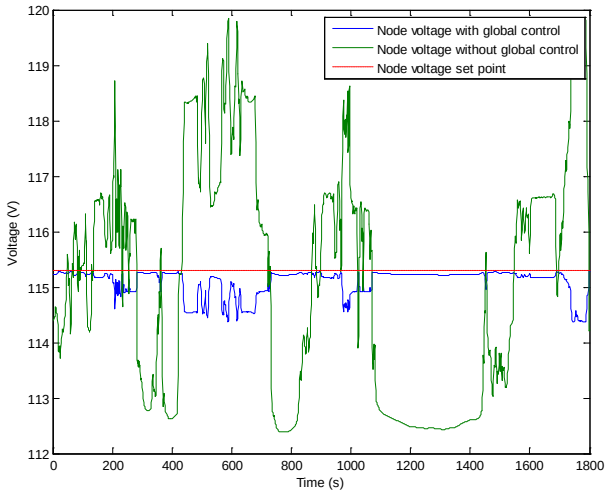

Figure 28: Phase A voltage measured at node 741 on the IEEE 37 node radial distribution test feeder with 1600 kW PV systems installed at nodes 727, 732, and 736.

Table 6.3: Voltage fluctuations with and without local control on the study interval for 37-node radial distribution feeder with 150 kW, 800 kW, and 1600 kW PV systems.

	150 kW systems		**800 kW systems**		**1600 kW systems**	
Measurement	Qc	No Qc	Qc	No Qc	Qc	No Qc
PU MSE_V at node 741	2.56×10^{-9}	3.36×10^{-6}	4.65×10^{-7}	8.91×10^{-5}	6.91×10^{-6}	3.31×10^{-4}
PU $Max_{\Delta V}$ at node 741	1.56×10^{-4}	6.35×10^{-3}	2.06×10^{-3}	2.37×10^{-2}	7.79×10^{-3}	6.23×10^{-2}
PU global MSE_V	17.9×10^{-9}	1.16×10^{-6}	9.98×10^{-8}	3.09×10^{-5}	1.73×10^{-6}	1.16×10^{-4}
PU global Max_{Ve}	4.10×10^{-4}	4.68×10^{-3}	2.23×10^{-3}	2.37×10^{-2}	7.79×10^{-3}	4.47×10^{-2}

Table 6.4: Reduction in voltage fluctuations for 37-node test system with PV systems installed at nodes 727, 732, and 736.

Reduction in	150 kW systems	800 kW systems	1600 kW systems
PU MSE_V at node 741	99.92%	99.48%	97.91%
PU $Max_{\Delta V}$ at node 741	97.55%	93.67%	87.48%
PU global MSE_V	99.98%	99.68%	98.51%
PU global Max_{Ve}	91.25%	90.56%	82.59%

Similar to the 13-node test feeder both the local and global MSE were reduced by approximately two orders of magnitude. The maximum local voltage variations and maximum global voltage errors were reduced in a similar fashion as was presented for the 13-node distribution test feeder. The studies performed for the 37-node distribution test feeder again demonstrated that the proposed approach is effective for reducing voltage fluctuations caused by the intermittency of PV generation.

6.6. Discussion on fast global reactive power control

The presented coordinated reactive power control showed significant reductions in voltage variations. It was determined that for a good control performance sensitivity matrices need to be determined close to the system operating point. The computational time to find new voltage sensitivity matrices was recorded as 2.9 seconds for the 13-node distribution test feeder and as 6.3 seconds for the 37-node distribution test feeder. The system used to perform these calculations was a Dell T1500 desktop computer using an Intel Core i-5 processor. Each test feeder had three PV sources. To determine the voltage sensitivity matrices by utilizing the classical sensitivity approach one thousand power

flows were performed for each source around its operating point. The computational time to calculate voltage sensitivity matrices increases as the system size increases. For this reason the voltage sensitivities for small systems can be updated with a parallel calculation model, but for much larger systems a pre-determined look-up table for sensitivities could potentially be more suitable.

The computational time of the quadratic program was measured between 2 and 4 milliseconds for the 13-node distribution test feeder and between 6 and 8 milliseconds for the 37-node distribution test feeder. The same Dell T1500 computer was also used for these calculations. A slight increase in computational time was observed with the size increase of the test system. The observed increase was small and did not affect the performance of the control. The fast computational times observed that the approach shows promise for on-line reactive power control in the Smart Grid distribution feeders with fast communication channel between the PV devices.

The coordinated control approach achieved reductions with in both test systems were significant. Both systems saw a large reduction in terms of MSE values. The local voltage variations and global voltage deviations also reduced similarly in both systems. Simulations, on both test feeders, have exhibited effectiveness of the proposed approach for reducing voltage fluctuations. The proposed method will also reduce the wear and tear of traditional controllers involving mechanical parts.

6.7. Conclusions

A new control approach for global reactive power control of multiple PV inverters was introduced in this chapter. The work presented is based on the original work discussed in [15]. The coordinated reactive power control of multiple PV inverters was

formulated as a QP problem. The problem was constrained by linear voltage sensitivities calculated at the feeder operating conditions. The sum of the squared voltage deviations from voltage set points was the objective to be minimized. The performance of the proposed control was studied with two test systems based on the IEEE 13-node and IEEE 37-node radial distribution test feeders and with one second solar irradiance data recorded at NREL Solar Measurement Grid. The results showed that the presented control algorithm is effective for on-line application in the Smart Grid distribution feeders to limit voltage fluctuations due to intermittency of PV generation.

7. DUAL-LAYER CONTROL RESULTS WITH FAST LOCAL CONTROL

In the previous chapters 3 and 5 distribution system wide VVC and local reactive power control of PV inverters were respectively discussed. This chapter combines the feeder wide MINLP based VVO approach and the fast local reactive power control of PV inverters to form a dual layer control approach that can be utilized for distribution systems. The theory and studies presented in this section are based on the original work discussed in [14].

7.1. Introduction

The study presented in this chapter combines the fast-acting reactive power control of PV inverters with the slower MINLP base VVO approach to form a dual-layer distribution feeder VVC. The fast-acting local inverter reactive power control is used to limit the voltage fluctuations during the computational period of the MINLP based VVC algorithm. The presented VVC approach first globally determines the optimal control settings for the traditional distribution feeder controls and set points for the reactive power injection for PV inverters. The local inverter reactive power control is utilized to maintain the feeder voltages close to the voltage levels determined by the MINLP based VVO algorithm. The basic idea of the dual-layer VVC is presented in Figure 29.

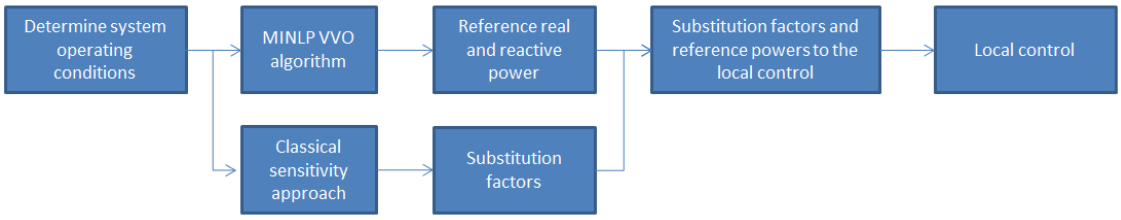

Figure 29: Dual-layer VVC flow chart

The first step in the presented dual-layer VVC is to determine the system operating conditions including loading and generation conditions. The system operating

conditions are sent to the MINLP based VVO algorithm and to the parallel calculation algorithm that determines the voltage sensitivities. The MINLP based VVO algorithm produces reference real and reactive power outputs and the substitution factors are calculated parallel to the MINLP algorithm. When the substitution factors and reference real and reactive power values are both determined they are sent to local PV reactive power controllers. The MINLP based VVO and parallel sensitivity calculations are defined as the first layer control and the local reactive power control of the PV inverters is defined as the second layer control. The local controllers limit the voltage variations in distribution nodes as described earlier in chapter 5.

The local control algorithm requires only periodic updates for the power reference values from the global VVC algorithm and substitution factors determined from the parallel sensitivity calculations. The rest of the data utilized in local control is completely local and independent from the first level of the dual-layer control. Multiple local controllers can work independently from each other with good results as shown in the chapter 5. The local control by the linear controller is very fast, and thus, can respond to any PV fluctuations in real-time. The results in section 7.3 illustrate how the PV inverters can limit the voltage fluctuations within the fifteen-minute intervals determined by the first control layer.

Together with the first layer control approach the local PV inverter controllers can maintain the voltage levels in the feeder very close to optimized voltage levels. Keeping the voltages at the optimized levels can improve the economics of the system by keeping load demand at a minimum. The control also improves in preventing power quality issues

such as voltage fluctuation and exceeded voltage bounds in the distribution feeder as the solar irradiance fluctuates.

7.2. Case study for 37-node radial distribution test feeder

To examine the dual-layer control approach a three-phase radial distribution feeder based on the IEEE 37 node radial distribution test feeder is used. The IEEE 37 node radial distribution test feeder is described, in detail, in [49] and [55]. A single line diagram of the test system is shown in Figure 15 in an earlier section. The system used in this study has the exact same components, including transformers, distribution lines, and the LTC as the IEEE test feeder. The feeder loading was also very unbalanced for the three phases. Each load was set to follow a normalized 15-minute loading pattern shown in Figure 30.

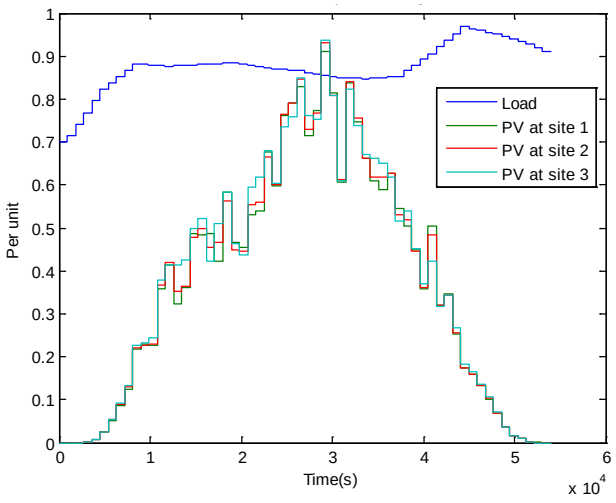

Figure 30: Normalized load level and expected PV generation levels for irradiance data collected on July 22, 2010.

The test feeder had three PV inverters connected to nodes 727, 732, and 736 shown in Figure 15. These PV inverters are able to control the reactive power injection independently for each phase. Figure 30 also displays the normalized PV generation

levels for 15-minute time intervals. For the case study two test cases were considered. In a first test case all three PV inverters had a rated power output of 150 kW each and in the second test case all three PV inverters had a rated power output of 450kW each. The substitution rates were chosen in a way that voltage variations are minimized for main feeder tie-nodes: 703, 708, and 734. The theory displaying how these substitution factors were determined is shown in earlier section 5.3. The nodes selected were electrically the closest to the nodes on the main feeder with respect to the PV inverters.

The power system loading varies throughout the day for this study. It was assumed that load changes to its new value every fifteen minutes. As mentioned previously the first layer control was selected to update the feeder control settings every fifteen minutes. Based on previous solar data a set point value for PV generation level is estimated and used for the VVO calculations. The estimated PV generation levels were used as the real power reference values for the local second control layer.

For the PV generation one second global irradiance data collected at NREL Solar Measurement Grid in Oahu, HI, was used. The specific data used for this study was collected between July 20, 2010 and July 29, 2010. The solar irradiance was measured between 5:00 am and 8:00pm for each day. Three measurement points were used and their specific locations were DH3, AP1, and AP6 on the NREL measurement grid [71]. Normalized 15-minute PV generation levels were estimated from 1-second irradiance data and illustrated in Figure 30. Normalized load levels and PV generation expectancies were used as the inputs for the first layer of optimal control.

The irradiance data used shows a strong correlation between the irradiance levels at the test locations. The strong correlation was expected due to similar cloud movement

patterns and illumination conditions as the three locations were within a close proximity to each other. For the fifteen-minute intervals the irradiance data was almost identical for the three locations, which is also supported by Figure 30.

Short-term generation variability is typically caused by the changes in irradiation such as shading due to cloud movement. This shading can be very rapid as demonstrated by the changes in PV generation for example in Figure 17 and Figure 25. Statistical studies performed for the irradiance data reveal the maximum change in irradiance levels as a function of time as illustrated in Figure 31. Site 1 in Figure 31 is defined the irradiance at node 727, site 2 is defined the irradiance at node 732, and site 3 is defined the irradiance at node 736. For the solar data used in this study it appears that the change in PV generation can be as much as 30% of the total PV generation in one second. As the time interval increases to 10 seconds the change can be almost 70% of the maximum PV output.

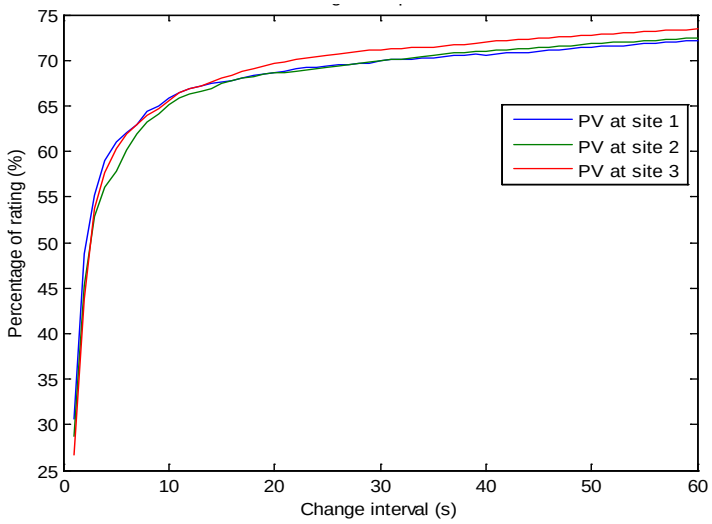

Figure 31: Maximum irradiance variation as a function of time

The proposed dual-layer control approach was applied to the 37-node test feeder with the described irradiance data and load data. The feeder voltages were determined by

performing a series of power flow calculations utilizing the ladder iterative power flow technique, which is described in [8]. The power flows were performed for each second as power generation conditions changed for each second. To demonstrate the improvements achieved over a more traditional VVC the voltage variability was compared to a case where second layer local control was not applied to compensate for the changes in real power outputs of PV generation sources. The results of the case study are discussed in section 7.3.

7.3. 37-node feeder case study results

The proposed dual-layer control approach was applied to the 37-node distribution test feeder, described in the previous section. The MINLP based VVO of the first layer was set to update the LTC positions and PV inverter reactive power injection set points every fifteen minutes as new load level and PV expectations levels became available. The objective of the dual-layer control was to minimize the real power drawn from the distribution substation. The first layer control provided also the real and reactive power set point values to the first layer control. The second layer control was set to continuously control the reactive power injection by the PV inverters to limit the changes in node voltages at the main feeder tie nodes. As discussed previously in Chapter 5 limiting the voltage fluctuation at the main feeder tie points also limits the voltage fluctuations downstream from the tie-node. Therefore, the control also targets the end of the feeder locations that are likely to operate closest to the ANSI specified voltage bounds.

The optimal LTC transformer tap-positions determined for a time interval between 5:00 am and 8:00 pm with July 22, 2010 solar irradiance data and 450 kW PV plants installed at nodes 727, 732, and 736 are illustrated in Figure 32. The tap-positions

were obtained with the first layer MINLP VVO algorithm using expected values for the PV generation. When comparing Figure 32 to Figure 30 a correlation between load levels, PV levels, and LTC tap-positions is apparent. High PV generation levels and low load levels appeared to result in lower tap positions whereas the low PV generation and high load conditions result in higher tap-positions of the LTC.

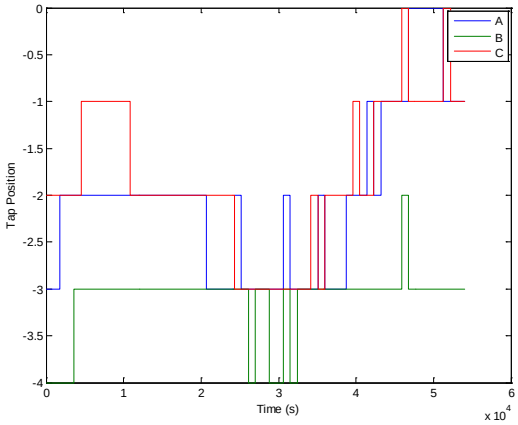

Figure 32: Optimal LTC tap-positions from 5:00 AM to 8:00 PM with solar irradiance data of July 22, 2010 with 450 kW PV systems at nodes 727, 732, and 736.

For the functionality of the dual-layer control a communication channel from the global VVO layer to the local reactive power controllers has to exist. Only a small amount of data is transmitted from the VVO layer to the distributed PV inverters. For this reason even a slow speed communication channel would be sufficient.

Figure 33 displays the power quality improvement achieved with the local reactive power control of PV inverters. The voltage variations on phase A at node 740 are observed with and without the local reactive power control for three 150 kW PV systems at nodes 727, 732, and 736. As illustrated in Figure 33 the system voltage variations caused by the irradiance fluctuations can be significant. These voltage variations can be significantly reduced and almost eliminated using a proper local control. As seen in

Figure 33 phase A node voltage is maintained close to a constant value during the 15-minute time interval. Similar behaviors are observed at the other nodes locations along the 37-node distribution test feeder.

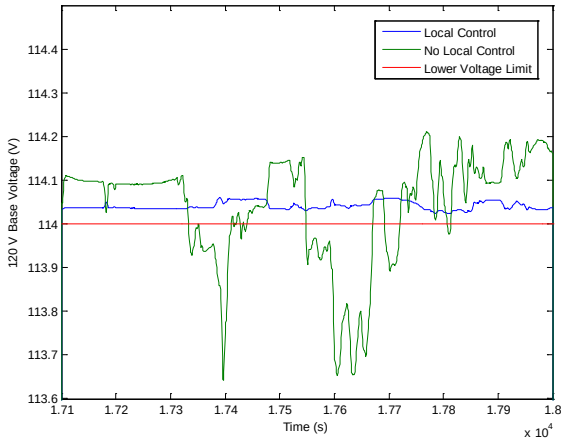

Figure 33: Voltage level at node 741 with and without the local control for 150 kW PV systems at nodes 727, 732, and 736.

The feeder voltages are also considered for a much longer time period with 450 kW PV systems in Figure 34. The voltage variations in phase A were recorded at feeder nodes 703, 734, and 741 to demonstrate the voltage variability at different nodes along the distribution feeder. The voltage variations were recorded for a 15-hour time interval, from 5 am to 8 pm for the irradiance data measured on July 22, 2010. During the first hours of operation the solar generation was low and only small variations in voltage levels were measured. The observed step voltage changes at node 703 were due to changes in the LTC tap-position. The large step voltage changes were only observed at node 703 due to its close proximity to the LTC transformer. As the distributed PV generation increased and irradiance variability became more apparent. The system without the local reactive power compensation showed large voltage variations at all of

the measured nodes. The application of fast reactive power compensation significantly reduced the voltage fluctuations throughout the 37-node distribution test feeder. The voltage fluctuations due to the changes in solar irradiance were significantly reduced for the entire system and the end of the feeder were observed not to exceed their ANSI specified voltage limits.

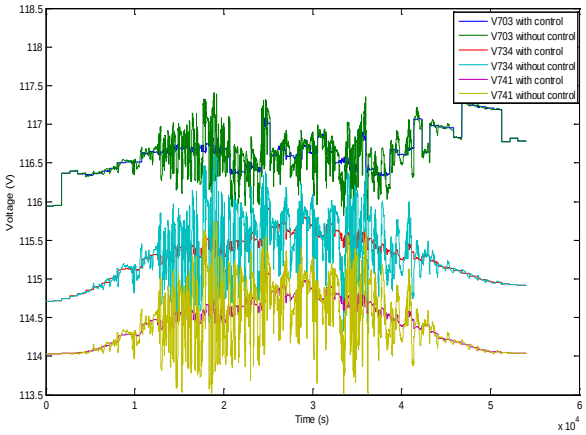

Figure 34: Phase A voltage variations observed at nodes 703, 734, and 741 with and without local control with 450 kW PV systems at nodes 727, 732, and 736.

Table 7.1 and Table 7.2 quantify the mitigation of voltage fluctuations. Table 7.1 demonstrates the voltage fluctuations at nodes 741 and 724 with and without the fast local reactive power control. The PV systems installed to nodes 727, 732, and 736 were 150 kW each for the case presented in Table 7.1. The first column of Table 7.1 shows the type of fluctuation that was measured. For example, the 'Mean fluctuation with local control' represents the mean voltage fluctuation with local control during the entire study horizon. The second through fourth columns display numerical values for each fluctuation at node 741 for phases A, B, and C. The fifth through seventh columns show numerical values for each fluctuation at node 724 for phases A, B, and C.

Table 7.1: Voltage fluctuations with and without the local control for 150 kW PV systems installed at nodes 727, 732, and 736 on 120V voltage base.

150 kW PV systems installed at nodes 727,732, and 736						
	Node741 (120 V base)			Node 724 (120 V base)		
Phase	A	B	C	A	B	C
Mean fluctuation with local control (mV)	7.6	5.6	12.2	1.2	3.3	9.1
Mean fluctuation without local control (mV)	61.9	49.3	55.8	22.8	17.1	21.2
Max. fluctuation with local control (mV)	49.5	40.6	82.8	15.3	30.4	65.0
Max. fluctuation without local control (mV)	422.0	336.1	647.0	157.4	118.0	147.7

Table 7.2 similarly displays the voltage fluctuations at nodes 741 and 724 with and without fast local control. The PV system sizes, installed at nodes 727, 732, and 736, are 450 kW each. The first column of Table 7.2 determines the type of voltage fluctuation measured. The second through fourth columns display numerical values for each fluctuation at node 741 for phases A, B, and C. The fifth through seventh columns show numerical values for each fluctuation at node 724 for phases A, B, and C.

Table 7.2: Voltage fluctuations with and without the local control for 450 kW PV systems installed at nodes 727, 732, and 736 on 120V voltage base.

450 kW PV systems installed at nodes 727,732, and 736						
	Node 741 (120 V Base)			Node 724 (120 V Base)		
Phase	A	B	C	A	B	C
Mean fluctuation with local control (mV)	19.5	15.8	37.2	3.8	10.8	28.3
Mean fluctuation without local control (mV)	181.9	145.1	164.6	66.9	50.2	62.9
Max. fluctuation with local control (mV)	132.5	126.3	266.8	*43.6*	96.1	210.1
Max. fluctuation without local control (mV)	1231	986	1171	457.6	344.8	431.6

The application of the local controllers significantly reduced the voltage fluctuations at the studied end of the feeder nodes. Table 7.1 and Table 7.2 demonstrated that both mean and maximum fluctuations from the optimized voltage values were considerably reduced with the application of the local reactive power control. The same phenomenon was observed in Figure 33 and Figure 34. Figure 33 and Figure 34 represent typical performance for the fast-acting local voltage control during short and long time intervals. Similar control performance was also observed when the rated power output of the PV plants was increased.

Table 7.3: Improvement achieved by local control for 150 kW PV systems installed at nodes 727, 732, and 736.

150 kW PV systems installed at nodes 727,732, and 736		
	Node 741	Node 724
Average decrease in mean fluctuations	84.8%	78.4%
Min. decrease in mean fluctuations	78.1%	57.1%
Max. decrease in mean fluctuations	88.6%	94.7%
Average decrease in max. fluctuations	87.6%	73.8%
Min. decrease in max. fluctuations	87.2%	56.0%
Max. decrease in max. fluctuations	88.2%	90.3%

The improvements in terms of fluctuation percentages, achieved with the local control of three 150 kW PV systems installed at nodes 727, 732, and 736, are shown in Table 7.3. The first column of Table 7.3 describes the type of improvement that was achieved. For example, the 'Average decrease in mean fluctuations' represents the average of the decrease in the mean fluctuations of the three phase voltages in the study horizon. The second and third columns show the decrease at node 741 and 724 respectively. As seen in Table 7.3 the local control reduced the mean voltage fluctuations on average by 84.8% at node 741. Demonstrated by Table 7.1 and Table 7.2 the magnitudes of voltage fluctuations at node 741 were larger than at node 724. The

average magnitude fluctuations at node 724 were reduced on average by 78.4%. The distant lateral location of node 724 to the PV plants yielded into considerably less voltage variations than the variations at node 741. The fluctuations at node 741 were larger due to its closer location to the PV generation.

Table 7.4 displays the improvements in terms of fluctuation percentages achieved with local control of three 450 kW PV systems installed at nodes 727, 732, and 736. Similar to Table 7.3 the first column describes the type of decrease achieved and the second and third columns show the decrease at node 741 and 724 respectively. The increase in plant sizes did not significantly affect the performance displayed in Table 7.4. The application of local control reduced the mean voltage fluctuations on average by 85.3% on node 741, and by 75.9% at node 724. Table 7.3 and Table 7.4 demonstrate the performance of the local control maintained its effectiveness with the increased PV penetration.

Table 7.4: Improvement achieved by local control for 450 kW PV systems installed at nodes 727, 732, and 736.

450 kW PV systems installed at nodes 727,732, and 736		
	Node 741	Node 724
Average decrease in mean fluctuations	85.3%	75.9%
Min. decrease in mean fluctuations	77.6%	55.0%
Max. decrease in mean fluctuations	89.3%	94.3%
Average decrease in max. fluctuations	84.5%	71.3%
Min. decrease in max. fluctuations	77.2%	51.3%
Max. decrease in max. fluctuations	89.2%	89.5%

For the studied nodes, the local reactive power control considerably reduced all voltage fluctuations. The overall system performance and power quality were thus improved considerably over VVC without local reactive power control

7.4. Discussion on dual-layer VVC approach with fast local control

This chapter presented an application of a dual-layer VVC for distribution systems with active participation for reactive power support by the PV inverters. The proposed algorithm included finding an optimal solution to the VVO problem by using a distribution feeder wide MINLP based VVO algorithm. In conjunction with the MINLP algorithm the proposed solution included local reactive power control by the solar inverters to reduce voltage fluctuations along the feeder. The proposed approach was compared to a VVO approach without the fast second layer local PV inverter reactive power control. For the studied test feeder the local reactive power control considerably reduced all voltage fluctuations. The overall system power quality was thus improved considerably over VVO without local reactive power control. The proposed algorithm was implemented to a modified IEEE 37 node radial distribution test feeder with three PV plants with various loading and generation conditions. The results obtained showed significant reductions in both the mean and the maximum voltage fluctuations were achieved with the application of the dual-layer VVC. The dual-layer approach with the MINLP based VVO and fast local reactive power control shows promise to be applied to on-line feeder VVC with distributed generation.

8. CONCLUSIONS

The work presented in this dissertation researches new methods for distribution system VVC and VVO. Chapters 3 and 4 presented a new method for formulating and solving a distribution system VVO as a MINLP problem. The proposed approach can solve the distribution system VVO without making assumptions, such as linearization, in the VVO problem formulation. The effectiveness of the MINLP was studied with a number of test feeders including the IEEE 13 node and IEEE 37 node radial distribution test feeders in Chapter 4 and the performance of the presented approach was validated.

The analytical VVO approach is limited by their computational times for large distribution systems and by the response times of mechanical distribution control devices. An approach to minimize voltage fluctuation at specific feeder nodes by use of local linear reactive power controllers was presented in chapter 5. The proposed algorithm considered a local reactive power control of multiple PV inverters on a distribution feeder to minimize voltage fluctuations at main feeder tie nodes. That allowed voltage fluctuations to be similarly limited at the downstream feeder nodes. The presented distributed was shown to be effective for reducing voltage fluctuations significantly. The results obtained displayed significant reductions in both the mean and maximum voltage fluctuations caused by the irradiance variations.

In order to prevent two or more DG units from taking counteracting control actions a novel approach for fast global reactive power control was presented in chapter 6. The approach utilizes quadratic programming constrained by classical sensitivity analysis to find optimized reactive power injections by the DG to minimize voltage variations across the feeder. The results of the case studies in chapter 6 displayed that the presented

coordinated control algorithm is effective for on-line application in the Smart Grid distribution feeders to limit voltage fluctuations due to intermittency of PV generation.

Finally the dissertation presented a dual-layer VVC approach. The presented MINLP based VVO approach was utilized for making the long term control decisions and proposed fast-acting local control approach was utilized for the short term control decisions. The effectiveness of the dual-layer VVC approach was studied with test system, real life variable utility load data, and with PV generation determined from measured irradiance patterns. The results obtained from case studies in chapter 7 exhibited significant reductions in both the mean and maximum voltage fluctuations achieved with the application of the dual-layer VVC. The dual-layer approach with the MINLP based VVO and fast local reactive power control shows promise for on-line feeder VVC with distributed generation.

REFERENCES

[1] D. I. H. Sun, et al., "Calculation of energy losses in a distribution system," *IEEE Transactions on Power Apparatus and Systems*, no. 4, 1980.

[2] S. A. Nasar and F. C. Trutt, *Electric power systems*. Boca Raton, FL, USA: CRC Press, 1999.

[3] J. J. Grainger and W. D. Stevenson, *Power System Analysis*. Singapore: McGraw-Hill, 1994.

[4] R. Billinton and D. Lakhanpal, "Impacts of demand-side management on reliability cost/reliability worth analysis," *IEE Proceedings on Generation, Transmission, and Distribution*, vol. 143, no. 3, pp. 225-231, 1996.

[5] K. P. Schneider, F. K. Tuffner, J. C. Fuller, and R. Singh, "Evaluations of conservation voltage reduction (CVR) on a national level," Pacific Nortwest National Laboratory PNNL Report 19596, 2010.

[6] ANSI, "American national standard for electric power system and equipment voltage ratings (60) hertz," 1996.

[7] G. W. Sunderman, "Conservation voltage reduction system, modeling, measurement, and verification," in *Proceedings of 2012 IEEE T&D Conference and Exposition*, Knoxville, TN, 2012, pp. 1-4.

[8] W. H. Kersting, *Distribution system modelling and analysis, 2nd Ed.* Boca Raton, FL: CRC Press, 2007.

[9] J. J. Grainger and S. Civanlar, "Volt/var control on distribution systems with lateral branches using shunt capacitors and voltage regulators - Part I: The overall

problem," *IEEE Transactions on Power Apparatus and Systems*, vol. 104, no. 11, pp. 3278-3283, 1985.

[10] S. Civanlar and J. J. Grainger, "Volt/var control on distribution systems with lateral branches using shunt capacitors and voltage regulators - Part 2: The solution method," *IEEE Transactions on Power Apparatus and Systems*, vol. 104, no. 11, pp. 3284-3290, 1985.

[11] S. Civanlar and J. J. Grainger, "Volt/var control on distribution systems with lateral branches using shunt capacitors and voltage regulators - Part 3: The numerical results," *IEEE Transactions on Power Apparatus and Systems* , vol. 104, no. 11, pp. 3291-3297, 1985.

[12] R. W. Uluski, "VVC in smart grid era," in *Proceedings of IEEE Power and Energy Society General Meeting*, Minneapolis, MN, 2010, pp. 1-7.

[13] E. A. Paaso, Y. Liao, and A. M. Cramer, "Formulation and solution of distribution system voltage and var control with distributed generation as a mixed integer non-linear programming problem," *Electric Power System Research*, vol. 108, pp. 164-169, 2014.

[14] E. A. Paaso, Y. Liao, and A. M. Cramer, "Dual-layer voltage and var control approach with active participation from distributed generation," *Submitted: IEEE Transactions on Smart Grid*, 2014.

[15] E. A. Paaso and Y. Liao, "Coordinated reactive power control of photovoltaic inverters to limit voltage variations on distribution feeders ," *Submitted: Electric Power Systems Research* , 2014.

[16] T. N. Samuel and N. K. Nohria, "Digital control and instrumentation for step-voltage regulators," *IEEE Transactions on Power Apparatus and Systems*, vol. 104, pp. 194-199, 1985.

[17] W. H. Kersting, "Distribution feeder voltage regulation control," *IEEE Transactions on Industry Applications*, vol. 46, no. 2, pp. 620-626, 2010.

[18] A. A. Sallam and O. P. Malik, "Power factor improvement," in *Electric distribution systems*. Singapore: Jon Wiley & Sons IEEE Press, 2011, ch. 9, pp. 361-379.

[19] Y. V. Joshi, S. S. Deshpandm, and S. G. Kahaleka, "Microprocessor based automatic power factor control," in *Proceeding of IEEE TENCON*, Beijing, China, 1993, pp. 326-329.

[20] T. B. Girotti, N. B. Tweed, and N. R. Houser, "Real-time VAR control by SCADA," *IEEE Transactions on Power Systems*, vol. 5, no. 1, pp. 61-64, 1990.

[21] M. E. Baran and Y. Hsu, "Volt/var control at distribution substations," *IEEE Transactions on Power Systems*, vol. 14, no. 1, pp. 312-318, 1999.

[22] S. J. Cheng, O. P. Malik, and G. S. Hope, "An expert system for voltage and reactive power control of a power system," *IEEE Transactions on Power Systems*, vol. 3, no. 4, pp. 1449-1455, 1988.

[23] M. M. A. Salama and A. Y. Chikhani, "An expert system for reactive power control of distribution system - Part 1: System configurations," *IEEE Transactions on Power Delivery*, vol. 7, no. 2, pp. 940-945, 1992.

[24] P. R. Laframbiose, G. Ferland, A. Y. Chikhani, and M. M. A. Salama, "An expert system for reactive power control of distribution system - Part 2: System

implmentation," *IEEE Transactions on Power Delivery*, vol. 10, no. 3, pp. 1433-1441, 1995.

[25] C. Pimpa and S. Premrudeepreechacharn, "Voltage control in power system using expert system based in SCADA system," in *Proceedings of IEEE Power and Energy Society Winter Meeting*, New York, NY, 2002, pp. 1282-1286.

[26] S. Rahimi, M. Marinelli, and F. Silvestro, "Evaluation of requirements for volt/var control and optimization function in distribution management systems," in *Proceedings of IEEE International Energy Conference and Exhibition*, Florence, Italy, 2012, pp. 331-336.

[27] R. Baldick and F. F. Wu, "Efficient integer optimization algorithms for optimal coordination of capacitors and regulators," *IEEE Transactions on Power Systems*, vol. 5, no. 3, pp. 805-812, 1990.

[28] F. C. Lu and Y. Y. Hsu, "Reactive power/voltage control in a distribution substation using dynamic programming," *IEE Proceedings - Generation, Transmission and Distribution* , vol. 142, no. 6, pp. 639-645, 1995.

[29] I. Roytelman, B. K. Wee, R. L. Lugtu, and T. M. Kulars, "Volt/var control algorithm for modern distribution management system," *IEEE Transactions on Power Systems* , vol. 10, no. 3, pp. 1454-1460, 1995.

[30] I. Roytelman, B. K. Wee, R. L. Lugtu, T. M. Kulars, and T. Brossart, "Pilot project to estimate the generalized volt/var control effectiveness," *IEEE Transactions on Power Systems*, vol. 13, no. 3, pp. 864-869, 1998.

[31] X. Feng, W. Peterson, F. Yang, G. M. Wickramasekara, and J. Finley,

"Implementation of control center based voltage and var optimization in distribution management system," in *IEEE Power and Energy Society Transmission and Distribution Conference*, 2010.

[32] X. Feng and F. Yang, "Voltage regulation optimization," U.S. Patent 8195338, Jun. 5, 2012.

[33] K. Warwick, A. Ekwue, and R. Aggarwal, *Artificial intelligence techniques in power systems*. Stevenage, United Kingdom: The Institute of Electrical Engineers, 1997.

[34] Y. Y. Hsu and F. C. Lu, "A combined artificial neural network-fuzzy dynamic programming approach to reactive power/voltage control in a distribution substation," *IEEE Transactions on Power Systems*, vol. 13, no. 4, pp. 1265-1271, 1998.

[35] V. Miranda, A. Moreira, and J. Pereira, "An improved fuzzy inference system to voltage/var control," *IEEE Transactions on Power Systems*, vol. 22, no. 4, pp. 2013-2020, 2007.

[36] R. H. Liang and Y. S. Wang, "Fuzzy-based reactive power and voltage control in a distribution system," *IEEE Transactions on Power Delivery*, vol. 18, no. 2, pp. 610-618, 2003.

[37] Z. Hu, X. Wang, H. Chen, and G. A. Taylor, "Volt/var control in distribution systems using a time-interval based approach," *IEE Proceedings - Generation, Transmission and Distribution*, vol. 150, no. 5, pp. 548-554, 2003.

[38] T. Senjyu, Y. Miyazato, A. Yona, N. Urasaki, and T. Funabashi, "Optimal distribution voltage control and coordination with distributed generation," *IEEE*

Transactions on Power Delivery, vol. 23, no. 2, pp. 1236-1242, 2008.

[39] K. Turitsyn, P. Sulc, S. Backhau, and M. Shertkov, "Options for control of reactive power by distributed photovoltaic generation," *Proceeding of IEEE*, vol. 99, no. 6, pp. 1063-1073, 2011.

[40] M. Braun, "Reactive power supplied by PV inverters - cost benefit analysis," in *Proceedings of European Photovoltaic Solar Energy Conference*, Milan, Italy, 2007, pp. 1-5.

[41] Y. Liao, et al., "Voltage and var control to enable high penetration of photovoltaic generation," in *North American Power Symposium*, Urban-Champaign, IL, 2012.

[42] M. B. Liu, C. A. Cañizares, and W. Huang, "Reactive power and voltage control in distribution systems with limited switching operations," *IEEE Transactions on Power Systems*, vol. 24, no. 2, pp. 889-899, 2009.

[43] A. Borghetti, "Using mixed integer programming for the volt/var optimization in distribution feeders," *Electric Power Systems Research*, vol. 98, pp. 39-50, 2013.

[44] G. Rochart, E. Monfroy, and N. Jussien, "MINLP problems and explanation-based constraint programming," in *Proceedings of 4th Workshop on Cooperative Solvers in Constraint Programming*, Toronto, Canada, 2004.

[45] P. Bonammi and J. Lee. (2007) BONMIN users' manual. Document. [Online]. https://projects.coin-or.org/Bonmin

[46] J. Currie and D. I. Wilson, "OPTI: Lowering the Barrier between Open Source Optimizers and the Industrial MATLAB User," in *Foundations of Computer-Aided Process Operations*, Savannah, GA, 2012.

[47] M. A. Duran and I. E. Grossmann, "An outer-approximation algorithm for a class of mixed-integer nonlinear programs," *Mathematical Programming*, vol. 36, no. 3, pp. 307-339, 1986.

[48] R. Fletcher and S. Leyffer, "Solving mixed integer nonlinear programs by outer approximation," *Mathematical Programming*, vol. 66, no. 1-3, pp. 327-349, 1994.

[49] W. H. Kersting, "Radial distribution test feeders," *IEEE Transactions on Power Systems*, vol. 6, pp. 975-985, 1991.

[50] T. A. Short, *Electric power distribution equipment and systems*. Boca Raton, FL, USA: CRC Press, 2006.

[51] H. Dawei, T. Habetler, M. J. Mousavi, and N. Kang, "A zip model-based feeder load modelling and forecasting method," in *Proceedings 2013 IEEE Power and Energy Society General Meeting*, Vancouver, Canada, 2013, pp. 1-5.

[52] K. Turitsyn, P. Sulc, S. Backhaus, and M. Chertkov, "Distributed control of reactive power flow in a radial distribution circuit with high photo voltaic penetration," in *Proceedings of IEE Power and Energy Society General Meeting*, Minneapolis, MN, 2010, pp. 1-6.

[53] National Alliance of Adavanced Technology Batteries, "Distributed Energy Storage: Serving National Interest," National Alliance of Adavanced Technology Batteries, 2010.

[54] IEEE PES Distribution System Analysis Subcommittee. (1991) IEEE 13 node test feeder. Document. [Online]. http://ewh.ieee.org/soc/pes/dsacom/testfeeders/

[55] IEEE PES Distribution System Analysis Subcommittee. (2010) IEEE 37 node test

feeder . Document. [Online]. http://ewh.ieee.org/soc/pes/dsacom/testfeeders/

[56] X. Liu, A. M. Cramer, and Y. Liao, "Reactive power control of photovoltaic inverters for mitigation of short term distribution system voltage variability," in *IEEE Power and Energy Society Transmission and Distribution Conference*, Chicago, 2014.

[57] M. Lave, J. Kleissl, and E. Arias-Castro, "High frequency irradiance fluctuations and geographical smoothing," *Solar Energy*, vol. 86, no. 8, pp. 2190-2199, 2012.

[58] A. Woyte, B. R., and J. Nijs, "Analyzing short-time irradiance fluctuations by their characteristic time scales," in *3rd World Conference on Photovoltaic Energy Conversion*, Osaka, Japan, 2003.

[59] W. Jewell and T. Unruh, "Limits on cloud-induced fluctuations in photovoltaic generation," *IEEE Transactions on Sustainable Energy*, vol. 5, no. 1, pp. 8-14, 1990.

[60] R. A. Messenger and J. Ventre, *Photovoltaic systems engineering*, 3rd ed. Boca Raton, FL, United States of America: CRC Press, 2010.

[61] M. A. Gomes de Brito, L. Galotto, L. P. Sampaio, G. A. e Melo, and S. A. Canesin, "Evaluation of the main MPPT techniques for photovoltaic applications," *IEEE Transactions on Industrial Electronics*, vol. 1, no. 3, pp. 117-124, 2010.

[62] S. Teleke, M. E. Baran, S. Bhattacharya, and A. Q. Huang, "Rule-based control of battery energy storage for dispatching intermitten renewable sources," *IEEE Transactions on Sustainable Energy*, vol. 1, no. 3, pp. 117-124, 2010.

[63] X. Li, D. Hui, and X. Lai, "Battery energy storage station (BESS) based smoothing control of photovoltaic (PV) and wind generation fluctuations ," *IEEE Transactions*

on Sustanable Energy, vol. 4, no. 2, pp. 464-473, 2013.

[64] T. D. Hund, G. S., and K. Barrett, "Grid-tied PV system energy smoothing," in *IEEE Photovoltaic Specialist Conference*, Honolulu, HI, 2010.

[65] N. Kakimoto, H. Satoh, S. Takayma, and K. Nakamura, "Ramp-rate control of photovoltaic generation with electric double layer capacitor ," *IEEE Transactions on Energy Conversion*, vol. 24, no. 2, pp. 465-473, 2009.

[66] A. Jamehbozorg, S. N. Keshmiri, and G. Radman, "PV output smoothing using energy capacitor systems," in *IEEE Southeastcon*, Nashville, TN, 2011.

[67] H. G. Yeh, D. F. Gayme, and S. H. Low, "Adaptive var control for distribution circuits with photovoltaic generation," *IEEE Transactions on Power Systems*, vol. 27, no. 3, pp. 1656-1663, 2012.

[68] J. Smith, R. Sunderman, R. Dugan, and B. Seal, "Smart inverter voltage and var control functions for high penetration of PV on distribution systems," in *IEEE Power and Energy Society Conference and Exposition*, 2011.

[69] S. Deshmukh, B. Natarajan, and A. Pahwa, "Voltage/var control in distribution networks via reactive power injection through distributed generation," *IEEE Transactions on Smart Grid*, vol. 3, no. 3, pp. 1226-1234, 2012.

[70] M. E. Baran and M. I. El-Markabi, "A multiagent-based dispatching scheme for distributed generators for voltage support on distribution feeders," *IEEE Transactions on Power Systems*, vol. 22, no. 1, pp. 52-59, 2007.

[71] National Renewable Energy Laboratory, "Solar measurement grid (1-year archive) 1-second global horizontal irradiance ," 2010.

[72] A. Woyte, V. V. Thong, R. Belmans, and J. Nijs, "Voltage fluctuations on distribution level introduced by photovoltaic systems," *IEEE Transactions on Energy Conversion*, vol. 21, no. 1, pp. 202-209, 2006.

[73] H. Xin, et al., "A distributed control for multiple photovoltaic generators in distribution networks," in *American Control Conference*, San Francisco, 2011.

[74] M. J. Reno, R. J. Broderick, and S. Grijalva, "Smart inverter capabilities for mitigating over voltage on distribution systems with high penetrations of PV," in *IEEE Photovoltaic Specialist Conference*, Tampa, FL, 2013.

[75] R. Aghatehrani and A. Golnas, "Reactive power control of photovoltaic systems based on the voltage sensitivity analysis," in *IEEE Power and Energy Socity General Meeting*, San Diego, CA, 2012.

[76] A. Samadi, R. Eriksson, L. Söder, B. G. Rawn, and J. C. Boemer, "Coordinated active power-dependent voltage regulation in distribution grids with PV systems," *IEEE Transactions on Power Delivery*, vol. PP, no. 99, p. 1, 2014.

[77] M. A. Kashem and G. Ledwich, "Multiple distributed generators for distribution feeder voltage support," *IEEE Transactions on Energy Conversion*, vol. 20, no. 3, pp. 676-684, 2005.

VITA

Esa Aleksi Paaso received the B.Sc. degree (summa cum laude) in electrical engineering from Western Kentucky University in 2009 and the MSEE degree in electrical engineering from the University of Kentucky in 2011. He is currently a PhD candidate in electrical engineering at the University of Kentucky. His research interests include voltage and var control, optimization of power distribution systems, distributed generation, renewable energy, and Smart Grid. He is a graduate student member of IEEE and the IEEE Power & Energy Society. He is also a member of Tau Beta Pi (TBP) and Omicron Delta Kappa (ODK) honor societies. During his graduate studies he served as Graduate Teaching Assistant for the Power and Energy Institute of Kentucky and held internships with Rautaruukki Oyj in Raahe, Finland, Nextlife Recycling in Frankfort, KY, and S&C Electric Company in Chicago, IL. Upon completion of his PhD degree he has accepted a job as Senior Smart Grid Specialist with Commonwealth of Edison (ComEd) in Oakbrook Terrace, IL.

Professional publications:

E. A. Paaso and Y. Liao, "Coordinated reactive power control of photovoltaic inverters to limit voltage variations on distribution feeders ," *Submitted: Electric Power Systems Research* , 2014.

E. A. Paaso, Y. Liao, and A. M. Cramer, "Dual-layer voltage and var control approach with active participation from distributed generation," *Submitted: IEEE Transactions on Smart Grid*, 2014.

E. A. Paaso, Y. Liao, and A. M. Cramer, "Formulation and solution of distribution system voltage and var control with distributed generation as a mixed integer non-linear programming problem," *Electric Power System Research*, vol. 108, pp. 164-169, 2014.

E. A. Paaso and Y. Liao, "Development of new algorithms for power system short-term load forecasting", International Journal of Computer and Information Technology, vol. 02, no. 02, 2013, pp. 201-209.

E. A. Paaso, "Investigation of new techniques for power system load forecasting," MSEE Thesis, University of Kentucky, Lexington, KY, 2011.

S. S. Wilson, L. Gurung, **E. A. Paaso**, and J. C. Wallace, "Creation of robot for subsurface void detection," *in Proceeding of IEEE Conference on Homeland Security*, Waltham, MA, 2009, pp. 669 – 676.